This is to certify that the

dissertation entitled

UNIT RESOLUTION AND PHOTO-FRAGMENTATION
IN A TANDEM TIME-OF-FLIGHT
MASS SPECTROMETER

presented by

Paul Raymond Vlasak

has been accepted towards fulfillment
of the requirements for

Ph.D. degree in Chemistry

Christie G. Enke
Major professor

Date Oct. 26, 1995

UNIT RESOLUTION AND PHOTO-FRAGMENTATION IN A TANDEM TIME-OF-FLIGHT MASS SPECTROMETER

By

Paul Raymond Vlasak

A DISSERTATION

Submitted to
Michigan State University
in partial fulfillment of the requirements
for the degree of

DOCTOR OF PHILOSOPHY

Department of Chemistry

1995

ABSTRACT

UNIT RESOLUTION AND PHOTO-FRAGMENTATION IN A TANDEM TIME-OF-FLIGHT MASS SPECTROMETER

By

Paul Raymond Vlasak

The goal of this work is the development of a dual reflectron tandem time-of-flight (TOF) mass spectrometer (MS) capable of collecting complete tandem mass spectrometry data sets on the chromatographic time scale. A system which can meet this goal must use sample efficiently and be capable of high mass spectral generation rates. In addition, the instrument must maintain unit resolution over the mass range of interest in order to be analytically useful.

The instrument described here uses an electron ionization source which accumulates ions between source extractions. Precursor ion separation occurs in a reflectron TOF analyzer, with a mass resolution of 1500 at the reflectron focal point.

Precursor selection and fragmentation are accomplished by intersecting a focused, high-energy laser pulse with a single, iso-mass ion packet at the focal point of the first mass analyzer. Unit mass resolution for selection has been demonstrated to m/z 158, while calculations indicate that

the real limit of unit mass resolution is about m/z 1200. The high degree of ion/photon overlap results in fragmentation efficiencies as high as 79% (for the molecular ion of bromobenzene) and efficiencies for a variety of ions similar to those observed for collisionally-induced dissociation in commercial tandem MS instruments. Product spectra are qualitatively similar to those obtained using commercial instrumentation.

Prior to fragmentation, the precursor ion packet is isolated by an interleaved comb ion deflection gate. Unit mass resolution for isolation has been demonstrated to m/z 167. Calculations indicate that the real limit of unit mass resolution is about m/z 300.

Upon dissociation, product ions retain a fraction of their kinetic energy equal to the fraction of mass retained. Thus, a relative kinetic energy range of nearly 100% results for the product ions. Using an acceleration stage to reduce this relative kinetic energy range and a novel, broad energy range focusing reflectron, a mass resolution of 300 for product ion spectra has been demonstrated.

This tandem mass spectrometer is capable of generating product spectra at the repetition rate of the laser while maintaining unit mass resolution over a mass range appropriate for gas chromatographic analyses.

for Deena, Thomas, and Dad

ACKNOWLEDGEMENTS

Many people contributed to this project, providing everything from labor to inspiration. First and foremost, I thank and acknowledge my advisor, Dr. Chris Enke. His guidance has been excellent, it has been appropriate, and it has been appreciated. Dr. Enke has taught me that confidence not only means knowing that one can do what others have done, but knowing that one can do what others have not done. I will strive to emulate his enthusiasm and creativity in my own pursuits.

Working with other students on this project has been both enjoyable and productive. I thank Dr. David McLane, Dr. Mary Seeterlin, Doug Beussman, Tina Erickson, Qinchung Ji, Ben Gardner, and Eric Hemenway, all of whom are esteemed friends and have my greatest respect as scientists.

I have learned from many excellent teachers over the years and I am grateful to all of them. I have been especially fortunate to have had Ms. Miesner, Ms. Davis, Mr. Costigan, Mr. McDougall, Mr. Detviler, Mr. Tressel, Mr. Young, Dr. Walters, Dr. Miessler, Dr. Hardgrove, Dr. Hanson, Dr. Abdella, Dr. Failletaz, Dr. Allison, Dr. Crouch, Dr. Enke,

Dr. Leroi, and Dr. McGuffin. I am especially grateful to Dr. Crouch, who served as my second reader, and the other members of my guidance committee, Dr. Leroi, and Dr. Reusch.

In addition to the students and faculty who have contributed to this project, I would like to acknowledge a number of other support persons. Mike Davenport, Russ Geyer, Harold Hilbert, and Marty Rabb all contributed to the design as well as the construction of the tandem TOF instrument. In addition, I would like to thank Tom Clarke, Ron Haas, Sam Jackson, Dick Menke, and Scott Sanderson.

Finally, I thank my family and friends for the support and encouragement that have allowed me to pursue this goal. My parents and grandparents taught me to be proud of myself and my work. My father instilled in me scientific curiosity. My brothers grew, shared, and explored with me. Deena, my patient and supportive wife, and Thomas, my child, are everything.

I did not get here on my own, and I am grateful to all of you.

TABLE OF CONTENTS

LIST OF TABLES

LIST OF FIGURES

Chapter 1: Introduction

1.1 Goal

The goal of this research is to continue the development of a tandem mass spectrometer (MS/MS) capable of greatly increasing the amount of MS/MS data obtainable from sample components as they elute from a chromatographic column. The characterizing power of MS/MS for pure sample introduced to the ion source for a sufficient period of time is tremendous. However, the characterizing power of MS/MS is limited for sample introduced chromatographically since current commercial instrumentation allows the collection of only a few mass scans during the elution time of a single component. This dissertation describes the development of a high speed tandem time-of-flight (TOF) mass spectrometer, with emphasis on the achievement of unit mass resolution for all aspects of instrument performance.

1.2 Tandem mass spectrometry

Tandem mass spectrometry (MS/MS) is the linking of two mass analyzers. Ions are initially created from solid, liquid, or gaseous sample in an ion source. These ions may consist of intact molecular ions or ionic fragments of the molecule. The first mass spectrometer is used to select ions

of a particular mass to charge (m/z) ratio from those produced in the source. Following this selection, a m/z-changing reaction occurs (in most cases a dissociation), either spontaneously or in response to induced energy in a reaction region. Energy can be induced by collision of the ions with a background gas (collision-induced dissociation or CID), collision of the ions with a surface (surface-induced dissociation or SID), or by irradiating the ions (photo-induced dissociation or PID). Ions which decay spontaneously outside of the ion source are referred to as metastable ions. The charged products of the reaction are then analyzed by the second mass spectrometer. The ions of a particular m/z value selected in the first mass analyzer are referred to as precursor ions. Ions resulting from the m/z-changing reaction are referred to as product ions, and ions resulting from fragmentation in the ion source are referred to as fragment ions. In the case of quadrupole ion traps or Fourier transform mass spectrometers (FTMS), the entire sequence occurs within one mass analyzer which performs both the initial selection and the analysis of product ions. When magnetic sector instruments, electric sectors, quadrupoles, or time-of-flight mass analyzers (TOF) are used, precursor selection and product analysis are performed in sequential mass analyzers.

1.2.1 Ion structure data

While the basic experiment remains unchanged, the role of the first mass analyzer varies depending on the type of ionization used and whether

or not the sample is a pure compound. In one case, a pure compound is introduced to the mass spectrometer and is ionized by a 'hard' ionization method (one which results in a high degree of fragmentation in the source) such as electron-impact ionization. Each *m/z* value observed in a normal mass spectrum for the pure compound can then be selected, the ion fragmented, and a mass spectrum for that *m/z* value ion obtained. In this case, the benefit of MS/MS is the increased structural information obtained and the ability to determine fragmentation pathways [1, 2]. Both mass analyzers provide ion structure data. In the majority of analyses, the complete MS/MS data set provides valuable additional information regarding the molecular structure of the sample compound.

1.2.2 Mixture data

If a 'soft' ionization method (one which results in little or no fragmentation of the sample molecule) such as chemical ionization or electrospray ionization is used, then the first mass analyzer can serve to separate different molecular ions from one another. This allows the introduction of a mixture directly to the mass analyzer, thereby eliminating the need to use chromatography to separate the compounds and greatly reducing analysis time. The fragmentation and subsequent mass analysis provide the structural information required to identify the compound [2, 3]. Operating in this way, tandem mass spectrometry is especially suited to trace analysis of targeted compounds in mixtures [2, 4, 5]. The first mass analyzer

is used to provide separation of a mixture rather than to provide ion structure data as was described in the previous section. Of course, isomers or other compounds having the same molecular weight cannot be separated with the first mass analyzer.

1.3 MS for chromatographic detection

Often gas chromatographs (GC) or high performance liquid chromatographs (HPLC) are interfaced to mass spectrometers and to tandem mass spectrometers. The combination of chromatographic resolving power and the sensitivity and selectivity of MS make these systems extremely powerful, explaining the popularity of these instruments in the scientific community. In this work, a GC was interfaced to the instrument as described below, and this thesis will refer primarily to GC applications.

1.3.1 Overlapping chromatographic peaks

If a mixture is not fully separated by chromatography, the normal mass spectra observed are a convolution of the spectra of the coeluting compounds. These overlapping spectra are exceedingly difficult to interpret unless mathematical methods can be employed to separate the spectra. Spectral subtraction can be used to remove background which may consist of column bleed, overlapping elutions, or both [6, 7]. Reverse library search algorithms (in which known spectra are compared to the sample spectrum to determine whether or not the compound is present) are effective when the

identities of compounds expected to be present are known [8-10]. In some cases, mathematical deconvolution of the overlapping spectra is possible based on a pure elution profile for a particular m/z value unique to each compound [11-14]. Alternatively, factor analysis has been used to determine components of coeluting mixtures [15, 16].

In chromatography/MS/MS, if compounds coelute, the first mass analyzer can be used to provide further separation, thereby increasing resolving power. If the chromatographic separation is complete, both mass analyzers can provide structural data and increase selectivity. For many applications, GC/MS or LC/MS provides adequate selectivity and sensitivity, whereas GC/MS/MS or LC/MS/MS is most often applied to complex mixtures in complex matrices such as analyses of environmental [17], food [18], or pharmaceutical [19, 20] samples.

1.3.2 Instrumentation

1.3.2.1 Mass filters

Most commercially available MS and MS/MS instruments are scanning mass spectrometers. These scanning instruments are also referred to as mass filters because they allow the passage of a single m/z value at a time, and the conditions of the mass spectrometer are scanned as a function of time to collect a mass spectrum. The scanning mass filters include quadrupoles, magnetic sectors, and combined electric and magnetic sectors

for normal mass spectrometry. The most common type of tandem mass spectrometer is the triple quadrupole mass spectrometer in which the first and third quadrupole are the mass filters and the center quadrupole serves as the reaction region. Tandem mass spectrometers based on electric and magnetic sectors are of varied geometry and involve 3 to 4 sectors in general, with the reaction region simply consisting of a field-free region between sectors.

Mass filters exhibit a trade-off between scan rate and sensitivity since increasing scan rate reduces the amount of time spent collecting each m/z value. Even when a mass filter is scanned slowly, the majority of ions produced in the source are always lost since all but one m/z value are being filtered away continuously. Most GC/MS analyses are performed at a scan rate that allows the collection of a few mass spectra per second in order to provide adequate sensitivity for monitoring capillary GC effluent.

An important consideration is the compatibility of sampling rate and chromatographic peak width. To maintain less than 0.1% error in peak height determination, at least 2.6 samples are required per peak (full width at half maximum height) [21]. This assumes that the peak shapes are Gaussian, that noise is negligible, and that the same sampling rate is maintained on either side of the peak for a considerable time. Description of the entire shape of the elution profile across a real chromatographic peak (not necessarily Gaussian) with the same level of accuracy in the presence of

noise may require 100 or more data points [22]. Since capillary GC typically results in peaks having widths on the order of a few seconds, the sampling rate normally used (a few Hz) is barely sufficient to allow quantitation based on peak height at a useful level of accuracy. This rate is not sufficient to allow effective mathematical deconvolution, which requires accurate description of the peak profile [12]. The fact that commercial MS detectors for GC barely provide adequate sampling rates illustrates an important obstacle in the development of a tandem mass spectrometer for GC detection.

Another difficulty associated with the relatively slow scan of mass filter instruments is that the sample pressure in the ion source can change significantly during the collection of a single spectrum. This results in a skewed spectrum. For example, if a spectrum is collected on the rising edge of a chromatographic peak, then the high m/z portion of the spectrum is enhanced, whereas the opposite is true if the spectrum is collected on the falling edge of a peak.

1.3.2.2 Batch array detectors

Batch array detection by ion trap mass spectrometry or time-of-flight (TOF) mass spectrometry can eliminate the skewing problem since ionization occurs for a period of time followed by detection of all of the ions formed during the ionization period. Unfortunately, the spectral generation rate is not significantly different for quadrupole ion trap mass spectrometers than for quadrupole mass spectrometers. Potentials are applied to the quadrupole

ion trap mass spectrometer in such a way as to sequentially eject ions of increasing m/z values through holes in one of the trap electrodes where a detector records ion signal. While sensitivity for the quadrupole mass spectrometer is inversely proportional to scan rate, the ion trap mass spectrometer is limited by the fact that the trap can hold a limited number of ions, therefore allowing a limited time for sample ionization, followed by an analysis period during which chromatographic effluent is lost. Also, scan rate is inversely proportional to mass resolution.

Ion trap mass spectrometers are capable of MS/MS experiments through the use of an excitation sequence which eliminates m/z values from the trap volume above and below the desired precursor m/z. Fragmentation by any of the common fragmentation techniques can then be implemented, followed by the collection of product spectrum in the usual manner.

TOF mass spectrometry is a pulsed technique where ions are periodically extracted from an ion source and subsequently separated according to m/z value in a field-free flight tube. A spectrum is collected as a function of time as the ions strike a detector at the end of the flight tube. TOF has the highest spectral generation rate of any mass analyzer, usually on the order of several kilohertz, limited only by the flight time of the largest m/z value. Collection of the large number of spectra produced by TOF for a sustained period of time, as is required for chromatographic analyses, requires the use of sophisticated data collection electronics. The integrating

transient recorder developed at Michigan State University [23-25] averages a specified number of individual transients (single spectra) and stores the summed spectra to disk for a spectral generation rate compatible with accurate description of elution profiles for GC/MS. A GC/TOF-MS instrument with a data collection system that operates on the TOF time scale has recently become commercially available [26].

1.3.2.3 True array detectors

True array detection can be accomplished either in a sector instrument with the use of a spatial array detector or by Fourier transform mass spectrometry (FTMS), again with the elimination of the spectral skewing problem. Spatial array detectors are very effective in improving sensitivity and spectral generation rate [27, 28]. These detectors are expensive, however, as are the sector instruments with which they are used. Either mass resolution or mass range is limited by the number of elements in the array. FTMS requires extremely low pressures within the instrument, so that the gas load of chromatography is an obstacle to this combination. Spectral generation rate for FTMS is low due to a trade-off between acquisition time and mass resolution. FTMS can be used to accomplish MS/MS in a manner similar to that described for ion trap mass spectrometers, with a period of time required for isolation of the precursor.

1.3.3 Greater challenge of chromatography/MS/MS

Using MS/MS as a chromatographic detector as opposed to MS amplifies the spectral generation rate requirements since the analyst would ideally collect a complete MS/MS data set during an elution. For tandem mass filter instruments, this would require a scan of the product analyzer for each m/z value in the normal mass spectrum. For commercially available chromatography/MS/MS instruments, only a small portion of the MS/MS data set can be collected during the elution of a single component.

Chromatography/MS/MS is usually performed in selected reaction monitoring (SRM) mode where a single or a few specific precursor/product combinations are monitored with the exclusion of the rest of the data set in a targeted analysis [2]. This method requires previous knowledge of the sample. If the pure compound is available, it can be characterized by MS/MS to find a unique fragmentation pathway for that compound which will allow its identification when analyzed in its matrix. Using SRM, entire chromatographic runs are dedicated to the detection of a single or a few compounds, while ability to monitor any other compound in the matrix is sacrificed. Despite these limitations and laborious method development requirements, the high degree of selectivity and sensitivity of MS/MS has proven itself extremely useful in many areas of research for both GC and LC applications.

1.3.4 Evolving chromatographic methods

Related to the spectral generation rate requirements associated with current MS and MS/MS instrumentation are the characteristics of the sample from the GC column. Specifically, the improvements in GC as a result of the development of capillary columns in the early 1980's dramatically affected the requirements of the mass spectrometer. Peak widths were reduced from around twenty seconds to a few seconds, and the amount of material introduced into the mass spectrometer was reduced to picograms. The performance of scanning mass spectrometers barely meets the challenge.

1.4 Overview of the tandem TOF instrument

Figure 1.1 is a diagram of the tandem TOF mass spectrometer developed in Professor Enke's laboratory. The electron-impact source ionizes gaseous sample introduced from a GC oven (not pictured) either continuously by direct-leak from a sample vial or by injection and chromatography. Outside of the oven, a heated transfer line (not pictured) serves to heat the column through which the sample stream enters the instrument. The spectral acquisition sequence begins with a function generator which generates a square wave. This signal simultaneously triggers the source pulsing circuit and a delay generator. In response to the trigger signal from the function generator, a 200 V pulse is applied to the back-plate of the

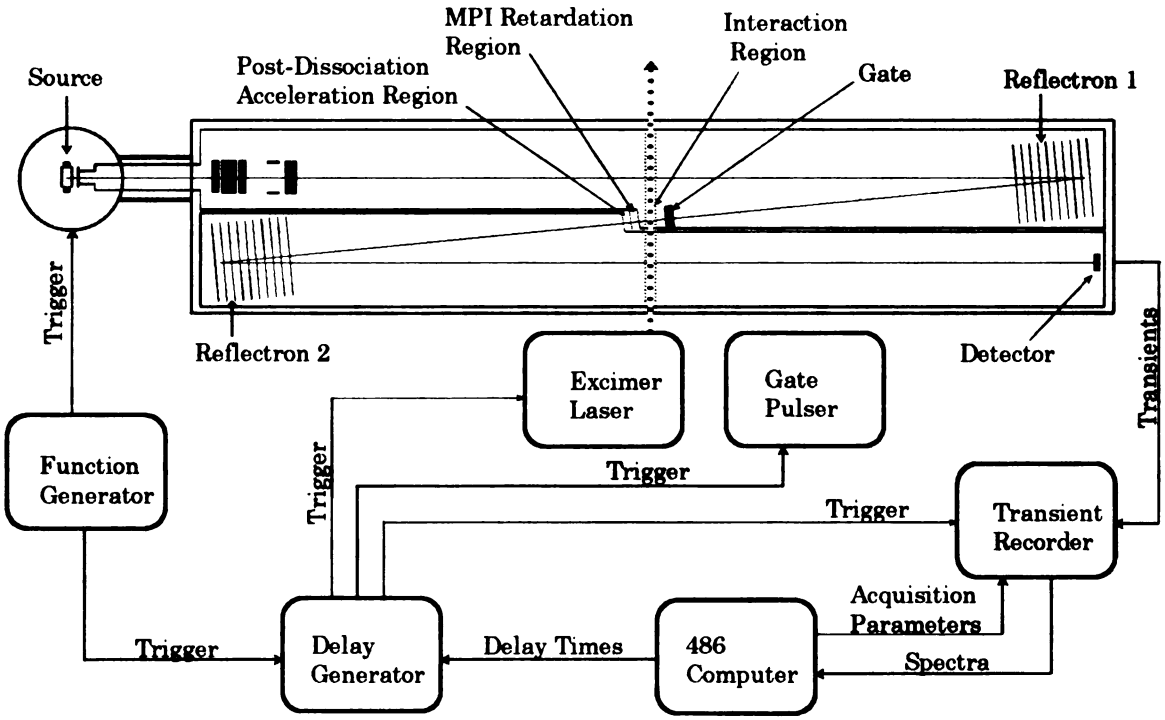

Figure 1.1 Schematic diagram of the tandem TOF mass spectrometer with instrument control and data collection system.

source, causing extraction of the ions into a secondary, static acceleration region of 550 V. The resulting ion beam is collimated with an einzel lens and steered with two sets of orthogonally oriented steering plates. The ion beam is then reflected by reflectron one and directed towards the interaction region. Iso-mass ion packets separate from one another through the first mass analyzer and are energy-focused by the reflectron at the position of the interaction region. The instrument chamber and vacuum system, sample introduction system, ion source, first mass analyzer, electronics, detectors, and instrument control and data collection systems are discussed in more detail in chapter 2.

Just prior to arrival at the interaction region, a gate device is used to isolate a single, chosen iso-mass ion packet by deflection of all other m/z values onto a path which will not result in collision with the detector. This step is not necessary for precursor selection since selection is determined later by the interaction of a laser pulse with the precursor ion packet. Rather, the gate serves to eliminate background. The firing of the gate is controlled by a delayed pulse from the delay generator, which is programmed from the computer. The gate device and its control electronics are discussed in detail in chapter 4.

The pulsed laser is timed (in a similar fashion) to irradiate the ion packet as it passes through the interaction region. Focusing of the laser pulse and the precursor iso-mass ion packet to a small volume results in high

efficiency fragmentation of the precursor ions. Pulsed-laser selection and the resultant photodissociation efficiencies are the subject of chapter 3.

After interaction with the laser pulse, the resulting product ions and unfragmented precursor ions enter the second mass analyzer. Besides the ion packet itself, a considerable population of neutral background gas exists in the interaction region. Multi-photon ionization of this background gas results in a large background signal. To prevent these ions from reaching the detector, a 20 to 30 V retardation field is created at the start of the second mass analyzer. This field does not discriminate against the sample ions. Immediately following this retardation field is an acceleration field of 1950 V which causes a separation of the product ions through the subsequent field-free flight. Ion optical elements, such as the ion gate and the grids used to create the retardation and acceleration fields, are placed on an optical rail which has been mounted parallel to the ion flight path in the interaction region. After dissociation and subsequent acceleration, a second reflectron is used to energy-focus and reflect the product ions onto the detector. A detailed description of the reflectron developed for the second mass analyzer is given in chapter 5. The signal as a result of each source pulse is referred to as a transient and is recorded by the transient recorder, where it can be averaged with other transients to improve signal-to-noise ratio. The averaged or single-shot spectra are then transferred to the computer hard drive for storage.

It is not evident in Figure 1.1 that the ion flight path is actually tipped with respect to the plane of the page (or the bottom of the instrument chamber). In other words, the source is higher than the interaction region which is higher than the detector. This arrangement avoids the possibility of the laser light striking ions in locations other than at the interaction region.

1.4.1 TOF provides high spectral generation rate and throughput

The achievement of more MS/MS data without a reduction in sensitivity requires the abandonment of tandem mass filters in favor of a mass array analyzer, at least for the product ion analysis stage. Also, a very high spectral generation rate is desirable. Due to their considerable isolation and analysis periods, FTMS and ion trap mass spectrometry are not suitable. As already discussed, the mass filters (sectors and quadrupoles) are also not suitable, with the possible exception of a sector instrument employing a spatial-array detector. TOF offers the advantage of unrivaled spectral generation rate and unrivaled efficiency when used in conjunction with an ion source that stores a considerable portion of the ions formed between pulsed extractions. Not only is it possible to perform array detection of product ion spectra with a tandem TOF arrangement, but it is possible to collect normal spectra at a similar rate simply by opening the gate and not firing the laser. Product spectrum generation rate is limited only by the repetition rate of the laser. The laser currently used has a maximum

repetition rate of 250 Hz, although other commercially available excimer lasers offer higher rates. A multiple sector MS/MS instrument utilizing a spatial array detector for product ion analysis can collect normal spectra only by scanning the first mass spectrometer.

1.4.2 PID provides high efficiency fragmentation

TOF is a pulsed technique which can produce dense iso-mass ion packets. Pulsed excimer lasers provide high energy pulses of light which can be focused to approximately the volume of the ion packet when the ion beam and light path are arranged orthogonally. As is discussed in chapter 3, this dense ion-photon overlap results in high efficiency fragmentation and high resolution selection of iso-mass precursor ion packets.

1.4.3 Unit resolution for TOF/PID/TOF analysis

Achieving the primary goal of this project is a useful demonstration only if unit mass resolution can be maintained for both stages of analysis over a mass range appropriate to GC analyses. The major portion of my work and of this thesis is devoted to the development of an ion optical arrangement that can meet this criterion despite the traditional reputation of TOF as a low resolution technique. Unit mass resolution has been demonstrated for precursor ion separation (chapter 2), isolation (chapter 4), and selection (chapter 3) as well as for product ion analysis (chapter 5).

1.5 Historical background

Despite the limitations of commercially available tandem mass spectrometers, the development of faster chromatography/MS/MS systems has been the focus of relatively few publications in the scientific literature. These are reviewed in section 1.5.1, below. Numerous tandem TOF instruments have been constructed for a variety of goals, as well as hybrid instruments which incorporate one TOF stage. These instruments are reviewed in section 1.5.2. Finally, since photo-induced dissociation is by no means a routine fragmentation method for MS/MS, relevant history regarding PID will be provided in section 1.5.3.

1.5.1 Instrumentation for high speed MS/MS

In 1983, Stults, *et al.* [29] introduced the concept of time-resolved ion momentum spectrometry (TRIMS). This method couples a magnetic sector with a TOF mass spectrometer. This MS/MS instrument is non-traditional in that the observed dissociation occurs between the source and the magnetic sector. The source is operated in pulsed mode while the magnet is scanned. The m/z value of the product ion and that of the precursor from which it originated is obtained from the known field strength of the magnet and the ion packet's flight time. When later combined with the MSU integrating transient recorder, the true power of this system was demonstrated by collecting a complete MS/MS data set for caffeine in 5 seconds, a spectral

generation rate compatible with packed-column GC [30]. This instrument is fundamentally limited by the scan rate of the magnet. A similar MS/MS method which uses an electric sector in place of the magnetic sector is called time-resolved ion kinetic energy spectroscopy (TRIKES) [29, 31]. This system offers advantages and capabilities similar to those of the TRIMS system.

Another approach to fast MS/MS was the coupling of a quadrupole analyzer with a TOF analyzer by Glish, *et al.* [32]. This instrument demonstrated a throughput advantage over tandem mass filter instruments, but gave poor product spectrum resolution and was limited in speed by its data acquisition system.

1.5.2 Tandem TOF and hybrid instruments

A variety of tandem TOF instruments and hybrid MS/MS instruments containing one TOF stage have been constructed for purposes other than for use as a chromatographic detector. The first use of TOF for analysis of product ions was the reported observation of metastable ions using linear TOF instruments (containing no reflectron) [33-39]. In these instruments, several grids were used to create a short retardation stage near the end of the flight tube which causes a slight time shift for ions which have undergone metastable decay. The product ions retain a fraction of the kinetic energy of the precursor ion equal to the fraction of mass retained by the product ion. Therefore, at a given retardation amplitude, the lower m/z portion of the product ion spectrum will be reflected by the field, while the higher m/z

portion will be transmitted. Slowly increasing the amplitude of the retardation field allowed the determination of the m/z of the product ion. While these demonstrations did not involve discrete, multiple stages of mass analysis, they did demonstrate the collection of product spectra using TOF. The product spectra collected in this manner are, of course, convoluted with the normal spectrum and are poorly resolved.

The next category of TOF instruments which allow the analysis of metastable ions is a modification of a single-stage reflectron TOF mass spectrometer. This category is differentiated from that already discussed by the use of a reflectron rather than a retardation stage to mass disperse product ions. A reflectron consists of an electric field which ions penetrate to a depth (or height if one considers a potential hill) corresponding to their kinetic energies. Ions with smaller kinetic energies penetrate the field less deeply than ions with greater kinetic energy. Reflectrons have primarily been used to compensate for flight time differences of iso-mass ions having a distribution of kinetic energy, as discussed in the instrument overview above. However, reflectrons can also (simultaneously) time disperse product ions on the basis of their fractionated kinetic energies. This method has been used with a variety of reflectron types to analyze metastable decay after multi-photon ionization (MPI) [40], ^{252}Cf fission fragment ionization or plasma desorption mass spectrometry (PDMS) [41-43], fast ion bombardment ionization or secondary ion mass spectrometry (SIMS) [44-45], electron

ionization [46], and, most recently, matrix-assisted laser desorption ionization (MALDI) [47-49]. Boesl, *et al.* [40] dropped the amplitude of the reflectron field slightly, causing undissociated ions to not be reflected, thereby differentiating between metastable and normal ions. In the SIMS and PDMS instruments [41-45], decompositions were identified by the detection of a neutral at a detector placed behind the reflectron, with the arrival time of the neutral 'correlated' to the precursor m/z which decomposed and the product ion which is then detected at the normal detector position. This technique requires a very low ion flux. The more recent instruments [46-49] employ an ion gate to isolate a precursor m/z (and products which have dissociated from that precursor m/z) so that any signal other than the precursor in the resulting spectrum can be attributed to metastable decay. Details regarding reflectrons and their use for product ion analysis are reviewed and discussed in more detail in chapter 5.

Single reflectron TOF analyzers have also been used with a variety of fragmentation techniques, where the dissociation is accomplished within the reflectron. Kaufmann, *et al.* [50] observed product ions caused by collision of precursor ions with a stainless steel mesh electrode near the front of the reflectron in a SIMS instrument. Later, Williams, *et al.* [51] introduced a solid plate near the back of the reflectron to cause SID of ions created by MPI, while Duncan's group [52, 53] employed laser PID at the turn-around

point of the ions in the back of the reflectron in their studies of metal cluster ions.

The true tandem TOF instruments consisting of discrete TOF analyzers can be classified according to whether they employ sequential linear TOF analyzers, one linear TOF and one reflectron TOF analyzer, or two reflectron TOF analyzers. Several linear TOF / linear TOF instruments have been constructed for a variety of purposes which use gate selection of ions prior to fragmentation and an acceleration stage in the second mass analyzer to accomplish mass dispersion of the product ions. Smalley's group [54, 55] and Geusic, *et al.* [56] accomplished photodissociation of cluster ions, Schey, *et al.* [57] performed SID of ions generated by electron ionization, and Jardine, *et al.* [58] demonstrated CID of ions produced by fast atom bombardment (FAB).

Two groups have constructed instruments which use a linear TOF analyzer followed by a reflectron TOF analyzer. Schey, *et al.* [59] describe an improved version of the instrument already mentioned above for SID of ions produced by electron ionization. Schlag's group [60, 61] has described two versions of an instrument which allows PID of ions produced by MPI. The two versions involve two different methods of reflectron focusing which are described in chapter 5.

Finally, the last classification of tandem TOF instruments is those which use two reflectron TOF analyzers. Only two instruments have this

geometry, one of which is the subject of this thesis. The other was constructed by Cornish and Cotter [62-65]. Cornish and Cotter use laser desorption ionization followed by CID via gas introduced to the chamber through a pulsed valve.

In general, the tandem TOF arrangements described above exhibit poor resolution for either precursor separation, product ion resolution, or both. The one exception is the tandem reflectron TOF instrument described by Cornish and Cotter [62-65]. This instrument is not compatible with GC, however, due to its laser desorption ion source.

Several hybrid instruments appear in the literature which use one TOF stage. In addition to those described in section 1.5.1 above, a magnetic sector / TOF instrument has been described by Gandy, *et al.* [66] which uses an electron ionization source and SID as the fragmentation technique. Russell's group [67] has demonstrated PID in a hybrid electric/magnetic sector / linear TOF instrument. More recently, this group substituted a reflectron TOF instrument for the linear TOF [68]. This instrument has been used in the neutral-ion correlation mode for collection of product spectra resulting from metastable decomposition and CID and has demonstrated excellent resolution for both precursor ion selection and product ion analysis.

1.5.3 Photodissociation as a fragmentation technique for MS

Photo-induced dissociation of organic ions is not routinely used as a fragmentation technique primarily due to the relatively low cross-sections

(about 10^{-17} to 10^{-19} cm^2) for the PID process as compared to those for CID (about 10^{-15} to 2×10^{-14} cm^2) [2]. Dunbar [69, 70] is credited with much of the pioneering work in the area of photodissociation of organic ions, performed in ion cyclotron resonance (ICR) mass spectrometers where the trapped ions can be irradiated for up to 3 seconds. A variety of light sources have been used to accomplish PID in ICR cells in the infrared [70-73], visible [74], and ultraviolet [75-77] regions. Unfortunately, due to the background of neutrals in the ICR cells, it is difficult to differentiate between ions that result from PID versus ions that result from ionization of the neutrals or CID of ions with the neutrals. ICR cells were once the only realistic option for PID experiments due to the nature of the light sources available, so that researchers were forced to deal with the problems associated with these experiments.

As light sources improved, photodissociation experiments in beam instruments became possible, reducing the problems associated with neutral background which hampered ICR experiments. Beynon's group [78, 79] first demonstrated ion photodissociation in a sector instrument arranging the ion beam coaxial to the light path, and Wagner-Redeker and Levsen [80] later reported a similar apparatus. McGilvery and Morrison [81] and Krailler and Russell [82, 83] have arranged the laser perpendicularly to the ion beam in quadrupole and sector instruments, respectively. Both groups later implemented a coaxial geometry to improve sensitivity.

Modern pulsed lasers have become an attractive option for PID due to their compatibility with pulsed ion sources [84] in sector instruments and with TOF mass spectrometers. As already mentioned in section 1.5.2, Smalley's group [54, 55] and Geusic, *et al.* [56] accomplished photodissociation of cluster ions in simple linear TOF / linear TOF instruments, while Duncan's group [52, 53] employed laser PID at the turn-around point of the ions in the back of a reflectron TOF instrument in their studies of metal cluster ions. Russell's group [67] has demonstrated PID in a hybrid electric/magnetic sector / linear TOF instrument, and Schlag's group [60, 61] has employed laser PID in a linear TOF / reflectron TOF instrument.

More complete histories of the utility of PID in mass spectrometry are available [12, 84, 85]. To date, the majority of work done with PID can be described as fundamental. Studies such as determining PID cross-section, investigating kinetic energy release upon dissociation, or investigating the effect of laser wavelength and power on photodissociation are among the most common [84]. Chapter 3 describes the implementation of laser PID in this dual reflectron tandem TOF instrument for the primary purpose of providing efficient fragmentation of precursor ions.

1.6 References

1 Yost, R. A.; Enke, C. G. *Amer. Lab.*, **1981**, 88-95.

2 Busch, K. L.; Glish, G. L.; McLuckey, S. A. *Mass Spectrometry / Mass Spectrometry: Techniques and Applications of Tandem Mass Spectrometry*, VCH Publishers, Inc.: New York, 1988.

3 Yost, R. A.; Enke, C. G. *J. Am. Chem. Soc.*, **1978**, *100:7*, 2274.

4 Hunt, D. F.; Shabanowitz, J.; Harvey, T. M.; Coates, M. L. *Anal. Chem.* **1985**, *57*, 525.

5 Glish, G. L.; Shaddock, V. M.; Harmon, K.; Cooks, R. G. *Anal. Chem.*, **1980**, *52*, 165.

6 Watson, J. T. *Introduction to Mass Spectrometry*, Raven Press: New York (1985).

7 Blaisdell, B. E.; Sweeley, C. C. *Anal. Chim. Acta* **1980**, *117*, 1.

8 Abramson, F. P. *Anal. Chem.* **1975**, *47(1)*, 45.

9 Dromey, R. G.; Stefik, M. J.; Rindfleisch, T. C.; Duffield, A. M. *Anal. Chem.* **1976**, *48(9)*, 1368.

10 Blaisdell, B. E.; Sweeley, C. C. *Anal. Chim. Acta* **1980**, *117*, 17.

11 Biller, J. E.; Biemann, K. *Anal. Letters*, **1974**, *7(7)*, 515.

12 McLane, R. D. *Ph. D. Thesis*, Michigan State University, **1993**.

13 McLane, R. D.; Vlasak, P. R.; Enke, C. G.; Yefchak, G. E.; Rodriguez, P. A.; Eddy, C. L.; Mazzone, M. A.; Pinkston, J. D. *Proceedings of the 40th ASMS Conference on Mass Spectrometry and Allied Topics*, Washington, DC, May 31 - June 5, 1992, 1171.

14 McLane, R. D.; Vlasak, P. R.; Enke, C. G.; Yefchak, G. E.; Rodriguez, P. A.; Eddy, C. L.; Mazzone, M. A.; Pinkston, J. D. (*in preparation for submission to Anal. Chem.*)

15 Malinowski, E. R.; McCue, M. *Anal. Chem.* **1977**, *49*, 284.

16 Knorr, F. J.; Futrell, J. H. *Anal. Chem.* **1979**, *51*, 1236.

17 Gale, B. C.; Fulford, J. E.; Thomson, B. A; Ngo, .A.; Tanner, S. D.; Davidson, W. R.; Shushan, B. I. *Adv. Mass Spectrom.* **1986**, *10*, 1467.

18 Trehy, M. L.; Yost, R. A.; Dorsey, J. G. *Anal. Chem.* **1986**, *58*, 14.

19 Nelson, C. C.; Foltz, R. L. *Anal. Chem.* **1992**, *64*, 1578.

20 Zirrolli, J. A.; Murphy, R. C. *J. Am. Soc. Mass Spectrom.* **1993**, *4*, 223.

21 Kelly, P. C.; Horlick , G. *Anal. Chem.* **1973**, *45(3)*, 518.

22 Chesler, S. N.; Cram, S. P. *Anal. Chem.* **1971**, *43*, 1922.

23 Erickson, E. D.; Enke, C. G.; Holland, J. F.; Watson, J. T. *Anal. Chem.* **1990**, *62(10)*, 1079.

24 Tecklenburg, R. E., Jr.; McLane, R. D.; Grix, R.; Sweeley, C. C.; Allison, J.; Watson, J. T.; Holland, J. F.; Enke, C. G.; Gruner, U.; Gotz, H.; Wollnik, H. *Proceedings of the 38th ASMS Conference on Mass Spectrometry and Allied Topics*, Tucson, AZ, June 3-8, 1990.

25 Holland, J. F.; Newcombe, B.; Tecklenburg, R. E., Jr.; Davenport, M.; Allison, J.; Watson, J. T.; Enke, C. G. *Rev. Sci. Instrum.* **1991**, *62(1)*, 69.

26 *Meridian Analytical Systems*, Okemos, MI (recently purchased by *Laboratory Equipment Company (LECO)*, St. Joseph, MI).

27 Tuithof, H. H.; Boerboom, A. J. H.; Meuzelaar, H. L. C. *Int. J. Mass Spectrom. Ion Processes* **1975**, *17*, 299.

28 Louter, G. J.; Boerboom, A. J. H.; Stalmeier, P. F. M.; Tuithof, H.H.; Kistemaker, J. *Int. J. Mass Spectrom. Ion Processes* **1980**, *33*, 335.

29 Stults, J. T.; Enke, C. G.; Holland, J. F. *Anal. Chem.* **1983**, *55*, 1323.

30 Eckenrode, B. A.; Watson, J. T.; Enke, C. G.; Holland, J. F. *Anal. Chem.* **1990**, *62*, 1362.

31 Pinkston, J. D.; Rabb, M.; Watson, J. T.; Allison, J. *Rev. Sci. Instrum.* **1986**, *57(4)*, 583.

32 Glish, G. L.; McLuckey, S. A.; McKown, H. S. *Anal. Instr.* **1987**, *16*, 191.

33 Hunt, W. W., Jr.; Huffman, R. E.; McGee, K. E. *Rev. Sci. Intrum.* **1964**, *35 (1)*, 82.

34 Hunt, W. W., Jr.; Huffman, R. E.; Saari, J.; Wassel, G.; Betts, J. F.; Paufve, E. H.; Wyess, W.; Fluegge, R. A. *Rev. Sci. Intrum.* **1964**, *35 (1)*, 88.

35 Hunt, W. W., Jr.; Huffman, R. E.; McGee, K. E. *J. Chem. Phys.* **1964**, *41 (9)*, 2709.

36 Ferguson, R. E.; McCulloh, K. E.; Rosenstock, H. M. *J. Chem. Phys.* **1965**, *42(1)*, 100.

37 Dugger, D. L.; Kiser, R. W. *J. Chem. Phys.* **1967**, *47(12)*, 5054.

38 Haddon, W. F.; McLafferty, F. W. *Anal. Chem.* **1969**, *41(1)*, 31.

39 Chait, B. T.; Field, F. H. *Int. J. Mass Spectrom. Ion Processes* **1981**, *41*, 17.

40 Boesl, U.; Neusser, H. J.; Weinkauf, R.; Schlag, E. W. *J. Phys. Chem.* **1982**, *86*, 4857.

41 Della Negra, S.; Le Beyec, Y. *Int. J. Mass Spectrom. Ion Processes* **1984**, *61*, 21.

42 Della Negra, S.; Le Beyec, Y. *Anal. Chem.* **1985**, *57*, 2035.

43 Brinklman, G.; Hakansson, P., Kjellberg, J.; Demirev, P.; Sundqvist, B. U. R.; Ens, W. *Int. J. Mass Spectrom. Ion Processes* **1992**, *114*, 183.

44 Standing, K. G; Beavis, R.; Bolbach, G.; Ens, W.; Lafortune, M.; Main, D.; Schueler, B.; Tang, X.; Westmore, J. *Anal. Instrum.* **1987**, *16*, 173.

45 Tang, X.; Beavis, R.; Ens, W.; LaFortune, F.; Schueler, B.; Standing, K. G. *Int. J. Mass Spectrom. Ion Processes* **1988**, *85*, 43.

46 Haberland. H.; Kornmeier, H.; Ludewigt, C.; Risch, A. *Rev. Sci. Intrum.* **1991**, *62(10)*, 2368.

47 Spengler, B.; Kirsch, D.; Kaufmann, R.; Jaeger, E. *Rapid Commun. Mass Spectrom.* **1992**, *6*, 105.

48 Kaufmann, R.; Spengler, B.; Lutzenkirchen, F. *Rapid Commun. Mass Spectrom.* **1993**, *7*, 902.

49 Kaufmann, R.; Kirsch, D.; Spengler, B. *Int. J. Mass Spectrom. Ion Processes* **1994**, *131*, 355.

50 Kaufmann, R.; Kirsch, D.; Rood, H.-A.; Spengler, B. *Rapid Commun. Mass Spectrom.* **1992**, *6*, 98.

51 Williams, E. R.; Fang, L; Zare, R. N. *Int. J. Mass Spectrom. Ion Processes* **1993**, *123*, 233.

52 LaiHing, K.; Cheng, P. Y.; Taylor, T. G.; Willey, K. F.; Peschke, M.; Duncan, M. A. *Anal. Chem.* **1989**, *61*, 1460.

53 Cornett, D. S.; Peschke, M.; LaiHing, K.; Cheng, P. Y.; Willey, K. F.; Ducnan, M. A. *Rev. Sci. Instrum.* **1992**, *63(4)*, 2177.

54 Brucat, P. J.; Zheng, L.-S.; Pettiette, C. L.; Yang, S.; Smalley, R. E. *J. Chem. Phys.* **1986**, *84(6)*, 3078.

55 Liu, Y.; Zhang, Q.-L.; Tittel, F. K.; Curl, R. F.; Smalley, R. E. *J. Chem. Phys.* **1986**, *85(12)*, 7434.

56 Geusic, M. E.; Jarrold, M. F.; McIlrath, T. J.; Freeman, R. R.; Brown, W. L. *J. Chem. Phys.* **1987**, *86(7)*, 3862.

57 Schey, K.; Cooks, R. G.; Grix, R.; Wollnik, H. *Int. J. Mass Spectrom. Ion Processes* **1987**, *77*, 49.

58 Jardine, D. R.; Morgan, J.; Alderdice, D. S.; Derrick, P. J. *Org. Mass Spectrom.* **1992**, *27*, 1077.

59 Schey, K. L.; Cooks, R. G.; Kraft, A.; Grix, R.; Wollnik, H. *Int. J. Mass Spectrom. Ion Processes* **1989**, *94*, 1.

60 Weinkauf, R.; Walter, K.; Weickhardt, C.; Boesl, U.; Schlag, E. W. *Z. Naturforsch.* **1989**, *44a*, 1219.

61 Boesl, U.; Weinkauf, R.; Schlag, E. W. *Int. J. Mass Spectrom. Ion Processes* **1992**, *112*, 121.

62 Cornish, T.; Cotter, R. J. *Rapid Commun. Mass Spectrom.* **1992**, *6*, 242.

63 Cornish, T. J.; Cotter, R. J. *Org. Mass Spectrom.* **1993**, *28*, 1129.

64 Cornish, T. J.; Cotter, R. J. *Anal. Chem.* **1993**, *65*, 1043.

65 Cornish, T. J.; Cotter, R. J. *Rapid Commun. Mass Spectrom.* **1993**, *7*, 1037.

66 Gandy, R. M.; Ampulski, R.; Prusaczyk, J.; Johnsen, R. H. *Int. J. Mass Spectrom. Ion Physics* **1977**, *24*, 363.

67 Tecklenburg, R. E., Jr.; Russell, D. H. *presented at the Pittsburgh Conference*, Atlanta, Georgia, March 1989.

68 Strobel, F. H.; Preston, L. M.; Washburn, K. S.; Russell, D. H. *Anal. Chem.* **1992**, *64*, 754.

69 Dunbar, R. C.; In *Gas Phase Ion Chemistry*, Bowers, M. T., Ed. Academic: New York, 1979, Volume 2.

70 Dunbar, R. C.; In *Gas Phase Ion Chemistry*, Bowers, M. T., Ed. Academic: New York, 1984, Volume 3.

71 Baykut, G.; Watson, C. H.; Weller, R. R.; Eyler, J. R. *J. Am. Chem. Soc.* **1985**, *107*, 8036.

72 Watson, C. H.; Baykut, G.;Battiste, M. A.; Eyler, J. R. *Anal. Chim. Acta* **1985**, *178*, 125.

73 Watson, C. H.; Baykut, G.; Eyler, J. R. *ACS Symp. Ser.* **1987**, 359.

74 Dunbar, R. C. *Anal. Instrum.* **1988**, *17*, 113.

75 Bowers, W. D.; Delbert, S.-S.; McIver, R. L. J. Am. Chem. Soc. 1984, 106, 7288.

76 Hunt, D. F.; Shabanowitz, J.; Yates, J. R. J. Chem. Soc., *Chem. Commun.* **1987**, 548.

77 Dunbar, R. C.; *J. Chem. Phys.* **1989**, *91*, 6080.

78 Kingston, E. E.; Morgan, T. G.; Harris, F. M.; Beynon, J. H. *Int. J. Mass Spectrom. Ion Processes* **1972**, *43*, 261.

79 Griffiths, I. W.; Mukhtar, E. S.; Harris, F. M.; Beynon, J. H. *Int. J. Mass Spectrom. Ion Processes* **1981**, *38*, 333.

80 Wagner-Redeker, W.; Levsen, K. *Org. Mass Spectrom.* **1981**, *16*, 538.

81 McGilvery, D. C.; Morrison, J. D. *Int. J. Mass Spectrom. Ion Physics* **1978**, *28*, 81.

82 Krailler, R. E.; Russell, D. H. *Anal. Chem.* **1985**, *57*, 1211.

83 Krailler, R. E.; Russell, D. H. *Int. J. Mass Spectrom. Ion Processes* **1985**, *66*, 339.

84 Tecklenburg, R. E., Jr.; Russell, D. H. *Mass Spec. Rev.* **1990**, *9*, 405.

85 Beussman, D. J. *Ph. D. Thesis*, Michigan State University, **1995**.

Chapter 2: Instrument design

The tandem reflectron TOF instrument has been developed and continues to develop as a team effort. I am the third student to contribute to this project, following Mary A. Seeterlin [1] and R. David McLane [2]. Mary's contributions involved primarily the design and construction of the vacuum chamber and pumping system, the instrument's electronics, the source, the first mass analyzer, and other ion optical elements. David's contributions involved the selection and installation of the laser, the development of the instrument control system and data collection system, and the development of the gas chromatograph / instrument interface. Although I have maintained, modified, and, in some cases, aided in the design and construction of these aspects of the instrument, included below is just a brief description of these developments. The aspects of instrument development for which I was primarily responsible are described in the following chapters.

Since my involvement, two more students have joined the tandem TOF project. Douglas J. Beussman joined the project shortly before David and Mary finished their degrees, taking over responsibility for laser maintenance and contributing to several aspects of instrument development that are described in the chapters below. Douglas' primary area of interest is the study of the photodissociation process itself, observing the effect of laser

power and wavelength on the efficiency of photodissociation and the specific fragmentation pathways for a variety of precursor ions. Tina Erickson has recently joined the tandem TOF effort on an official basis; however, her interest in the project has led her to assist with experiments for some time. Specifically, she has facilitated the evolution of the instrument control and data collection systems as various components are added and replaced. She plans to continue Douglas' efforts in the study of the photodissociation process.

2.1 Chamber & vacuum system

The instrument chamber is constructed of 0.75 inch stainless steel and has inner dimensions of 60 inches long by 11 inches wide by 9 inches tall. The top of the instrument chamber has three removable access panels to allow easy access to all areas of the instrument. A variety of flanges contain appropriate electrical and mechanical feed-throughs.

The source housing is a 6-way cross mounted on the end of the instrument chamber. A viewport is attached to the top of the source housing. Two turbomolecular pumps (Pfeiffer, Hudson, NH) are used to evacuate the chamber. One, a TPH 270, is mounted directly underneath the source while the second, a TPH 510, is mounted on the underside of the chamber itself, accomplishing differential pumping of the source chamber and main chamber. These pumps are backed by two D16A rotary-vane rough pumps

(Leybold Vacuum Products, Export, PA). The pressures achieved are measured with two ionization gauges mounted on the instrument, one on the source housing and the other on the chamber itself. The normal working pressure of the instrument is between 3 and 6 $\times$ 10^{-7} torr for the main chamber. The pressure in the source chamber varies widely depending on the rate of sample introduction. Without any sample flow, the pressure is typically between 5 $\times$ 10^{-8} and 1 $\times$ 10^{-7} torr. The design and construction of the vacuum chamber is described in more detail elsewhere [1].

2.2 Electronics

The electronics which supply power for various instrument components were designed and constructed in-house by Mary Seeterlin and Martin Rabb. High voltage supplies provide DC voltages for the instrument's ion optical elements. Most of these voltages are achieved through the use of a course and fine adjust on the front panel. The course consists of a switch which allows a choice of 5 ranges. The fine consists of a high performance potentiometer which allows adjustment of the voltage within 2 volts of the desired value. Most of the electrode voltages are achieved by the voltage dividers between three power supplies, one of which is a positive supply, usually adjusted to about 350 V. The others correspond to the 'field-free' voltages of the first and second mass analyzers (generally -550 and -2500 V. Other instrument components which require voltages more negative than the

second field-free, such as the einzel lens, or cause a significant load, such as the detectors, incorporate additional supplies.

A 200 V pulse is applied at a fixed frequency to the source back plate and represents the only dynamic voltage with the exception of the gate circuitry which are described in more detail in chapter 4. The source pulse is of adjustable width and amplitude, and the source pulser itself is mounted in a box directly behind the source housing. In addition to the high voltage supplies and the source pulsing circuitry, a low voltage, high current supply provides power for the source filaments.

2.3 Sample introduction

Gaseous samples are introduced into the mass spectrometer by use of a gas chromatograph (model 5890, Hewlett-Packard, Palo Alto, CA), which is interfaced to the source of the tandem TOF by a heated transfer line (Finnigan, San Jose, CA) mounted orthogonal to the source housing. A column is placed into the transfer line with the end of the column just inside the source region. The gaseous molecules are allowed to spray into the source region, where electron impact ionization occurs. Inside the GC oven, the column can either be attached to the heated GC injection port or to a glass sample vial. The first mode allows controlled injections of sample followed by gas chromatographic separation. When the column is attached to the vial, a continuous flow of sample is introduced into the mass spectrometer,

generally without carrier gas, on the basis of pressure differential between the vacuum chamber and the (heated) vial. This is useful when a sample is required to be present for long periods of time, such as for instrument tuning and studies on the laser PID spectroscopy of ions.

2.4 Source

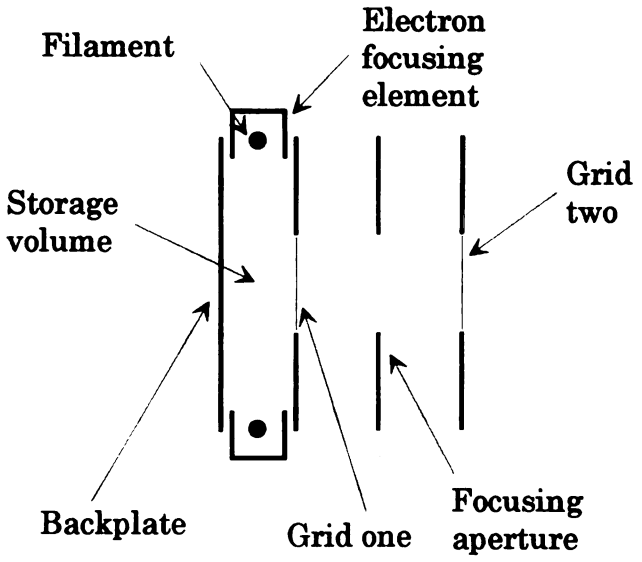

Figure 2.1 The electron ionization storage source.

The ion source currently used in the TOF/TOF instrument is based on a design introduced by Grix, *et al.* [3] and is illustrated in Figure 2.1. Two opposing, electron-emitting, 0.018 cm diameter, rhenium filaments are connected in series and positioned within electron focusing elements. The

electron focusing elements are held at a negative voltage with respect to the body of the source and the filament, while the filament is held at about 70 V more negative than the body of the source in order to direct the electrons between the back-plate and grid one of the source with about 70 eV energy. Sample is continuously introduced into the source where it is ionized in the electron beam. Periodically, the back plate of the source is pulsed to approximately 200 V, causing ions to be accelerated out of the source into an acceleration field formed by grid one and grid two.

Essential to the achievement of high sensitivity is the ability of the source to accumulate a significant fraction of the ions that are produced between the extraction pulses. It is believed, as Studier postulated in 1963 [4], that ion loss is limited by the creation of a potential well between the back-plate and grid one as a result of the negative space charge of the dense, well-focused electron beam. The efficiency of ion storage has been demonstrated and measured experimentally [1, 5]. At an extraction rate of 500 Hz, the maximum rate for the Questek excimer laser, storage is about 25% efficient. In addition to the sensitivity improvement by ion accumulation, the ion bunching caused by simultaneous extraction and focusing results in a great improvement in signal-to-noise ratio. All ions of a particular m/z value that are accumulated in the source between extractions arrive at the detector within a few tens of nanoseconds. The peak detector current is therefore several orders of magnitude greater than the average ion

current. The development, design, and construction of the source is described in more detail elsewhere [1].

Source tuning is accomplished by iterative, empirical adjustment of the voltages applied to each electron repeller, the source back plate (between extractions), the first grid, the focusing aperture between the first and second grid, and the bias voltage of the filament while monitoring peak intensity and peak width. The voltage of the second grid is set at the first field-free voltage and is not adjusted. The filament current is generally held at about 3.0 A.

2.5 First mass analyzer

About 21 cm beyond the source, an einzel lens is employed to collimate the ion beam produced in the source. The voltage on the einzel lens is adjusted empirically based on ion signal intensity. In addition, a set of orthogonally oriented pairs of steering plates just beyond the einzel lens are used for minor steering of the ion beam into the first reflectron, also empirically tuned to achieve maximum ion signal at a detector placed at the focal point of the reflectron. The potential of the first mass analyzer is held at -550 V. To accomplish this, shields were constructed from stainless steel mesh. These are isolated physically (and electrically) from the inner surfaces of the source chamber using ceramic spacers.

A nearly linear acceleration field is established during the source extraction pulse. The potential drop from the center of the source to the field-free region is 650 V. Due to the spatial distribution of ions in the source, a kinetic energy distribution is created since ions at the back of the source receive more energy (and therefore higher velocity) than ions of the same mass near the front of the source. At some point in the flight tube, a minimal flight time distribution is created at a position called the space-focus plane where ions originating near the back of the source overtake ions created near the front. In addition to the spatial distribution in the source, there is an energy distribution which degrades resolution in linear TOF. Wiley and McLaren demonstrated resolution improvements in linear TOF by using an adjustable two-stage acceleration to space-focus ions at the detector [6].

Mamyrin, *et al.* [7] demonstrated a method of improving resolution using a reflectron. In this approach, ions are accelerated using a steep extraction field, resulting in a space-focus plane near the source. As iso-mass ion packets travel toward the reflectron, the ions with more energy and higher velocity lead those of lower energy. The reflectron employed by Mamyrin consisted of a retarding field and a reflecting field formed by two grids and a back-plate. Ions of higher energy penetrate the reflecting field to a greater depth than iso-mass ions of lower energy and spend more time in the reflectron. Upon reflection, higher energy ions are again 'behind' lower energy ions. Eventually an image of the distribution at the space-focus plane

is created at the detector. The reflectron allows an extended effective flight length, providing more time for iso-mass ion packets to become separate from one another without a corresponding spread in the iso-mass ion packet width as observed in linear TOF.

Wollnik, *et al.* [8] further improved upon the reflectron TOF instrument by using grid-free reflectrons. These devices do not suffer from ion transmission losses due to collisions with the grid material or loss of resolution associated with the field perturbations in the vicinity of the wire mesh [9]; and they also serve to focus the ion packets radially. The first stage of mass analysis in the tandem TOF instrument was designed and constructed using a combination of the above technologies. Upon placing a detector at the interaction region of the TOF/TOF, a mass resolution of 1500 (FWHM) is routinely observed [1]. This effective bunching of ions at the interaction region is essential to achieving maximum efficiency in the tandem TOF mass spectrometer.

The first reflectron consists of 9 stainless steel electrodes and a stainless steel back-plate. Each electrode is a 0.051 cm thick stainless steel ring with an outer diameter of 10.2 cm and an inner diameter of 6.35 cm. The electrodes are separated from each other by 1.05 cm ceramic spacers for a total reflectron length of 10.5 cm. Potentials are supplied to four of the nine electrodes, with 5 MΩ resistors linking the others in series. The reflectron is attached to the instrument chamber by three posts, two of which are

connected to external motion feedthroughs (MDC Vacuum Products, Hayward, CA) which allow the direction of the axis of the reflectron to be adjusted. Tuning is accomplished by an empirical, iterative process.

2.6 Instrument control and data collection system

The timing sequence of the experiment is started by a square wave pulse from a function generator (Datapulse, Culver City, CA). This wave simultaneously triggers the pulser for the source back-plate, a delay generator (model 4222, LeCroy, Chestnut Ridge, NY), and a digital storage oscilloscope (model 9450, LeCroy, Chestnut Ridge, NY). The four-channel delay generator is controlled through a General Purpose Interface Bus (GPIB) connection (National Instruments, Austin TX) by a 486/33 computer (Zenith, St. Joseph, MI) running LabWindows® (National Instruments, Austin, TX). A LabWindows® instrument control program was written [2], which allows the delay on each channel to be independently set in 1 ns increments. The delay generator provides a 5 V pulse with a rise time of less than 1 ns and pulse width of 100 ns to both the gate pulsers and the external trigger of the excimer laser. The gate pulser delay is set such that the ion packet or range of ion packets desired is allowed to pass, while others are deflected. The laser discharge pulse is timed such that the photons arrive at the interaction point at the same time as the ion packet of interest. The detector anode is connected to the input of the digital storage oscilloscope

through a terminated 50 Ω BNC cable, allowing signal transients to be captured, averaged, and stored. A GPIB connection between the oscilloscope and the computer allows the resulting averaged spectrum to be captured and stored to disk, using the LabWindows® control program. More detail on the gate pulser control system is provided in chapter 4 below, while the instrument control and data collection systems in general are described in more detail elsewhere [2].

2.7 Detectors

Detection of the ions at the end of the second mass-analyzer is achieved through the use of a dual microchannel, chevron-type detector (modified model TOF-2003, Galileo, Sturbridge, MA). Two 40 mm diameter microchannel plates (MCPs) are used to provide a gain of approximately 10^7. A conical anode is contained in a shield, tapering to a BNC vacuum feedthrough such that the entire anode and following cable are matched at 50 Ω.

A second, removable detector with 25 mm microchannel plates has been constructed and mounted on a sliding carrier such that it can be placed anywhere along the optical rail beyond the interaction region. This allows detection and verification of ions after the interaction region components, ion focusing at the interaction region, and crude spectra to be collected just beyond the interaction region in order to test the photodissociation process.

This simple detector does not have an impedance-matched anode, and significant 'ringing' is observed after the individual mass peaks.

2.8 References

1 Seeterlin, M. A. *Ph. D. Thesis*, Michigan State University, **1993**.

2 McLane, R. D. *Ph. D. Thesis*, Michigan State University, **1993**.

3 Grix R.; Gruner, U.; Li, G.; Stroh, H.; Wollnik, H. *Int. J Mass Spectrom. Ion Processes* **1989**, *93*, 323.

4 Studier, M. H. *Rev. Sci. Instrum.*, **1963**, *34(12)*, 1367.

5 Yefchak, G. E.; Puzycki, M. A.; Allison, J.; Enke, C. G.; Grix, R.; Holland, J. F.; Li, G.; Wang, Y.; Wollnik, H. *Proceedings of the 38th ASMS Conference on Mass Spectrometry and Allied Topics,* Tuscon, Arizona, June 3-8, 1990, 540.

6 Wiley, W. C.; McLaren, I. H. *Rev. Sci. Instrum.* **1955**, *26(12)*, 1150.

7 Mamyrin, B. A.; Karataev, V. I.; Shmikk, D. V.; Zagulin, V. A. *Sov. Phys.-JETP* **1973**, *37(1)*, 45.

8 Wollnik, H.; Przewloka, M. *Int. J Mass Spectrom. Ion Processes* **1990**, *96*, 267.

9 Bergmann, T.; Martin, T. P.; Schaber, H. *Rev. Sci. Instrum.* **1989**, *60(3)*, 347.

Chapter 3: Precursor selection and fragmentation

3.1 Photo-induced dissociation as a fragmentation method

As described in chapter 1, photo-induced dissociation is not routinely used as a fragmentation method for tandem mass spectrometry. However, PID is uniquely suited to the fragmentation needs of our tandem time-of-flight mass spectrometer for several reasons. With this instrument, iso-mass ion packets are focused to temporal and spatial dimensions that are very similar to those of our focused laser pulse. The resulting high degree of spatial and temporal overlap provides optimal PID efficiency despite the relatively low cross-sections for the PID process. Simultaneously, PID yields high resolution selection of the precursor ion packet of interest. As opposed to collision-induced dissociation (CID) and surface-induced dissociation (SID), the product ions formed by PID do not have the associated additional kinetic energy distribution acquired from a collisional process. The amount of energy introduced to precursor ions is precisely known when PID is used, while CID and SID are characterized by broad distributions of deposited energy [1]. In addition, there is no gas load introduced to the mass spectrometer by the PID process as there is when CID is used.

Photo-induced dissociation has been widely observed, predominantly in conjunction with photon ionization, but also as a process separate from the ionization event. A brief history of the use of PID in mass spectrometry is given in chapter 1. The wide-spread adoption of PID as a fragmentation technique in the future will depend greatly on the type of instrumentation which is in routine use. Since the scanning mass spectrometers prevalent today do not generally operate in pulsed mode, they cannot exhibit the performance advantage with the pulsed laser PID that is described below for the tandem TOF instrument. While the trapping instruments may be configured to facilitate high efficiency PID by pulsed laser, they are not capable of mass spectral acquisition rates comparable to the repetition rates of modern excimer lasers (500 Hz or more). To date, the only system which accomplishes this level of efficiency for photo-fragmentation while collecting product spectra at a rate compatible with the GC time scale is the tandem TOF instrument presented here.

3.2 The laser, optics, and light tube

The laser used for the studies described in this thesis is a Questek (Lambda-Physik, Acton, MA) 2580vβ excimer. This laser is capable of producing radiation of several wavelengths depending on the gas mixture used. All photodissociation data presented in this thesis were collected using the ArF line at 193 nm (6.4 eV per photon). Operating at 20 Hz, this laser

produces approximately 150 mJ per pulse. The pulse width of the laser is approximately 17 ns.

A cylindrical plano-convex fused silica (Dynasil 1100) lens (Newport, Irvine, CA) of 300 mm focal length is used to focus the laser beam to an area approximately 2 cm high by 1 mm wide at the interaction region inside the mass spectrometer. Two fused silica interferometer flats (Newport, Irvine, CA) are positioned on flanges mounted to the outside of the mass spectrometer in order to allow photons to pass into the instrument and exit the other side where they are collected in a beam dump device.

Since the laser beam is of sufficient power to ablate metal, holes have been cut in the shield material to create an unimpeded path for the laser beam. To prevent field leakage through these holes, a tube has been constructed and placed through the holes such that the focused laser beam can pass through the tube without interacting with the shields or any other metal component inside the instrument. This tube is held at the potential of the first field-free region (–550 V). Since the 'light tube' spans both field-free regions, a second, shorter tube is slid over the first tube which spans the width of the second field-free region. This tube is held at the same voltage as the second field-free region shield (–2500 V). The two tubes are electrically isolated from each other by a thin sheet of Kapton® (E.I. du Pont de Nemours, Wilmington, DE). Two 22 mm high by 34 mm wide holes have been cut out of opposite sides of the light tube where it intersects the ion flight

path. Ions traveling from the ion source to reflectron 1 pass over the light tube, ions traveling from reflectron 1 to reflectron 2 pass through the light tube, and ions traveling from reflectron 2 to the detector pass under the light tube.

3.3 Ion/photon overlap

For precursor ion selection we rely on the laser pulse interacting with exactly one precursor m/z value. Two factors affect our ability to accomplish unit resolution for selection over the m/z range of interest. The first is the precision and accuracy with which we are able to time the laser pulse with respect to the ion packet. The instrument control system which accomplishes the precision timing of the laser pulse is briefly described in chapter 2 and is described in detail elsewhere [2]. Laser delay time can be controlled in 1 ns increments, and the jitter in the laser thyratron discharge is less than 2 ns. The second factor is the relative dimensions of the ion packet and the laser pulse and their overlap over the period of the laser pulse in the interaction region.

3.3.1 Calculated overlap

In order to predict the resolution for precursor selection that is possible with our system, a calculation of the interaction of the laser pulse and the ion packet is required. The laser pulse is focused to a width of approximately 1 mm at the interaction region. It is about 17 ns in duration. The mass

resolution of the ions at the interaction region is about 1500 ($t/2\Delta t$ definition, full width at half maximum). The kinetic energy of the ion beam is approximately 650 eV. The effective flight distance of the first mass analyzer is 2.4 m. Given these values, one can easily determine that any iso-mass ion packet (regardless of its m/z value) is about 0.8 mm in length (FWHM) at the interaction region. Next, one needs to consider two things: first, adjacent m/z values are closer together in space (and time) as the m/z value increases; and, second, the ion packet moves a significant distance during the 17 ns laser pulse. Lower m/z value ions travel farther during the 17 ns laser pulse than higher m/z value ions. The limit of unit resolution for selection occurs when the separation between adjacent ions (measured from peak center to peak center) is equal to one half the sum of the laser pulse width at the interaction region, the iso-mass ion packet width, and the distance the iso-mass ion packet moves during the laser pulse. Using this formula, one can determine that the upper m/z limit for unit resolution of selection (FWHM) occurs at around m/z 1200. For GC applications, this mass range is more than adequate. Focusing the laser beam to less than 1 mm in width or improving precursor separation would allow greater resolution for precursor selection.

Figure 3.1a illustrates the interaction of a laser pulse with a m/z 157 ion packet. If the laser pulse is timed such that the photons at the midpoint

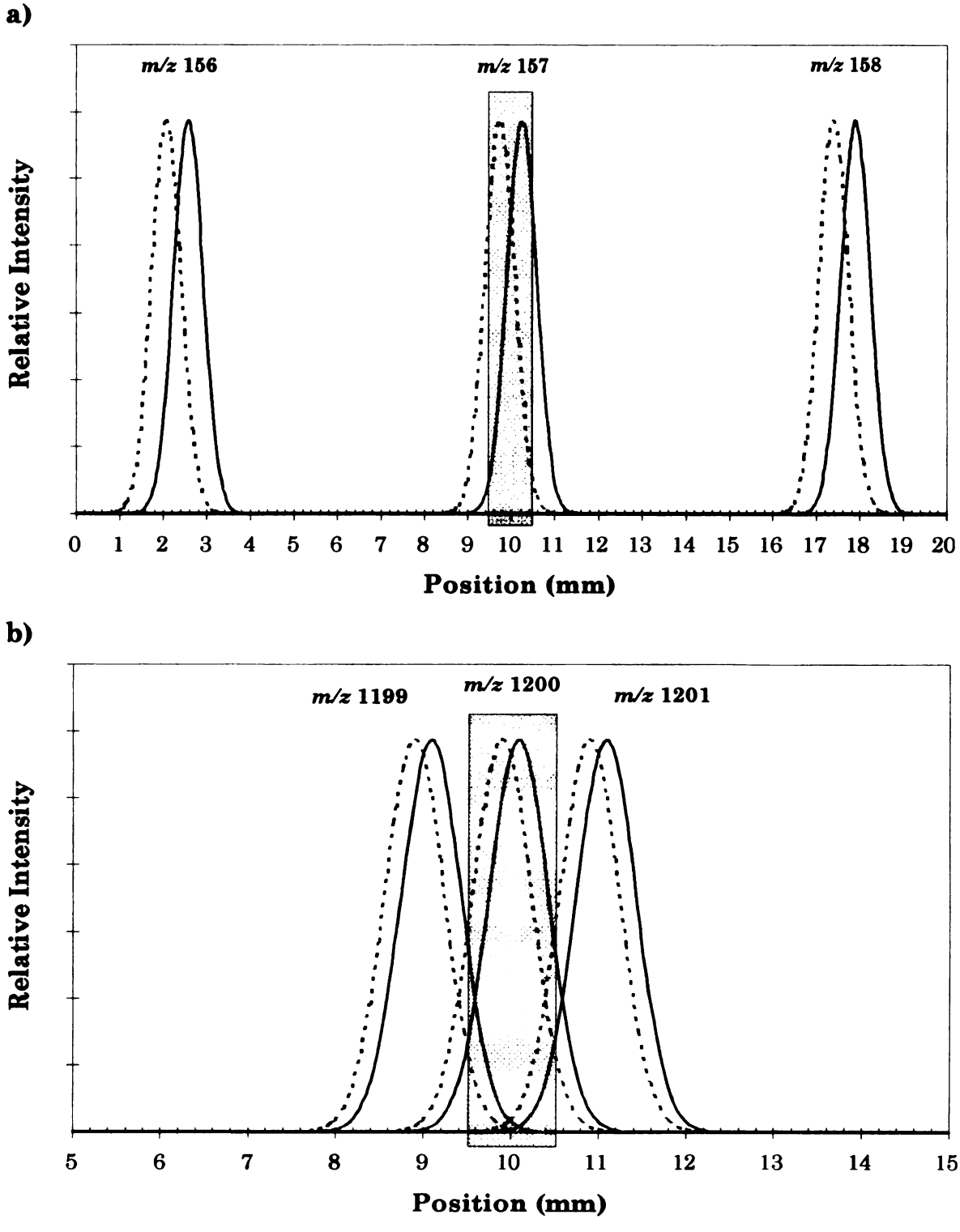

Figure 3.1 Selection of precursor iso-mass ion packet by laser light at **a)** m/z 157, and **b)** m/z 1200. (note different scales).

of the laser pulse reach the interaction region at the same time as the midpoint of the ion packet, approximately 97% of the selected ion packet is overlapped by some portion of the laser pulse, with no overlap or interference of neighboring m/z ion packets. The laser pulse is indicated by the shaded rectangle. The solid line indicates the position of the ion packet at the beginning of the laser pulse, while the dotted line indicates the position of the ion packet at the end of the laser pulse (17 ns later). At m/z 1200, as depicted in Figure 3.1b, 92% of the precursor ion packet is overlapped by some portion of the laser light. However, 11% of each of the adjacent m/z values is overlapped by some portion of the laser light as well. (Note that peak width was measured at half maximum rather than at baseline in the above calculation.) This model assumes Gaussian ion peak shapes and makes no compensation for the varying intensity of the laser light across its width or from the front of the laser pulse to the back. Since the excimer laser pulse is expected to have 'hot spots' in the beam cross-section and to have a maximum intensity in the temporal center of the pulse, these assumptions are not strictly valid. The assumptions made about the laser pulse characteristics will tend to result in a conservative estimate for the limit of unit resolution for precursor ion selection.

3.3.2 Observed overlap

Figure 3.2A is a spectrum of the molecular ion region of bromobenzene. Ions in this spectrum have traveled through the entire instrument to the normal detector position. With the laser on and the delay time between source extraction and laser firing set such that the laser pulse arrives at the interaction region at the same time as the precursor ions, interaction between the ions and photons occurs. Figures 3.2B-3.2D are the spectra obtained when the laser delay times are set at 86.40 μs, 86.70 μs and 86.97 μs to coincide with the ion packet arrival times for m/z values 156, 157 and 158, successively. The depletions associated with each of these times, being limited to the selected ion, demonstrate the effectiveness of precursor selection by laser timing adjustment. Calibration of delay times is easily accomplished due to the linear dependence of flight time on the square root of m/z. The ion arrival time jitter and laser thyratron discharge jitter were both measured to be less than 2 ns. Once the instrument is calibrated, selection of a new precursor ion simply involves changing the laser delay time to the calculated value for the desired precursor m/z value. In addition, the day to day arrival time drift is less than 100 ns. Recalibration requires only 3-4 attempted laser delays. The bromobenzene example demonstrates that we are able to select only one precursor m/z value with the laser, as is expected

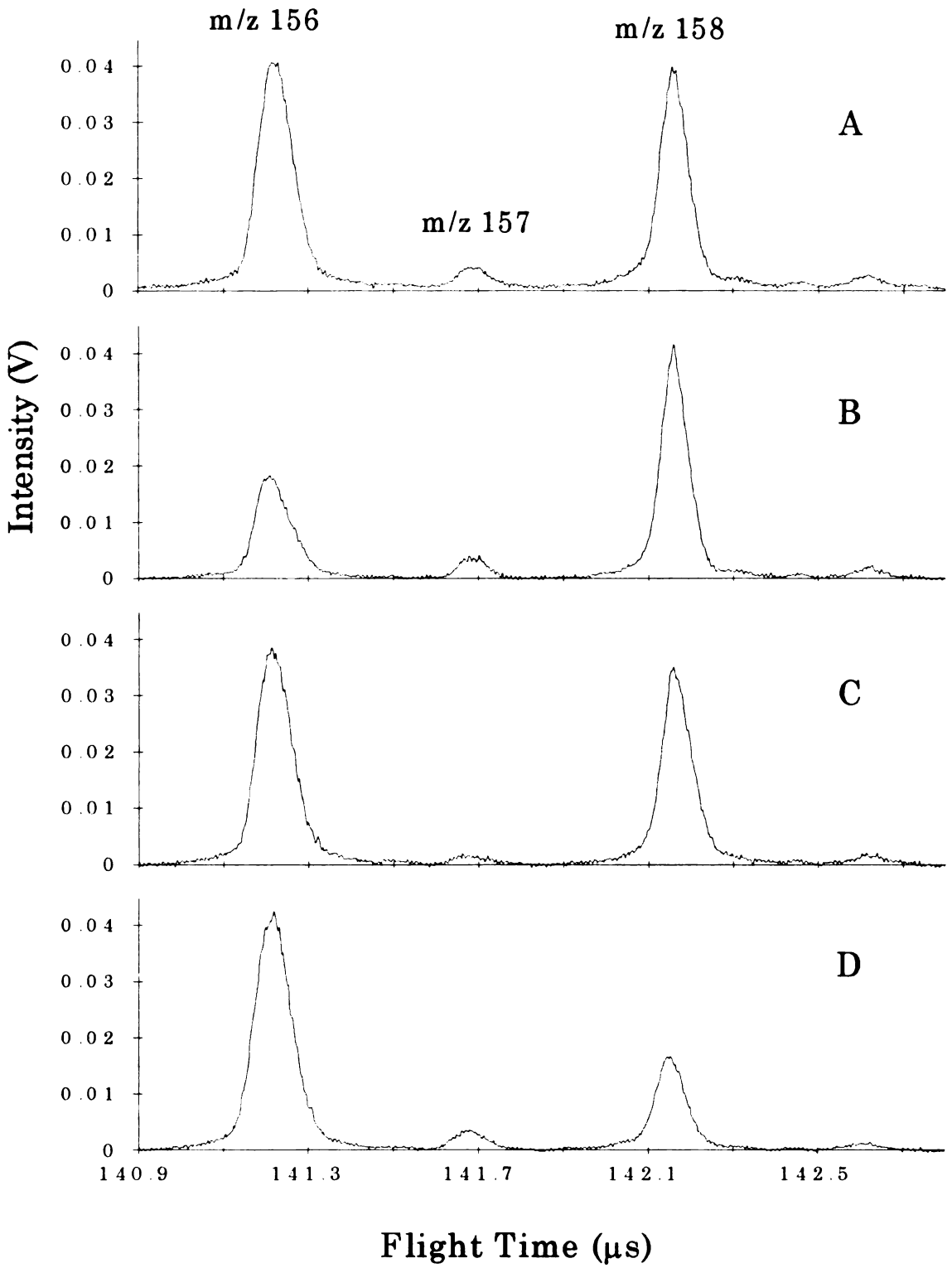

Figure 3.2 Precursor selection by pulsed-laser photodissociation.

based on the calculations outlined above. Precursor ion areas have been depleted by 55.2%, 56.3%, and 51.8% for *m/z* 156, 157, and 158, respectively.

3.4 Photo-fragmentation efficiency

Besides providing high resolution of selection, focusing the laser pulse and iso-mass ion packet to a small volume results in high photodissociation efficiencies. The photodissociation efficiency can be expressed by $\phi\sigma$, where ϕ is the photon density and σ is the photodissociation cross-section. When the excimer laser, operating with ArF (193 nm), provides 150 mJ of energy per pulse focused to a 2 cm by 1 mm area, the photon density is 7.3×10^{18} photons/cm^2. Given that PID cross-sections for small organic ions are on the order of 10^{-17} to 10^{-19} cm^2 [1, 3], photodissociation efficiencies near 100% are expected for some ions in this instrument.

The efficiency of the PID process is determined by the efficiency of fragmentation and the efficiency of collection of the ions. We can let P and P_0 represent the precursor ion current with and without laser excitation, respectively, and ΣF_i the total current of all fragment ions. The fragmentation efficiency is $E_F = \Sigma F_i / (P + \Sigma F_i)$, the collection efficiency is $E_C = (P + \Sigma F_i) / P_0$, and the overall PID efficiency is the product $E_{PID} = E_F \times E_C$ [4]. To perform these efficiency studies, a detector was placed approximately 20 cm beyond the interaction region, with the acceleration

region in place as described in chapter 1. This arrangement allows us to study the PID process independent of the effects of the second reflectron.

Using this configuration, the product spectrum for the molecular ion (m/z = 156) of bromobenzene was collected (Figure 3.3). The precursor ions have been separated by their m/z-dependent velocities and focused at the detector. This product spectrum was obtained by subtracting the laser off spectrum from the laser on spectrum. Ion peaks at t = 93.60 μs, 93.39 μs, 92.95 μs, 92.50 μs and 91.50 μs correspond to products ions with 6, 4, 3, 2, and 1 carbon atoms, respectively. The calculated fragmentation efficiency, collection efficiency and overall PID efficiency are 56%, 116%, and 65%, respectively. The fragments observed in this product spectrum are similar to those observed in a normal 70 eV electron impact mass spectrum. Compared to the EI spectrum, the relative intensities of the lower m/z fragment ions are enhanced in this PID product spectrum.

Product spectra for precursor ions from bromobenzene, toluene, nitrobenzene, acetophenone, triethylamine, N,N-diethylformamide, N-methylacetamide, glycine anhydride, and cyclohexene were collected. The compounds and precursor ions chosen demonstrate photo-fragmentation of odd-electron, even-electron, aromatic and non-aromatic species. Efficiencies are given in Table 1. In most of these studies, reflectron one was tuned to energy-focus at the detector rather than at the interaction region to improve

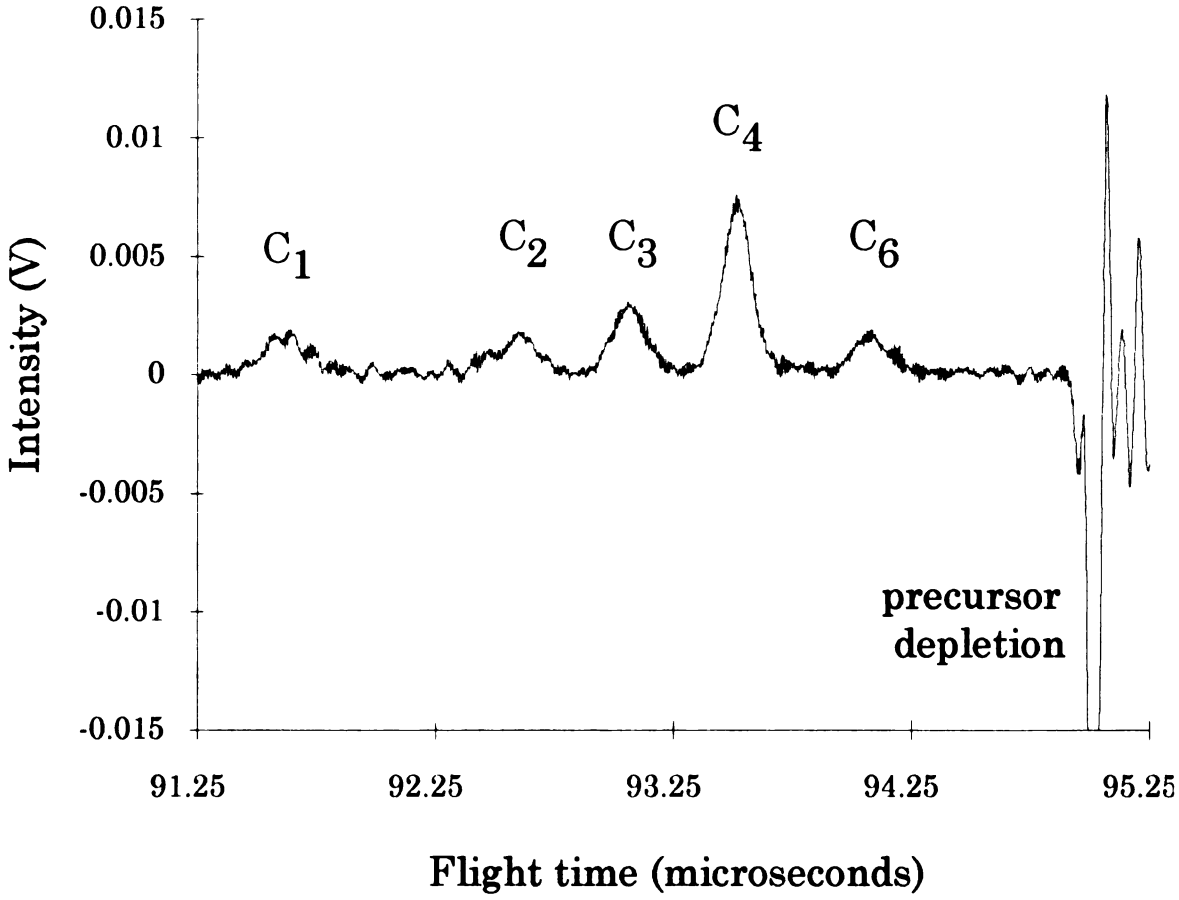

Figure 3.3 Product spectrum for *m/z* 156 (molecular ion) of bromobenzene.

Table 3.1 PID efficiencies for a variety of precursor ions

Compound	Precursor Ion *m/z*	Laser Pulse Energy (mJ)	Fragmentation Efficiency (%)	Collection Efficiency (%)	PID Efficiency (%)
bromobenzene	156	150	56	116	65
	77	160	30	93	28
	156*	130	79	132	104
	77*	130	44	113	50
toluene	91	110	39	103	40
nitrobenzene	123	140	66	137	91
acetophenone	105	140	54	107	58
triethylamine	86	110	27	119	32
N,N-diethyl-formamide	86	100	24	99	24
N-methyl-acetamide	73	120	29	94	27
glycine anhydride	114	100	28	100†	28
cyclohexene	67	140	12	91	11

*Precursor ions were focused at the interaction region instead of at the detector.
†A collection efficiency of 100% was assumed.

product ion resolution. This results in reduced PID efficiencies. When reflectron 2 is used in the final instrument configuration to focus the product ions, the optimal focus will be achieved at both the interaction region and at the detector. To determine the effect of improved focusing on PID efficiency, two precursor ions (indicated by asterisks in Table 1) were studied with the focus at the interaction region. As hypothesized, PID efficiencies were increased. Collection efficiencies of greater than 100% were sometimes observed. This is believed to be the result of greater detector gain for ions with higher velocity (lower m/z) [5].

The overall PID efficiencies of between 11% and 100% are comparable to the high efficiencies achievable in the CID process in a triple quadrupole instrument (65% for n-hexane) [4]. These results give evidence that PID can be an analytically useful fragmentation technique when implemented in a system with high ion/photon overlap.

3.5 References

1 Busch, K. L.; Glish, G. L.; McLuckey, S. A. *Mass Spectrometry / Mass Spectrometry: Techniques and Applications of Tandem Mass Spectrometry*, VCH Publishers, Inc.: New York, 1988.

2 McLane, R. D. *Ph. D. Thesis*, Michigan State University, **1993**.

3 Dunbar, R. C.; In *Gas Phase Ion Chemistry*, Bowers, M. T., Ed. Academic: New York, 1979, Volume 2.

4 Yost, R. A.; Enke, C. G.; McGilvery, D. C.; Smith, D.; Morrison, J. D. *Int. J. Mass Spectrom. Ion Physics* **1979**, *30*, 127-136.

5 Meier, R.; Eberhardt, P. *Int. J. Mass Spectrom. Ion Processes* **1993**, *123*, 19-27.

Chapter 4: Precursor isolation

4.1 Elimination of interference

As demonstrated in chapter 3, when pulsed-laser photodissociation (PID) is used as the fragmentation method, it is possible to interact the laser pulse with a single m/z value ion packet, thereby accomplishing selection of the precursor ion packet from an ion beam in TOF mass spectrometry [1]. However, the resulting product spectrum may overlap the portion of the normal ion spectrum having lower m/z values than the laser-selected precursor as well as (potentially) product ion spectra due to metastable decomposition of other m/z values [2, 3]. Figure 4.1a is a convoluted spectrum of toluene containing the normal spectrum of toluene and the product spectrum of m/z 91 of toluene. This interference can be effectively eliminated by subtracting a 'laser off' spectrum from a 'laser on' spectrum. Such a difference spectrum is shown in Figure 4.1b, where the peaks due to the normal spectrum have been subtracted away and the product spectrum can be clearly seen. These product spectra were collected using a reflectron TOF analyzer which is described in chapter 5, accounting for the much improved mass resolution as compared to Figure 3.3. The precursor ion signal appears as a negative peak due to the subtraction.

a)

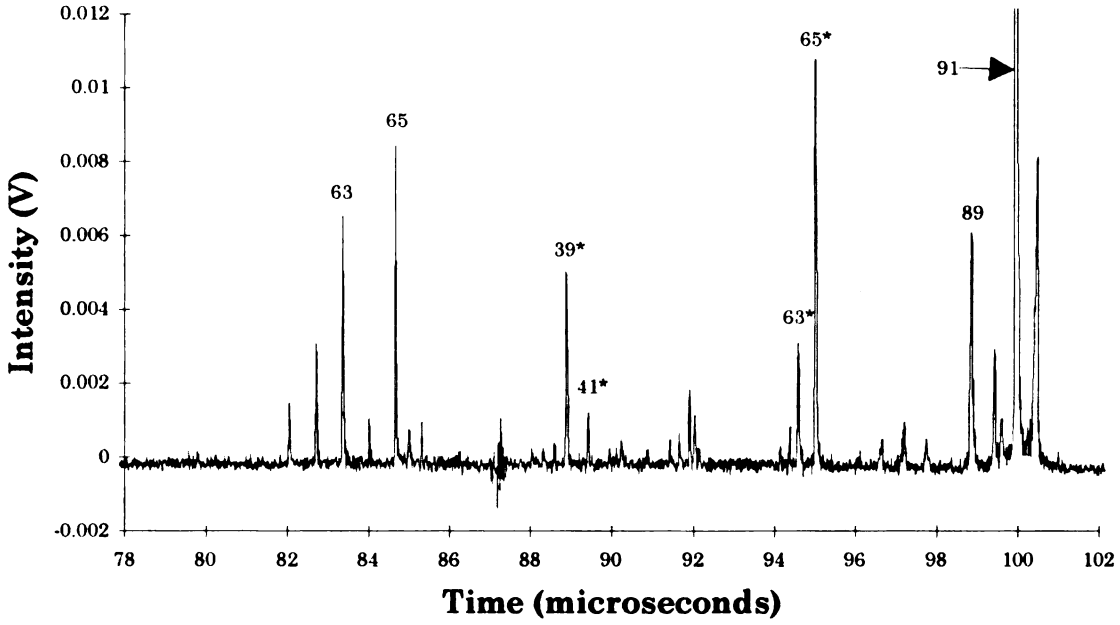

b)

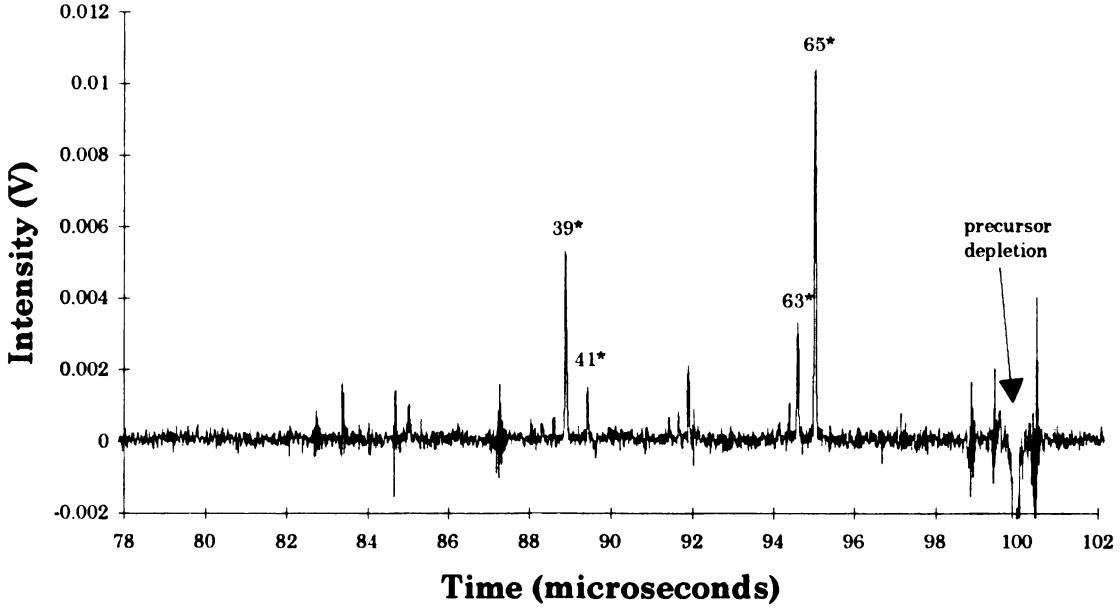

Figure 4.1 Product spectra of *m/z* 91 of toluene **a)** with convoluted normal spectrum, and **b)** with normal spectrum subtracted. (* indicates product ion peak).

The subtraction of spectra requires that the 'laser off' spectrum be collected very near in time to the 'laser on' spectrum in order to avoid peak intensity fluctuations associated with the changing sample pressure in the source region. This could be accomplished by operating at twice the repetition rate of the laser and alternately collecting product and normal spectra. However, this scheme introduces several difficulties that would increase the complexity of the data collection system because alternate transients would have to be collected in alternate channels for summing in real-time. Also, either the subtraction of spectra would have to occur in real-time or else twice the usual number of spectra would have to be collected.

A more effective approach is to isolate the selected precursor ion packet prior to fragmentation by elimination of all others. This can be accomplished through the use of an ion gate, which deflects unwanted ions on a trajectory which will not result in collision with the detector. In this mode, the product spectrum can be collected without normal spectrum interference or interference from metastable decomposition of other m/z values as long as unit resolution for isolation is maintained. Ultimately, precursor selection is accomplished through the overlap of the laser pulse and the ion packet of interest as described in chapter 3. This method of precursor isolation has the added benefit of reducing chemical noise which is often limiting in mass spectrometry [4].

4.2 Other applications of ion gates

4.2.1 Precursor selection

When collision-induced dissociation (CID) [5, 6] or surface-induced dissociation (SID) [7] is used as the activation method for tandem TOF mass spectrometry, an ion gate must be used to select a particular m/z packet for dissociation with rejection of all others. Without m/z selection, unlike the case for pulsed-laser PID, many m/z value ions may be fragmented, and the resulting spectra are convolutions of multiple, overlapped product and normal spectra. A pulsed gas valve has been used to introduce collision gas for CID in a tandem TOF instrument [6], but the duration of the burst in the interaction region (about 200 μs) is too long to accomplish selection.

4.2.2 Preventing detector saturation

Elimination of low-mass ions or ions of little interest may be important to avoid detector saturation which can limit detector response to ions of interest. Examples of this include elimination of ions formed from the gas chromatography (GC) carrier gas for GC/MS applications and elimination of matrix ions in matrix-assisted laser desorption / ionization (MALDI) mass spectrometry. Another use of gate devices for TOF instruments is the temporal encoding of continuous ion beams [8].

4.3 Gating methods

Two deflection devices have been described in the literature for ion beam modulation and/or gating purposes in TOF mass spectrometry. These devices are deflection plates and interleaved comb ion deflection systems, both of which will be described and compared below. Three distinct methods for ion beam modulation have been identified [8] for use with deflection plate gating devices. The work described below is concerned only with the normal 'gate mode' of operation, and the other modes of operation are not considered. However, the advantages of the interleaved comb ion deflection gate device over deflection plate devices as outlined below should apply to all three modes of operation.

In order to achieve m/z selection in TOF mass spectrometry, the gate device is held in its closed or deflecting state until the iso-mass ion packet of interest is about to reach the deflecting field created by the gate device. At this time the gate is electronically switched to its open or non-deflecting state, the ion packet passes through the volume that the deflecting field previously occupied, and then the gate is switched to its closed state again.

4.3.1 Deflection plates

Early devices for ion beam modulation consist of parallel plates between which the ion beam passes. The potential of one or both of the plates are modulated to create, alternately, a deflecting field and a non-deflecting

field in order to achieve selection of the desired portion of the ion beam. Descriptions and examples of the use of this type of ion gate in TOF mass spectrometry are prevalent in the literature [5-15].

4.3.2 Interleaved comb ion deflection gate

The interleaved comb ion deflection gate consists of a plane of closely spaced parallel wire segments. Alternate wire segments are connected, creating two distinct wire sets which are electrically isolated from one another. An ion beam traveling orthogonal to the plane of wire segments is unaffected by the device (excepting collisional interactions) when the wire sets are held at the potential of the field-free flight path. However, when the wire sets are held at opposite potentials of equal magnitude with respect to the field-free potential, approximately half of the ions are deflected to one side and the rest of the ions to the other side, depending on the polarity of the field which the particular ion passes through.

This interleaved comb device was first proposed by L. B. Loeb to H. F. Lusk for use as an electron filter [16]. Lusk's preliminary studies showed that if a high frequency RF potential was applied between the alternating wire sets, that electrons should be eliminated from an ion beam with little effect on the slower ions. Use of this device as an electron filter was demonstrated by A. M. Cravath [17] and later by N. E. Bradbury and R. A. Nielsen [18]. The device was first used for m/z selection in the ion gate mode for TOF mass spectrometry by R. Weinkauf, *et al.* [2]. Several groups,

including this one, are using the interleaved comb ion deflection gate for m/z selection in TOF mass spectrometry [2, 3, 19-21].

4.3.3 Comparison

The inherent advantage of the interleaved comb ion deflection gate over the deflection plate gate is related to the physical dimensions of the field which is produced by this device in the closed (or deflecting) state. In TOF mass spectrometry, consecutive iso-mass ion packets of increasingly higher m/z values are closer together in time and space. Decreasing the length of the deflection field without reducing the angle of deflection is therefore very important in improving resolution of selection. Using SIMION [22], a computer program which predicts electric field shapes and ion motion, the interleaved comb ion deflection gate was compared with deflection plates. Both devices were configured to accomplish an angle of deflection of about 10°. With wire spacing of 1 mm and ± 250 V applied to alternate wire segments (relative to the field-free potential) in the interleaved comb ion deflection gate, the field produced extends about 1.1 mm in both directions from the device center. The limit of field effect was defined as the ± 5 V equi-potential contour lines. Equi-potential contours (at ± 5 V, ± 50 V, and ± 100 V) and ion trajectories through the device as modeled in SIMION are shown in Figure 4.2a.

a)

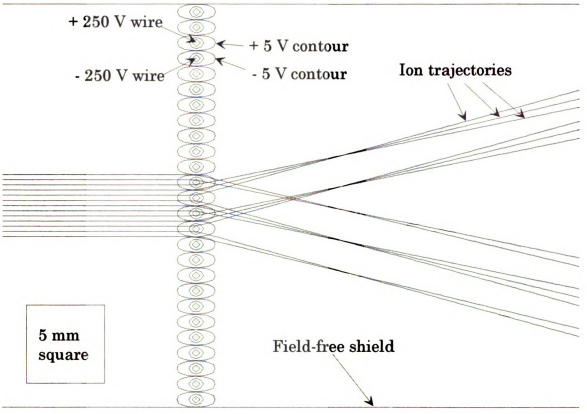

b)

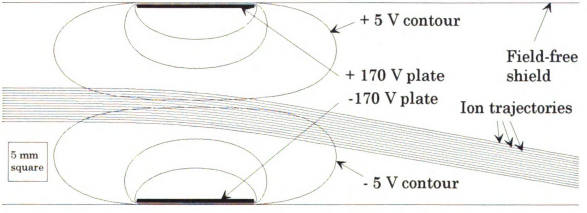

Figure 4.2 SIMION models showing equi-potential contours and ion trajectories for **a)** the interleaved comb ion deflection gate, and **b)** a deflection plate gate (note different scales).

For a set of deflection plates 15 mm wide and 25 mm apart with ± 170 V applied, the field extends at least 18 mm in both directions from the device center, again using the ± 5 V equi-potential contours as the limit of field effect. Equi-potential contours (at ± 5 V, ± 50 V, and ± 100 V) and ion trajectories through the device as modeled in SIMION are shown in Figure 4.2b. The model presented here depicts a limiting case of placing the shield electrodes (at field-free potential) very near to the deflection plates. As the distance between the shield electrodes and the deflection plates increases, the field produced by the deflection plates extends even farther in both directions.

The large difference in the length of the deflection field for the two devices can be explained by two factors. First, the large field strength produced by the closely spaced wire segments results in efficient deflection for the interleaved comb device. Also, the field produced by this device is canceled as the distance from the wires increases due to the equal and opposite potentials on the adjacent wire segments. It is crucial that the wires are perfectly co-planar for effective cancellation of the field.

4.4 Instrumentation

Little description has previously been provided in the literature concerning interleaved comb ion deflection gate devices. Here a detailed account of the device itself and suitable electronics which achieve the desired

pulse shapes for the gate mode of m/z selection are presented, similar to the information presented in reference [23].

4.4.1 Interleaved comb ion deflection gate device

A drawing of the interleaved comb ion deflection gate constructed in our laboratory is shown in Figure 4.3. Two continuous, stainless-steel, 0.076 mm diameter wires (California Fine Wire, Grover City, CA) form a plane of 26 wire segments as shown in Figure 4.3b (front view). Two Vespel® (E.I. du Pont de Nemours, Wilmington, DE) blocks (A & B) are held apart by #6-32 threaded rods (C & D) inserted in holes in the Vespel blocks with nuts at both ends. The tension on the wires serves to hold the blocks together on the threaded rods. As can be seen in Figure 4.3a (top view), a row of 0.38 mm holes are drilled in the Vespel block to hold the wire segments 1 mm apart. Since the two wires must be electrically isolated, each wire is wound around a different #3-48 threaded rod (E & F) suspended above the holes on either side of the row of holes. A congruent assembly is employed at the bottom of the gate. The ends of the wires are anchored by pinching them between two nuts and two washers on the suspended rods (E & F). Electrical contact is made to the wires through threaded rods E & F. The effective area of the gate is approximately 25 mm by 50 mm.

It was observed that the wire segments did not form a perfect plane due to the effect of one wire being wound around threaded rod E, to the back,

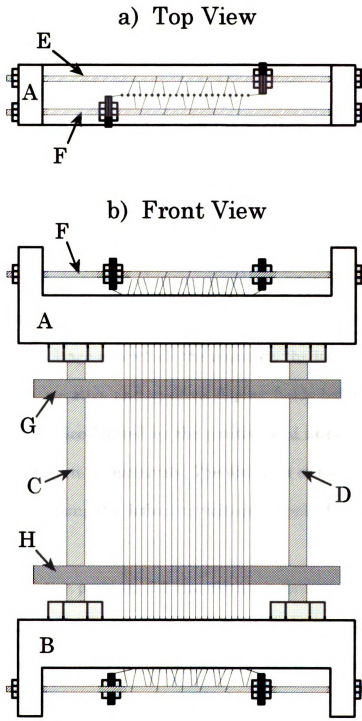

Figure 4.3 The interleaved comb ion deflection gate device.

and the other wire being wound around threaded rod F, to the front. The result was that alternate wire segments arced out of the plane in opposite directions very slightly. The field produced by this imperfect device was not canceled effectively as the distance from the wires increased. In fact, a net positive field was generated on one side of the gate and a net negative field was generated on the other. The fields produced by a planar gate device and a non-planar gate device are compared in Figure 4.4 as modeled in SIMION. Experimentally, the imperfect device caused an arrival-time shift in the selected iso-mass ion packet. Depending on which wire set received the positive deflecting voltage and which the negative, the ion packet was either accelerated by the negative and positive sloping fields before and after the gate, respectively, or decelerated by the positive and negative sloping fields before and after the gate, respectively. The direction of the arrival-time shift was reversed by reversing the deflecting voltages supplied to the two wires in the gate.

To eliminate this problem, 2.6 mm diameter ceramic rods (G & H) were inserted in front of threaded rods C & D, but behind the plane of wires, so that all of the wire segments arc in the same direction and form a plane. The ceramics are effectively held in place by the tension of the wires and the threads on rods C & D (see Figure 4.3). After the ceramic rods were inserted, no arrival-time shift was observed.

a)

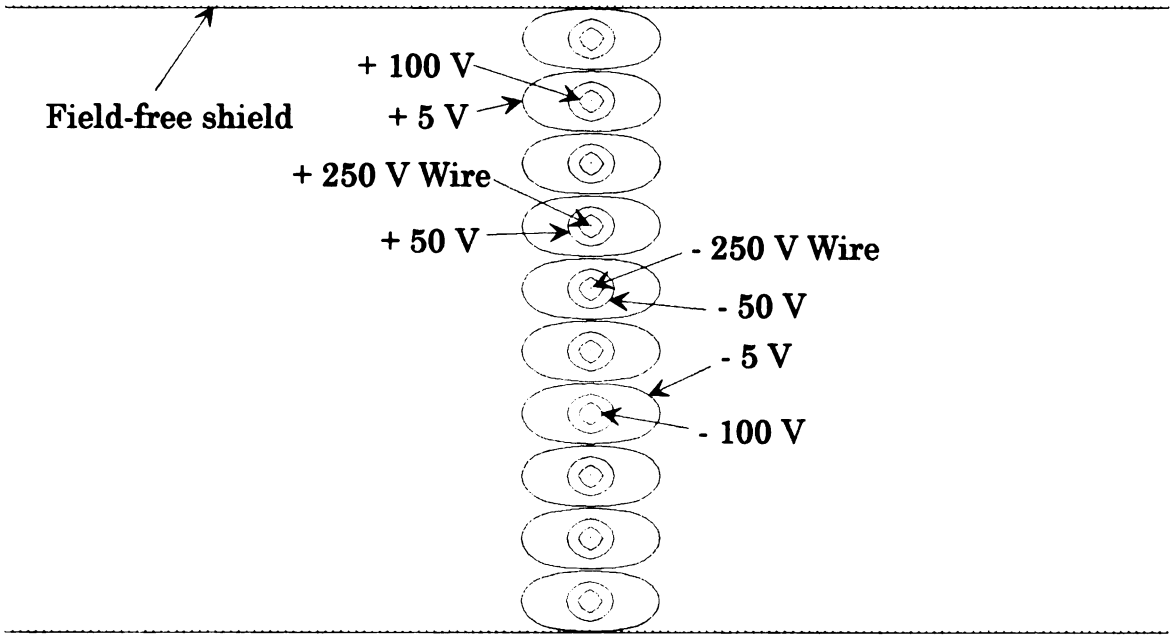

b)

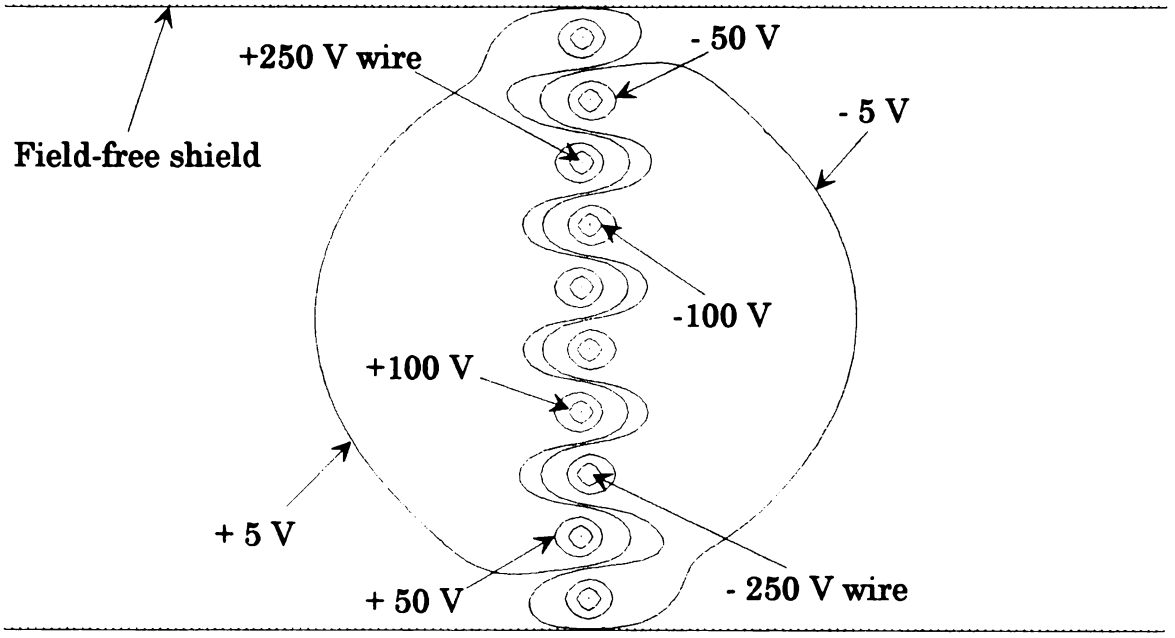

Figure 4.4 SIMION models showing equi-potential contours for **a)** the planar gate device, and **b)** the non-planar gate device.

Tension on the wires is adjusted by rotating the nuts on rods C & D, sliding the ceramic rods G & H up or down, or adjusting the position at which the ends of the wires are anchored. To achieve uniform tension across the plane, the individual wire segments are manually massaged.

4.4.2 Electronics

4.4.2.1 Description

Figure 4.5 is an overview of the electronics built for gate control. A TTL level trigger from the ion source extraction rate time base is routed through a LeCroy 4222 programmable delay generator (PDG) in a CAMAC frame which is interfaced to the host computer using a general purpose interface bus (GPIB). Delayed trigger pulses from the PDG range from 170 ns to 16.7 ms with 1 ns resolution. This delayed pulse is used to trigger a programmable pulse width generator (PPWG) circuit, which is described in detail elsewhere [23]. The PPWG circuit produces complementary pulses of variable width from 11 ns to 2561 ns in 10 ns steps. Due to unequal propagation delays throughout the system, an edge alignment circuit was built into the PPWG circuit. The pulse width is specified in the Lab Windows® (National Instruments, Austin, TX) instrument control program as an 8-bit word which is applied to the PPWG through a National Instruments model AT-MIO-16F-5 board.

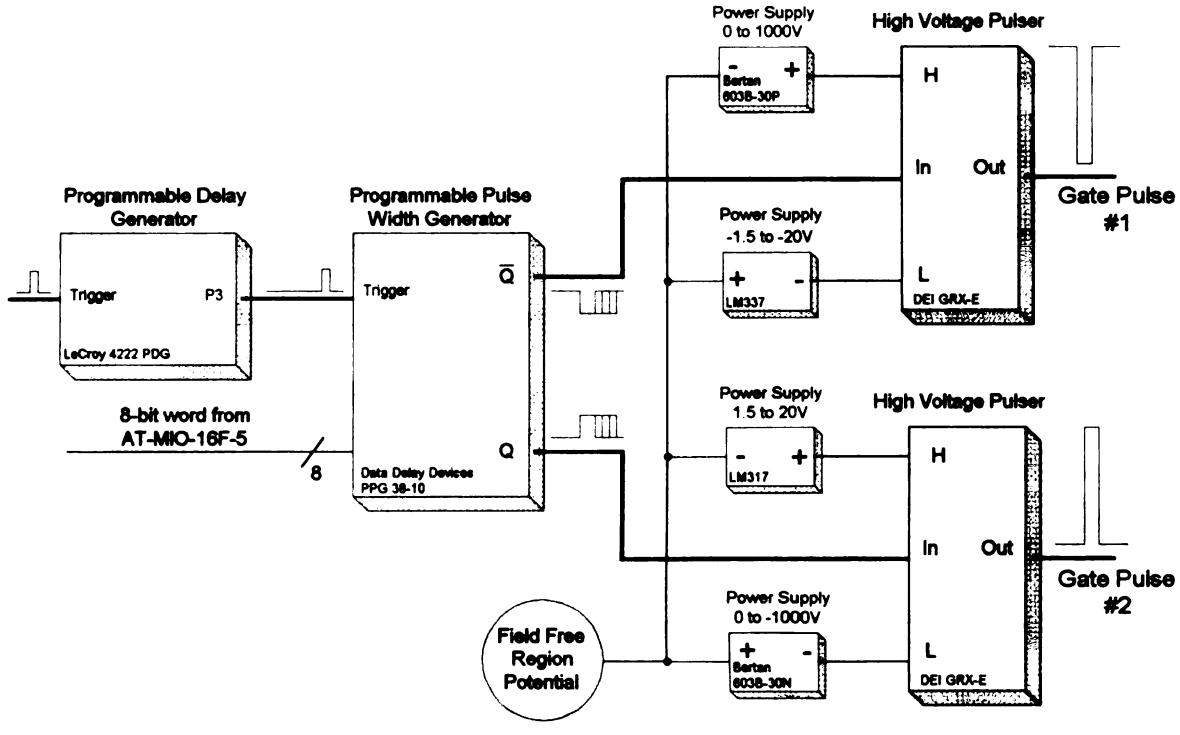

Figure 4.5 Overview of electronics used to produce complementary gate pulses.

The complementary pulses from the PPWG trigger a pair of GRX-1.5K-E pulse generators (Directed Energy, Inc. (DEI), Fort Collins, CO) which supply the high voltage pulses applied to the gate device. One pulser switches from a positive deflection voltage to the field-free region potential. The other unit switches from the negative deflection voltage to the field-free region potential. Positive and negative deflection voltages are supplied by separate positive and negative high voltage power supplies floating at the field-free region potential. The DEI units do not have full rail-to-rail swings and therefore the low (or high) input must be offset below (or above) the field-free region voltage. Low voltage power supplies with adjustable linear regulators provide the ± 5 to 10 volts needed. The outputs from the DEI pulsers are routed through impedance-matched 50 Ω cables about 60 cm long to an impedance-matched vacuum feed-through. Inside the vacuum chamber, insulated wires (not impedance matched) about 20 cm long connect the pulser output to rods E & F of the gate device (see Figure 4.3).

4.4.2.2 Pulse shapes

Typical pulse shapes are shown in Figure 4.6, where output signals from the DEI pulsers are plotted versus elapsed time since ion source extraction. The line labeled V_{ff} indicates the field-free potential. Rise and fall times are on the order of 30 ns for the ± 250 V pulses.

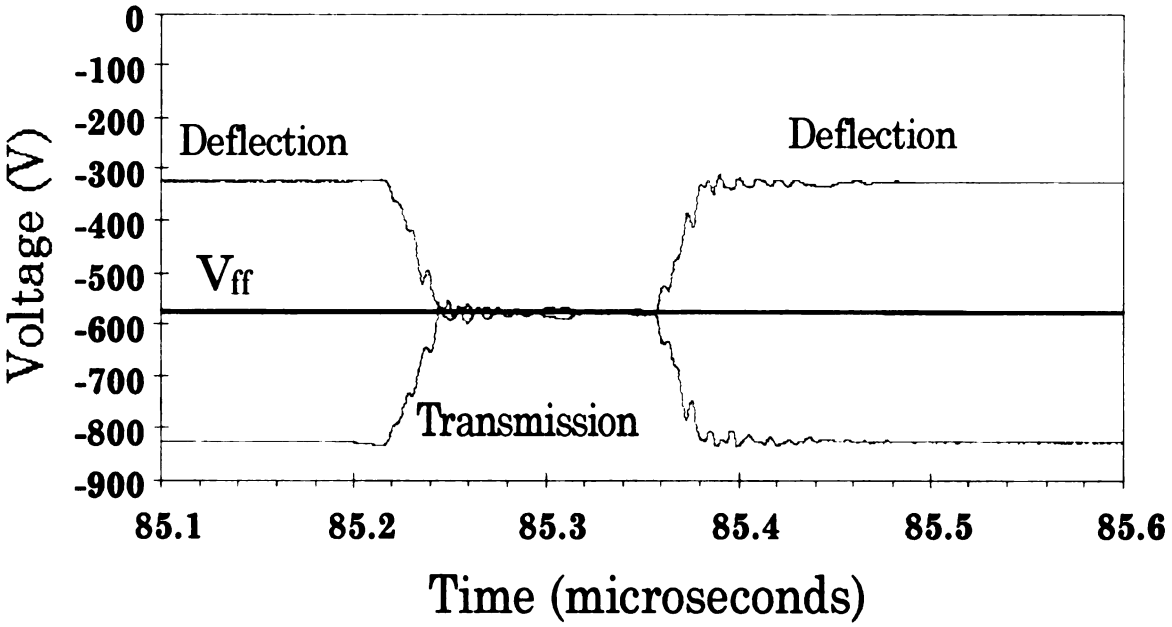

Figure 4.6 Typical pulse shapes produced by the DEI pulsers.

4.5 Performance

Performance of the interleaved comb deflection gate was characterized in the tandem TOF mass spectrometer [3, 20, 23]. The first reflectron TOF analyzer was focused at the position of the gate device by placing a detector 4 cm beyond the gate (as near as possible). A mass resolution of about 2000 was observed at this position for ions having energies of approximately 650 eV. The detector was then placed 15 cm beyond the gate device. Just prior to the gate device, an aperture limited the beam diameter to 12.7 mm, while the diameter of the active area of the detector is 25 mm. Figure 4.7a is a spectrum showing the molecular ion region of diphenylmethane

(MW = 168). During the gate closed period, the wires are set to potentials of ± 250 V with respect to the field-free voltage. The gate was operating with an appropriate time delay and a wide gate pulse (1.28 μs) in order to select the entire region.

Figure 4.7b is the same spectral region with the time delay adjusted appropriately and the gate pulse narrowed to 140 ns in order to select the *m/z* 167 ion packet. Optimization of the gate delay and gate pulse width was accomplished sequentially. First, the gate delay was adjusted to as high a value as possible without reducing the intensity of the peak corresponding to the chosen *m/z* value. Next, the gate pulse width was set to as small a value as possible without reducing the intensity of the peak. In this manner, both edges are optimized for maximal resolution of isolation on both sides of the object peak. One might consider use of the gate to actually make the precursor peak narrower and hence improve mass resolution. However, in this experimental arrangement, it was observed that setting the gate delay too high or the pulse width too narrow resulted in both a narrowing of the peak and a reduction in its intensity.

The spectrum in Figure 4.7c was collected under the same conditions as for Figure 4.7b except that the trigger signals to the two pulsers were reversed in order to eliminate just the *m/z* 167 ion packet. By integration of

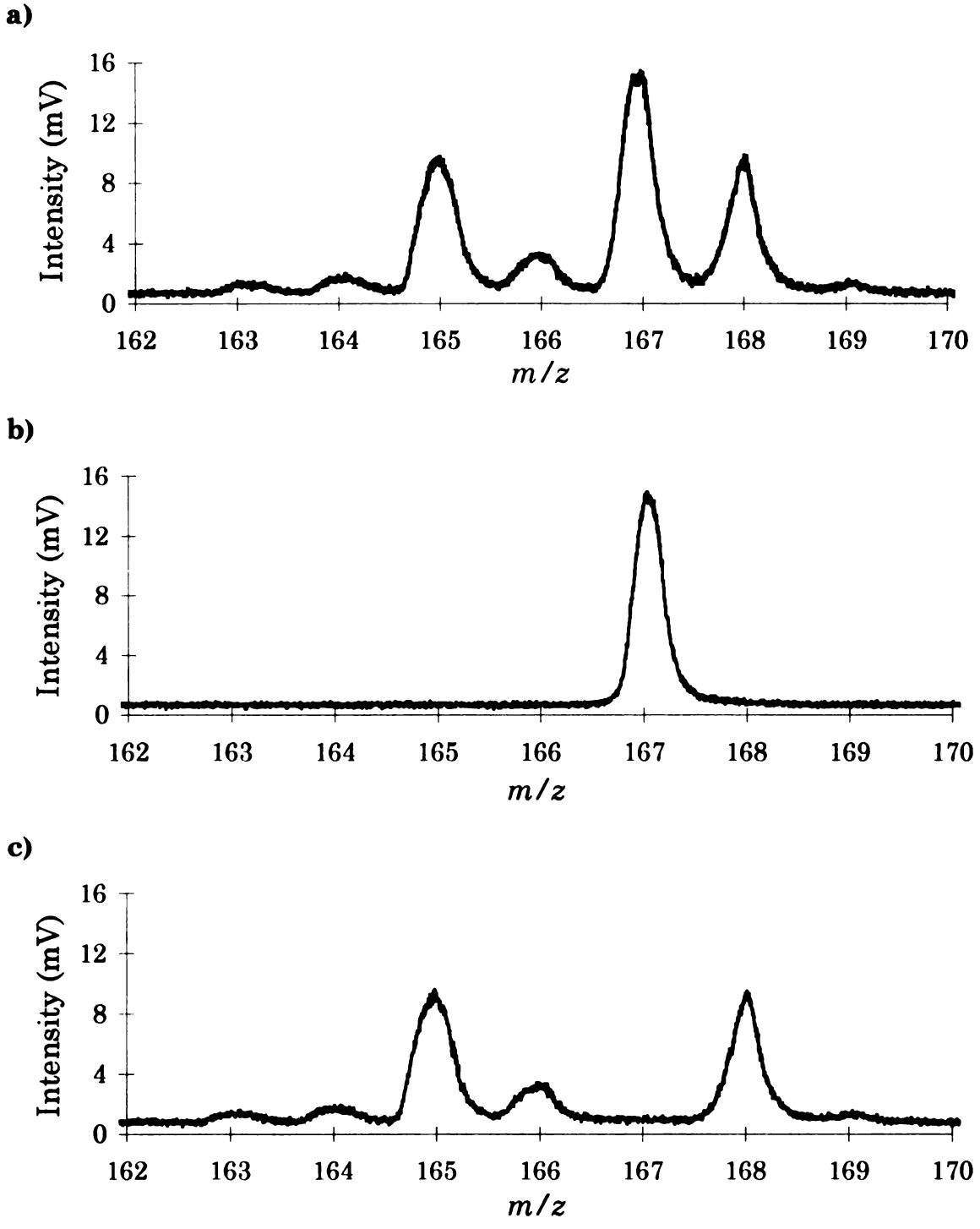

Figure 4.7 TOF mass spectra of the molecular ion region of diphenylmethane for gate pulse width of **a)** 1.28 μs, **b)** 140 ns, and **c)** 140 ns with gate trigger signals reversed.

the m/z 167 for the spectra in Figures 4.7a and 4.7b, the peak area for the isolated peak in Figure 4.7b was 88% of the area for the corresponding peak in Figure 4.7a. Hence, little reduction in transmission occurs.

The potential difference required to achieve complete elimination of ions for this experimental arrangement was investigated by slowly increasing the potentials of the deflecting voltage supplies. It was observed that below ± 175 V, signal due to coherent ion arrival could be observed. The 350 V potential difference between the wire segments of the interleaved comb ion deflection gate, according to SIMION modeling, should result in a deflection angle of about 8.5°. The angle expected to be required by simple geometrical considerations is 7.2°. This investigation represents fairly good agreement between the theoretical model and the experimental results. Several factors could account for the minor discrepancy, such as uncertainties in the positions of the gate, aperture, and detector. With greater significance, it is likely that the ion beam is not collimated and/or that the beam is not perfectly parallel with the rail on which the ion optical elements are mounted. Since the detector is placed at a much greater distance from the gate during normal operation of the tandem TOF instrument, the deflection angle required is smaller than that required for the previous study.

The data presented in Figure 4.7 demonstrates unit resolution for selection over a mass range of at least 167 in our tandem TOF mass spectrometer. Based on ion packet width, distance between the ion packets,

the flight distance influenced by the gate deflection field (as determined by SIMION), and the pulse rise and fall times, unit resolution over a mass range of at least 300 is possible. The limit of unit resolution for isolation occurs when the separation between adjacent ions (measured from peak center to peak center) is equal to the sum of the width of the gate deflection field, the iso-mass ion packet width (FWHM), and the distance the iso-mass ion packet moves during the pulse rise (or fall) time. The work presented here represents a significant improvement over previously demonstrated capabilities in ion packet isolation. The performance of the interleaved comb ion deflection device is dependent on a number of factors, including mass resolution at the gate position, energy of the ions, angle of deflection required, distance between wire segments in the device, jitter in timing delays, pulse height, pulse width, pulse rise-times, pulse stability (extent of ringing and droop), and extent to which the pulse shapes are complementary. We expect that the interleaved comb ion deflection device will be widely used for precursor ion selection (or isolation) in tandem TOF instruments and for other applications where modulation of an ion beam is necessary.

For GC analyses, a mass resolution for isolation of 300 should be adequate for the majority of applications. For this tandem TOF instrument, pulsed-laser PID allows unit resolution for selection to m/z 1200 (see chapter 3). Isolation of ion packets above m/z 300 will still be an effective method of eliminating the vast majority of interferences along the time

domain. In the worst case, two neighboring m/z values on either side of the ion packet of interest would be allowed to pass, and these would be reduced in intensity. The neighboring m/z value(s) of lower mass than the precursor ion packet would obscure only the upper few percent of the product spectrum mass range. The neighboring m/z value(s) of greater mass than the precursor ion packet will not interfere unless significant metastable decay of these ions occurs. A product spectrum for m/z 91 of toluene for which the gate was used to eliminate interference from the normal ion spectrum is presented in chapter 5 (see Figure 5.10).

4.6 References

1 Seeterlin, M. A.; Vlasak, P. R.; Beussman, D. J.; McLane, R. D.; Enke, C. G. *J. Am. Soc. Mass Spectrom.* **1993**, *4*, 751.

2 Weinkauf, R.; Walter, K.; Weickhardt, C.; Boesl, U.; Schlag, E. W. *Z. Naturforsch.* **1989**, *44a*, 1219.

3 Beussman, D. J.; Vlasak, P. R.; McLane, R. D.; Seeterlin, M. A.; Enke, C. G. (*submitted to Anal. Chem.*)

4 Busch, K. L.; Glish, G. L.; McLuckey, S. A. *Mass Spectrometry / Mass Spectrometry: Techniques and Applications of Tandem Mass Spectrometry*, VCH Publishers, Inc.: New York, 1988.

5 Jardine, D. R.; Morgan, J.; Alderdice, D. S.; Derrick, P. J. *Org. Mass Spectrom.* **1992**, *27*, 1077.

6 Cornish, T. J.; Cotter, R. J. *Anal. Chem.* **1993**, *65*, 1043.

7 Schey, K.; Cooks, R. G.; Grix, R.; Wollnik, H. *Int. J. Mass Spectrom. Ion Processes* **1987**, *77*, 49.

8 Yefchak, G. E.; Schultz, G. A.; Allison, J.; Enke, C. G.; Holland, J. F. *J. Am. Soc. Mass Spectrom.* **1990**, *1*, 440.

9 Bakker, J. M. B. *J. Phys. E: Sci. Instrum.* **1974**, *7*, 364.

10 Bloomfield, L. A.; Geusic, M. E.; Freeman, R. R.; Brown, W. L. *Chem. Phys. Lett.* **1985**, *121*, 33.

11 Pinkston, J. D.; Rabb, M.; Watson, J. T.; Allison, J. *Rev. Sci. Instrum.* **1986**, *57(4)*, 583.

12 Brucat, P. J.; Zheng, L.-S.; Pettiette, C. L.; Yang, S.; Smalley, R. E. *J. Chem. Phys.* **1986**, *84(6)*, 3078.

13 Haberland, H.; Kornmeier, H.; Ludewigt, C.; Risch, A. *Rev. Sci. Instrum.* **1991**, *62(10)*, 2368.

14 Cornett, D. S.; Peschke, K.; LaiHing, K.; Cheng, P. Y.; Willey, K. F.; Duncan, M. A. *Rev. Sci. Instrum.* **1992**, *63(4)*, 2177.

15 Kaufmann, R.; Spengler, B.; Lutzenkirchen, F. *Rapid Commun. Mass Spectrom.* **1993**, *7*, 902.

16 Loeb, L. B. *Basic Processes of Gaseous Electronics*, University of California Press: Berkely, 1961.

17 Cravath, A. M. *Phys. Rev.* **1929**, *33*, 605.

18 Bradbury, N. E.; Nielsen, R. A. *Phys. Rev.* **1936**, *49*, 388.

19 Boesl, U.; Schlag, E. W.; Walter, K.; Weinkauf, R. U. S. Patent # 5,032,722, 1991.

20 Beussman, D. J.; Vlasak, P. R.; Erickson, T. A.; Davenport, M. R.; Enke, C. G. *presented at the 43rd ASMS Conference on Mass Spectrometry and Allied Topics*, Atlanta, Georgia, May 22, 1995.

21 Hoyes, J. B.; Curbishley, S. G.; Doorbar, P.; Tatterton, P.; Bateman, R. H.; Beer, B.; Lockett, J. *Proceedings of the 42nd ASMS Conference on Mass Spectrometry and Allied Topics*, Chicago, Illinois, May 29 - June 3, 1994, 682.

22 Dahl, D. A.; Delmore, J. E. *SIMION PC/PS2 Version 5.0 (real mode)*, 1988, Idaho Falls National Engineering Laboratory, EG&G Idaho Inc., P.O. Box 1625, Idaho Falls, ID 83415.

23 Vlasak, P. R.; Beussman, D. J.; Davenport, M. R.; Enke, C. G. (*submitted to Rev. Sci. Instrum.*)

Chapter 5: The second mass analyzer

5.1 Requirements

The requirements of the second mass analyzer are different from that of the first due to the nature of the sample ions. When acceleration occurs from an ion source, each iso-mass ion packet has approximately the same kinetic energy distribution as other iso-mass ion packets. In contrast, the ions that are accelerated after PID in the tandem TOF instrument have m/z-dependent energies. Upon dissociation, the ions and neutrals retain approximately the velocity distribution of the precursor ion packet assuming that the translational energy release upon dissociation is not significant. These ions have a relative kinetic energy range of nearly 100%, however, ranging from a small fraction of the precursor energy for low m/z product ions to the entire precursor energy for undissociated precursor ions, according to the equation:

$$U_{prod} = U_{prec} \cdot \frac{m_{prod}}{m_{prec}} \qquad (1)$$

where U_{prod} and U_{prec} are the energies of the product and precursor ion, and m_{prod} and m_{prec} are the masses of the product and precursor ion, respectively.

5.2 Reflectron TOF

5.2.1 Background

In reflectron time-of-flight (TOF) mass spectrometers employing electron ionization sources, the application of an extraction field to the source volume creates a minimal spatial/temporal distribution for iso-mass ions outside of the ion source at a position called the space-focus plane [1-4]. There is a significant distribution of the kinetic energy of these ions as a result of their initial spatial and energy distributions. The reflectron, or ion mirror, is used to reproduce the spatial/temporal distribution of the space-focus plane at the surface of an ion detector, thereby improving mass resolution by increasing flight time (and the separation between adjacent iso-mass ion packets) without increasing significantly the temporal width of the iso-mass ion packets [2-6]. Generally, the relative kinetic energy range of ions accelerated from the source is small (< 10%), and most reflectron time-of-flight instruments described in the literature have been designed to effectively focus these small energy ranges.

5.2.2 One-stage and two-stage reflectrons

The most common reflectrons in use are one-stage and two-stage reflectron designs which provide first-order and second-order energy compensation, respectively. Homogeneous fields (stages) are created with the use of wire mesh 'grids'. The prescribed geometry of the reflectron field, in

both cases, is an analytically derived function of instrument variables [2, 6]. Figure 5.1 is a plot of $2 \cdot \Delta T/T$ versus ion energy for three reflectron solutions where T is the arrival time of an ion having average velocity and ΔT is the difference between T and actual arrival time. Taking the inverse of the difference between the extreme vertical values over a specific energy range on this chart gives an estimate of mass resolution for that energy range. Curve A is for an optimized single-stage reflectron, curve B is calculated according to reference 2 where simplifying assumptions were made in deriving the solution for a two-stage reflectron, and curve C is a solution calculated using MathCad 5.0 [7], a numerical solving program, giving a result similar to that described in reference 6 for a two-stage reflectron. This chart is calculated using values which match the reflectron focusing problem for the second mass analyzer in the tandem TOF instrument. It can be seen that these simple reflectrons provide excellent energy compensation for small deviations in ion energy. Boesl, *et al.* [8] note that for larger energy ranges (> 10%), the two-stage reflectron can be re-configured to give somewhat improved resolution over that specific energy range.

5.2.3 Grid-free reflectrons

Several grid-free reflectron designs have also been described [5, 9-13]. The ability to energy focus without the use of grids is an advantage since the grids limit transmission via ion collisions with the wires and scattering of

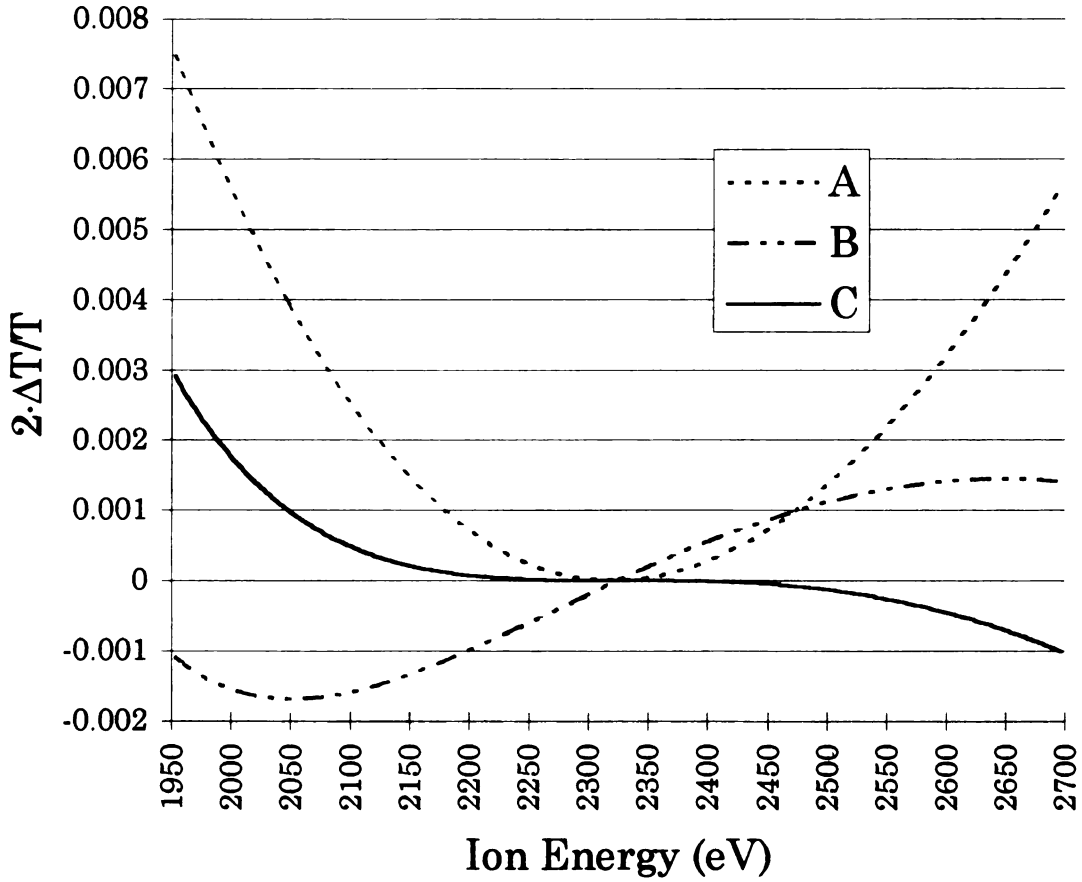

Figure 5.1 A plot of $2 \cdot \Delta T/T$ as a function of ion energy for homogeneous field reflectrons.

ions which pass near the wires [14]. In addition, throughput can be improved by the radial focusing of the ion beam in the cylindrically-symmetric, inhomogeneous reflectron field. Grix, *et al.* [5] report that an energy range of greater than 10% can be effectively focused using a grid-free design. This is the type of reflectron which is used in the first mass analyzer of the tandem TOF instrument.

5.2.4 Perfectron

Rockwood [15] has developed a method giving infinite order correction which uses a parabolic field in a device termed a 'perfectron'. The perfectron contains no field-free region, and the focal points of the perfectron are at the reflectron entrance. A preliminary version of this instrument resulted in a resolution of 125, because of poor pulse response of the electronics and deviations from the ideal parabolic field in a grid-free design. The difficulty of achieving a parabolic field and the unconventional design (lacking field-free distance) prohibit its use in the current tandem TOF instrument.

5.3 Reflectron TOF for product ion analysis

Several reflectron focusing methods have been used to improve mass resolution for product ion analysis in TOF mass spectrometers. These methods fall into two main categories segregated by whether or not the product ions (resulting from either an induced dissociation or a metastable decomposition) are accelerated after dissociation.

5.3.1 Separation within the reflectron

Without post-dissociation acceleration, separation of product ions from one another and from the precursor ion packet from which they originated is accomplished entirely within the reflectron on the basis of the reduced energy for product ions (see Equation 1). This results in a correspondingly smaller residence time in the reflectron. No separation occurs in the field-free regions since here the product ion packets have approximately the same velocity distribution as the precursor ion packet from which they originated.

Early demonstrations involved metastable decompositions occurring after ionization by a ^{252}Cf plasma desorption source [16, 17] and a secondary ion (SIMS) source [18] using a single reflectron for normal ion and product ion analysis. Decompositions were identified by the detection of a neutral at a detector placed behind the reflectron, with the arrival time of the neutral 'correlated' to the precursor m/z which decomposed and the product ion which is then detected at the normal detector position. In general, one-stage reflectrons are advantageous in this configuration since mass calibration is accomplished as a linear function of time. Schlag's group [8, 19] used a linear TOF / reflectron TOF arrangement, in which dissociation was accomplished by intersecting a laser pulse with the precursor ion packet at the space-focus plane of the linear TOF analyzer. This instrument incorporated an ion gate to isolate a particular precursor m/z thus eliminating the need for the correlation technique. The potentials of a two-stage reflectron were scanned

to consecutively focus product ions of different m/z values at a detector with a fixed arrival time. Cornish and Cotter [20] also incorporated an ion gate in their dual reflectron TOF instrument in which precursor ions are fragmented by collisionally-induced dissociation (CID) at the focal point of a first reflectron TOF analyzer, and the products are analyzed in a second reflectron TOF analyzer. Initially, a single-stage reflectron was used. A later modification involving an empirically-generated, curved reflectron field improved resolution and resulted in a non-linear time vs. mass relationship, with calibration accomplished by fitting the data to a third-order polynomial by means of non-linear regression analysis [21, 22].

5.3.2 Separation by post-dissociation acceleration

The other major product ion analysis method involves a post-dissociation acceleration step in which m/z-dependent velocities are imparted to the product ions. This acceleration results in separation of iso-mass ion packets in the field-free region with the primary role of the reflectron being energy-focusing.

Schey, *et al.* [23] focused product ions produced by surface-induced dissociation in a linear TOF / reflectron TOF tandem mass spectrometer. The reflectron was grid-free and allowed energy focusing over a range of greater than 10%. Because the target surface was at a higher potential than the field-free region, the ions were essentially decelerated prior to dissociation and accelerated after dissociation. Since the reflectron could not compensate

for the energy spread due to partitioning, overall resolution was improved by optimizing for one product ion at a time. Schlag's group [8] also incorporated a post-dissociation acceleration stage in the linear TOF / reflectron TOF instrument described above. The acceleration reduced the relative kinetic energy range to the point where a two-stage reflectron could adequately compensate. This focusing method regained the ability to collect a complete mass spectrum from each ionization pulse, which was lost in the scanning method described above, but resulted in lower mass resolution than for the scanning method.

5.4 Product ion analysis in the tandem TOF instrument

5.4.1 Post-dissociation acceleration

In the tandem TOF instrument, our goal is to collect a complete product spectrum from every source extraction. For this reason, the incorporation of a scanning process such as that used by Schlag's group [8, 19] is not desirable. We chose to use an acceleration stage beyond the dissociation step, such that separation occurs within the entire flight path beyond the acceleration. Here, a reflectron serves primarily to focus the energy distribution rather than to act as both a separation and an energy-focusing device.

The acceleration is accomplished by means of a pair of grids placed about 1 cm apart approximately 2 cm beyond the interaction region. These

grids are aligned on the previously mentioned optical rail which is mounted parallel to the ion flight path below the interaction region. The first grid is held at the field-free potential of the first mass analyzer (-550 V) while the second grid is held at the field-free potential of the second mass analyzer (-2500 V). Besides imparting m/z-dependent velocities to the product ions, this acceleration reduces the relative kinetic energy range from nearly 100% (see Equation 1) to about 32%.

5.4.2 Elimination of interference due to MPI

In addition to providing efficient dissociation of precursor ions, the laser pulse causes multi-photon ionization (MPI) of neutral background gas in the interaction region. We observed that some portion of these ions drift toward the acceleration stage and are accelerated into the second mass analyzer. Figure 5.2a illustrates the background that is generated as a result. The large, noisy signal at the left is the electrical ringing associated with the discharge of the laser thyratron. The large, broad signal following is due to MPI interference, while the sharp peaks are the molecular ion region of bromobenzene (m/z 156-159). In the example shown, the laser was timed so that it did not cause photodissociation of the bromobenzene. The detector was placed on the optical rail about 20 cm beyond the interaction region.

In order to eliminate this background, a third grid was introduced beyond the interaction region between the acceleration grids such that the

a)

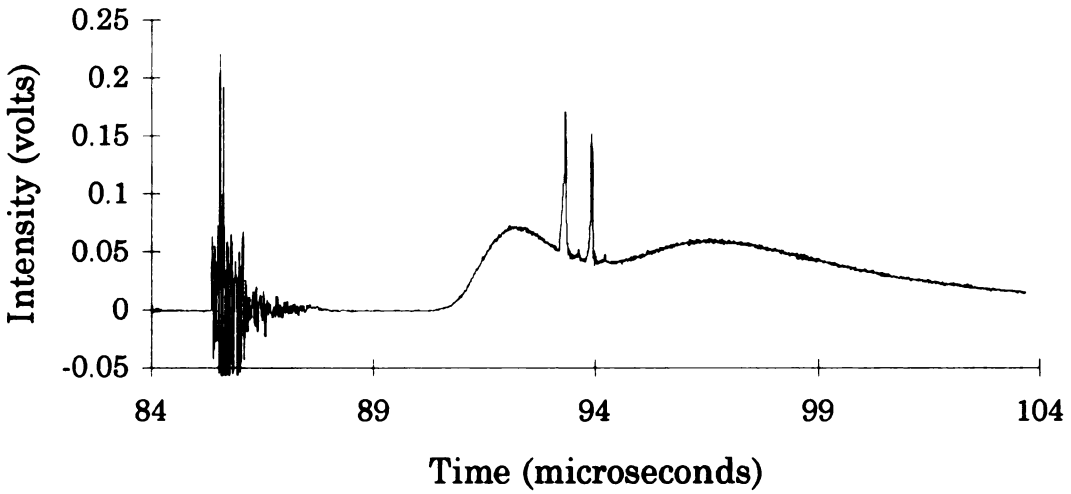

b)

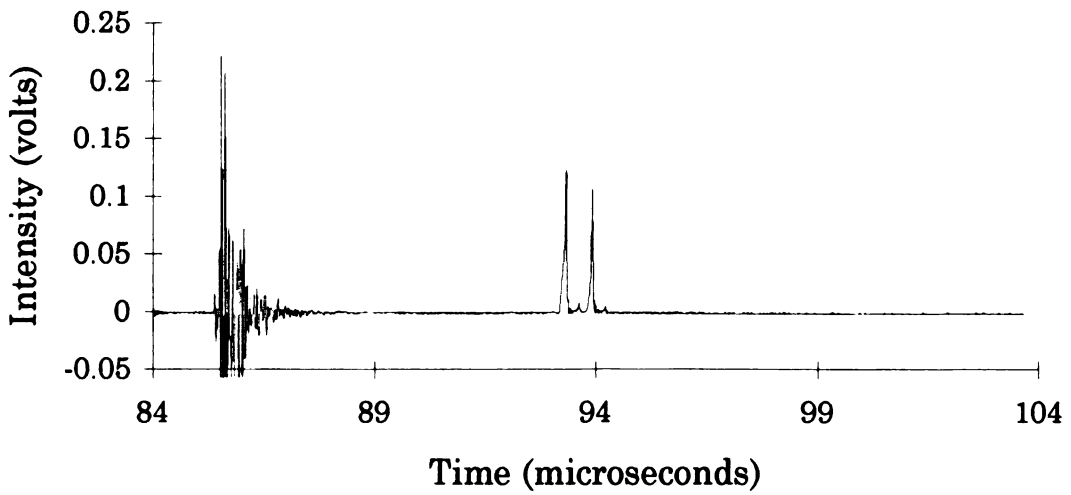

Figure 5.2 Molecular ion region of bromobenzene **a)** without MPI elimination field and **b)** with MPI elimination field.

grids are spaced about 1 cm apart, with the first grid placed about 2 cm beyond the interaction region. A potential about 20 V more positive than the first field-free potential is applied to the center grid. The ions produced by MPI have only thermal velocities, while product ions and undissociated precursor ions retain some percentage of the acceleration energy introduced by the first mass analyzer. This retardation field stops the ions produced by MPI, but allows the product ions to pass with the exception of approximately the lowest 3% of the mass range. Figure 5.2b illustrates the effective elimination of the MPI interference.

5.4.3 Grid-free reflectron for product ion analysis

Initially, a grid-free reflectron was incorporated in the second mass analyzer [24]. This analyzer was expected to focus a larger energy range than homogeneous field designs. The first photodissociation experiments performed in this instrument involved the molecular ion of bromobenzene (*m/z* 156 or 158). After depletion of either of these precursor ion signals by proper adjustment of laser timing, no product ions were observed. It was expected that the major fragment ion resulting from the photodissociation process would be *m/z* 77. Because *m/z* 77 had a significantly different energy than the precursor ion, for which reflectron 2 had been optimized, it was postulated that the resolution was simply too poor for any product peak to be observed [24].

In response to this hypothesis, the next experiments involved the fragmentation of the molecular ion of toluene (m/z 92), which was expected to yield a product ion at m/z 91. Since the loss of a very small mass percentage gives a product ion having nearly the same kinetic energy as the precursor, it was expected that this product ion packet should be nearly as well focused as the precursor. This product ion was indeed observed. It was also found that adjusting the potentials of the reflectron to bring lower energy ions into focus allowed the observation of m/z 77 from the bromobenzene molecular ion [24]. Recognizing that the relatively slow process of scanning reflectron voltages was inconsistent with the goals of this project, we set out to find or develop a different focusing solution.

5.4.4 Linear TOF mass analyzer

Although a reflectron capable of meeting the focusing needs of the second mass analyzer was eventually developed as described in section 5.5 below, the investigation of photodissociation as a fragmentation method continued using a short, linear TOF mass analyzer. This analyzer was implemented simply by placing a detector about 20 cm beyond the interaction region. Depending on the nature of the investigation, reflectron 1 was either tuned at the interaction region by temporarily placing a detector there, or tuned at the position of the detector 20 cm beyond. The former configuration provides maximal ion/photon overlap and therefore maximal

photodissociation efficiency, while the latter configuration results in improved resolution for both precursor and product spectra.

Operating the instrument in this manner allowed the observation of entire product ion spectra and the determination of PID efficiencies for a number of ions as discussed in chapter 3. As expected, however, the resolution of the product spectra was quite poor. Figure 5.3 is a product spectrum for bromobenzene obtained while the focus of reflectron 1 was at the detector position. This spectrum is a subtraction of the 'light off' spectrum from the 'light on' spectrum having been collected prior to the introduction of the ion gate. In the subtracted spectrum, the precursor ion depletion is observed as a negative peak. The positive product ion peaks are labeled with the number of carbon atoms present. The resolution of this spectrum is not adequate to differentiate between product ions varying by one mass unit.

5.5 A broad kinetic energy range focusing reflectron

As outlined above, the second mass analyzer in the tandem TOF instrument must be capable of focusing a relative kinetic energy range of about 32%. Coincidentally, another instrumentation project in this research group also requires focusing of ions having a relatively broad energy range (~30%). This project is the construction of a mass spectrometer in which ions are extracted from an ion trap storage device and analyzed by

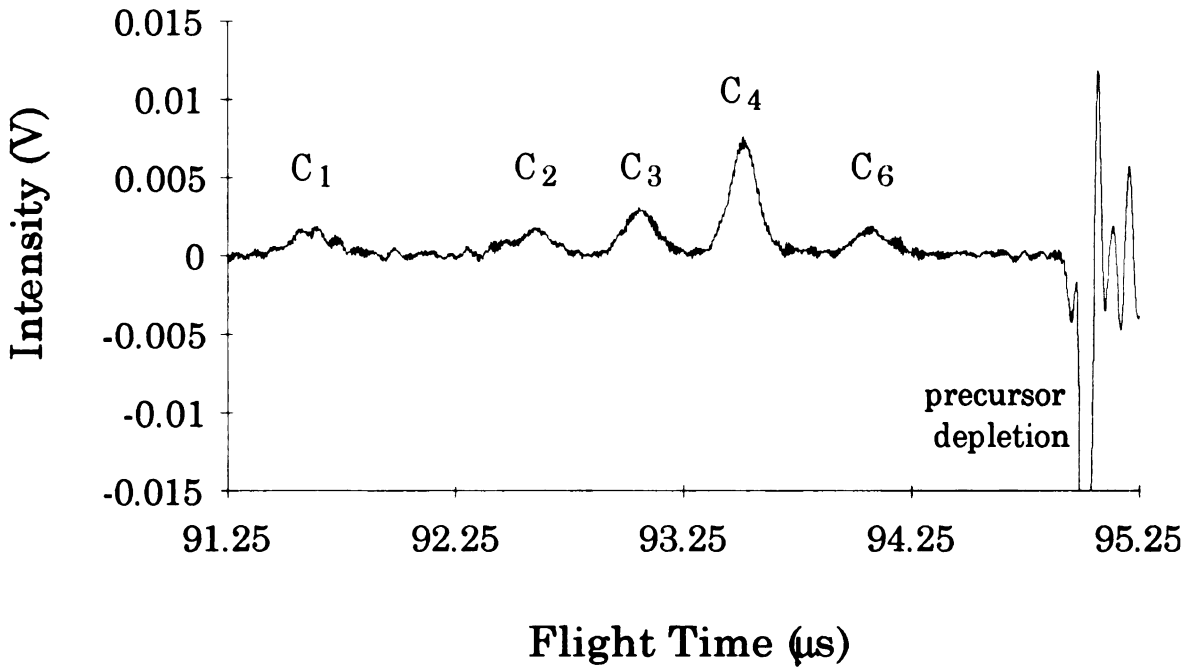

Figure 5.3 Product spectrum from *m/z* 156 of bromobenzene collected using a short, linear TOF analyzer.

time-of-flight (IT/TOF) [25, 26]. The storage device serves to accumulate continuously produced ions between extractions, thus increasing sensitivity. Ions in the trap occupy a relatively large volume compared to traditional electron ionization sources and are subjected to a large extraction potential. The spatial distribution of ions within the ion trap storage device becomes a broad relative energy distribution upon extraction and subsequent acceleration. In addition, energy induced by the trapping field will contribute to the energy distribution. In the IT/TOF, each iso-mass ion packet has a broad energy distribution (~30%), unlike the situation in the tandem TOF instrument. In the latter case, each iso-mass ion packet has a narrow distribution, but the energy range is broad over the mass range of the product ions. Despite this difference, the goal for reflectron design in the IT/TOF is very similar to that in the tandem TOF instrument.

Since our goals were similar, the development of the broad kinetic energy reflectron design method described below was a collaborative effort between Qinchung Ji, whose Ph. D. research is the development of the IT/TOF, and the tandem TOF group. This method involves a numerical calculation step to establish an electrostatic voltage profile followed by a computer simulation step which allows us to achieve the desired field profile using a practical device.

5.5.1 Calculation of a profile

The reflectron field profile is established in a front to back manner, beginning with the lowest energy ions that need to be focused and persisting until the entire energy range of interest is covered. The profile used for the tandem TOF instrument contains a linear and a non-linear field region. The profile for the non-linear field region is determined by specific, practical instrument parameters, namely: field strength and length of the linear field region, kinetic energy range of the ions to be focused, angle between the flight path of the ions in the field-free region and the axis of the reflectron, and length of the field-free region. This profile is generated as a series of linear segments, such that the nodes of the segmented curve correspond to the positions of virtual grids in a theoretical reflectron. The potential applied to each grid is calculated so that iso-mass ions having exactly enough energy to reach a grid, stop there, and change direction will have the same total flight time as iso-mass ions reaching each of the other grids. Ions which turn around at positions other than at grids will have slightly different flight times.

Suppose the lowest energy ion to be focused has energy U_1. Our strategy is to construct a first reflectron segment from two parallel grids placed a distance L_1 apart so that an ion having energy U_1 would stop exactly at the second grid. In order to achieve this, the field-free voltage is applied to the first grid, and a voltage V_1 is applied to the second:

$$V_1 = \frac{U_1}{z} \cos^2\alpha \qquad (2)$$

where α is the angle between the flight path in the field free region and the axis of the reflectron, and z is a single, positive charge.

The length of the flight path outside of the reflectron (field-free region) is L_{ff}, which is the sum of the distance from the initial space-focus plane to the face of the reflectron and the face of the reflectron to the reflectron focal point (often the detector position). The flight time (t) of a hypothetical, singly-charged positive ion having energy U_1 (which would come to a complete stop with respect to the reflectron axis at the position of grid two) can be calculated from:

$$t = \frac{L_{ff}}{v_{ff}} + \frac{2 \cdot L_1}{\bar{v}_1} \qquad (3)$$

where v_{ff} is the velocity of the ion in the field-free region given by:

$$v_{ff} = \sqrt{\frac{2 \cdot U_1}{m}} \qquad (4)$$

where m is the mass of the ion. The average velocity ($\bar{v}_1$) of the ion in the space between grid one and two (parallel to the reflectron axis) is given by:

$$\bar{v}_1 = \frac{1}{2} \cdot v_{ff} \cdot \cos\alpha \qquad (5)$$

The factor of two in the second term of Equation 3 comes from the fact that the ion traverses the field between grids one and two twice. The average velocity of the ion in the space between grid one and two ($\bar{v}_1$) is simply the

average of its velocity parallel to the reflectron axis at the position of grid one ($v_{ff} \cdot \cos \alpha$), and its velocity at the position of grid two (zero). All terms in Equation 3 (fully expanded) are known or measurable physical quantities with the exception of m, which may be arbitrarily chosen as long as its value is kept constant throughout. Therefore a flight time (t) can be calculated for any given set of conditions.

Having established a flight time (t) for an ion of energy U_1, we wish to establish a second field between grid two and a third grid placed a distance L_2 behind grid two. The flight time for an ion stopping at this third grid is given by the equation:

$$t = \frac{L_{ff}}{v_{ff}} + \frac{2 \cdot L_1}{\bar{v}_1} + \frac{2 \cdot L_2}{\bar{v}_2} \qquad (6)$$

where the velocity terms are now:

$$v_{ff} = \sqrt{\frac{2 \cdot (U_1 + U_2)}{m}} \qquad (7)$$

$$\bar{v}_1 = \frac{v_{ff} \cdot \cos\alpha + \sqrt{\frac{2 \cdot U_2}{m}} \cdot \cos\alpha}{2} \qquad (8)$$

$$\bar{v}_2 = \frac{1}{2} \cdot \sqrt{\frac{2 \cdot U_2}{m}} \cdot \cos\alpha \qquad (9)$$

where U_2 is the additional energy that the ion must have (above U_1) to exactly reach grid three. Also, V_2 is the potential difference between grid two and three where:

$$V_2 = \frac{U_2}{z}\cos^2\alpha \qquad (10)$$

Using the flight time (t) calculated from Equation 3, all terms in Equation 6 (fully expanded) are known values with the exception of U_2 which we solve for numerically using MathCad® [7].

The remainder of the reflectron field segments are calculated using MathCad® according to the general equation for the nth stage (n > 2):

$$t = \frac{L_{ff}}{v_{ff}} + \sum_{i=1}^{n-1}\frac{2\cdot L_i}{\bar{v}_i} + \frac{2\cdot L_n}{\bar{v}_n} \qquad (11)$$

where the general velocity terms are:

$$v_{ff} = \sqrt{\frac{2\cdot\sum_{j=1}^{n} U_j}{m}} \qquad (12)$$

$$\bar{v}_i = \frac{v_{ff}\cdot\cos\alpha + \sqrt{\frac{2\cdot\sum_{j=i+1}^{n} U_j}{m}}\cdot\cos\alpha}{2} \qquad (13)$$

$$\bar{v}_n = \frac{1}{2}\sqrt{\frac{2\cdot U_n}{m}}\cdot\cos\alpha \qquad (14)$$

Note that the U_n term (the unknown variable) appears 2·n times in Equation 11 when this equation is fully expanded, illustrating the need to use a numerical solving program such as MathCad® to determine the unknown. V_n is found according to:

$$V_n = \frac{U_n}{z}\cos^2\alpha \qquad (15)$$

For the tandem TOF instrument, a potential profile was calculated for the second reflectron containing 12 segments using the above method. This reflectron was configured for a drift length (L_{ff}) of 188.6 cm, the distances between the grids (L_1 to L_{12}) as given in Table 5.1, the angle (α) between the flight path and the reflectron axis of 2 degrees, 1650 eV as the lowest energy to be focused (U_1), and 2700 eV as the highest energy that can be focused. The actual calculated potentials to be applied to the grids (relative to the field-free potential) and the energies of hypothetical ions reaching each grid are given in Table 5.1, while Figure 5.4 graphically shows the profile beyond grid two. Generally, the profile is curved through the first several grids and becomes more linear towards the back of the reflectron. To obtain a more exact field curvature, electrodes were placed more densely in the initial curved portion of the reflectron, as can be seen in Table 5.1 and Figure 5.4. As will be discussed later, the shape of the calculated profile depends on the values chosen for L_{ff}, U_1, and L_1 through L_{12}. The profile shown in Figure 5.4 is the result of several iterations of input parameters, restricted by the size and physical shape of our vacuum chamber (originally designed around a relatively short, grid-free reflectron) and the actual energy spread of product ions given the possible range of accelerating voltages for this instrument. The profile shown in Figure 5.4 is one which can focus ions in the energy range of interest and meets the physical size restrictions in our tandem TOF instrument.

Table 5.1 Reflectron configuration by segment

Segment	Length (cm) [a]	Energy of Ion (eV) [b]	Calculated Potential (V) [c]	Adjusted Potential (V) [d]
1	1.054	1650.00	1647.99	1647.99
2	0.527	1773.79	1771.63	2590
3	0.527	1865.44	1863.17	1910
4	0.527	1945.10	1942.73	1920
5	0.527	2018.35	2015.89	2015
6	0.527	2087.51	2084.97	2095
7	0.527	2153.81	2151.19	2175
8	1.054	2279.87	2277.09	2278
9	1.054	2401.28	2398.36	2403
10	1.054	2519.53	2516.46	2526
11	1.054	2635.59	2632.38	2635.5
12	1.054	2750.14	2746.79	2745

[a] distances of linear field regions between grids
[b] energies of ions that would exactly reach each grid
[c] calculated potentials for the fully gridded reflectron
[d] empirically adjusted potentials used in the final, two-grid reflectron

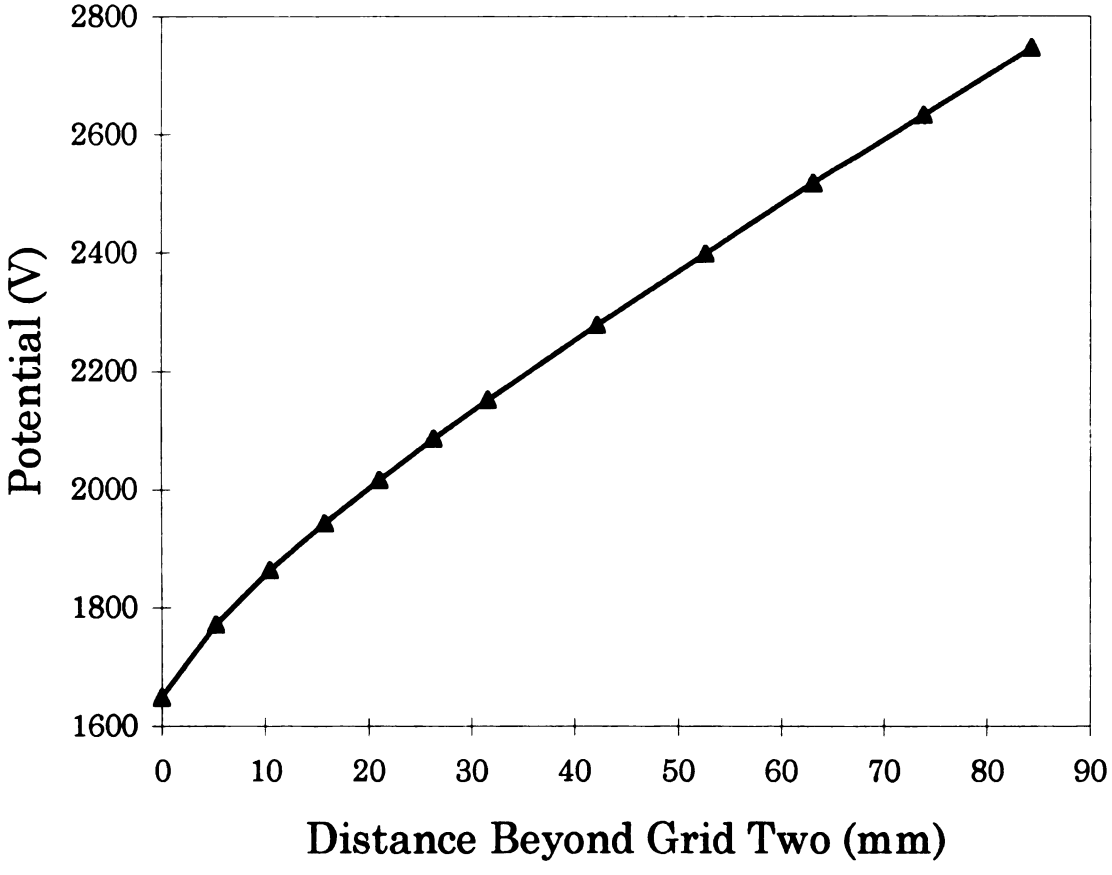

Figure 5.4 Calculated profile for the non-linear portion of the reflectron.

As mentioned previously, only iso-mass ions which stop exactly at grid positions are expected to have exactly the same flight times. The flight times for ions having energies which cause them to turn around between electrode positions can be calculated. Figure 5.5 is a plot of $2 \cdot \Delta t/t$ (where t is the time for an ion which turns around at a grid position, and Δt is the difference between the flight time for a particular ion and the time for an ion which turns around at a grid position) for ions in the range of 1650 to 2700 eV for the calculated reflectron field profile. Calculations were made at 1 eV intervals for the purpose of preparing this plot. Positions where the curve dips toward zero indicate grid locations. It can be seen that in the front of the reflectron, where the curvature of the voltage vs. distance profile is greatest (see Figure 5.4), $2 \cdot \Delta t/t$ exceeds 0.016 which corresponds to a mass resolution of about 50. In the back of the reflectron, where the voltage vs. distance profile is more linear, the flight time deviations for ions turning around between grids are smaller. However, there is a jump to larger deviations between 2100 eV and 2200 eV. This corresponds to the change from closely spaced grids in the front of the reflectron to more widely spaced grids in the back (see Table 5.1).

For the purposes of developing an effective focusing profile, U_1 was set to a value 300 eV lower than the lowest possible energy for the product ions. This was done to take advantage of the smaller deviations in the back of the

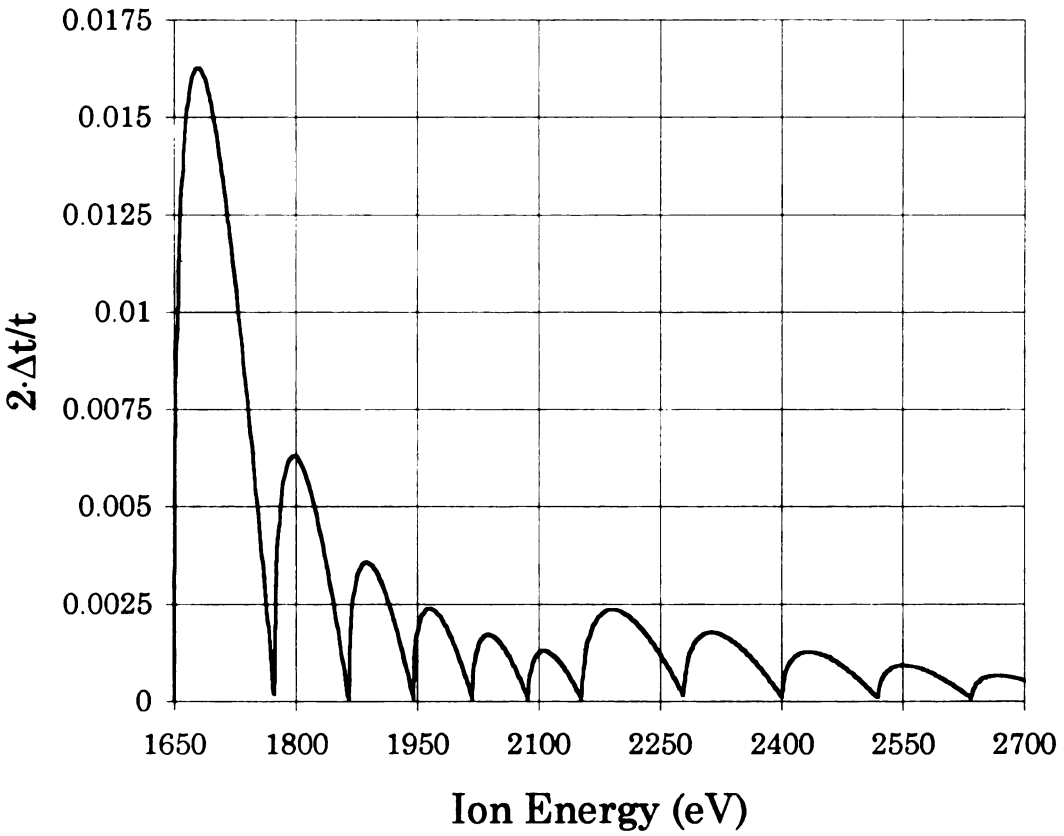

Figure 5.5 A plot of $2 \cdot \Delta t/t$ as a function of ion energy for the fully gridded reflectron.

reflectron and to avoid the large deviations expected for the front part of the reflectron. In Figure 5.5, the portion of the reflectron in which ions turn around is from 1950 eV to 2700 eV. It can be seen that $2 \cdot \Delta t/t$ is less than 0.0025 (Resolution > 400) for this energy range. This predicted resolution is greater than that predicted for optimized two-stage reflectrons. Also, this reflectron is about half as long as the two-stage design.

5.5.2 SIMION modeling to achieve desired profile

Having calculated a potential profile expected to focus iso-mass ions in a kinetic energy range of 1950 eV to 2700 eV, we next constructed a model of the 12 stage reflectron in SIMION [27]. SIMION is a program designed to predict electric fields based on position, shape, and voltage applied to graphically entered electrodes and to predict the motion of charged particles in the fields produced. Figure 5.6a is the SIMION reflectron, with the heavy lines indicating electrodes and the light lines indicating equi-potential contours. The reflectron is cylindrically symmetric. Grid one (at field-free potential) is on the left, with the solid back-plate at the right. A shroud extends from the first grid around the other, higher potential electrodes to preserve the field-free drift space. The potentials corresponding to the equi-potential contour lines are the applied potentials as given in Table 5.1. The contours, of course, follow the conductive electrodes, with minimal leakage of the field-free potential into the spaces between the electrodes near the edges.

a)

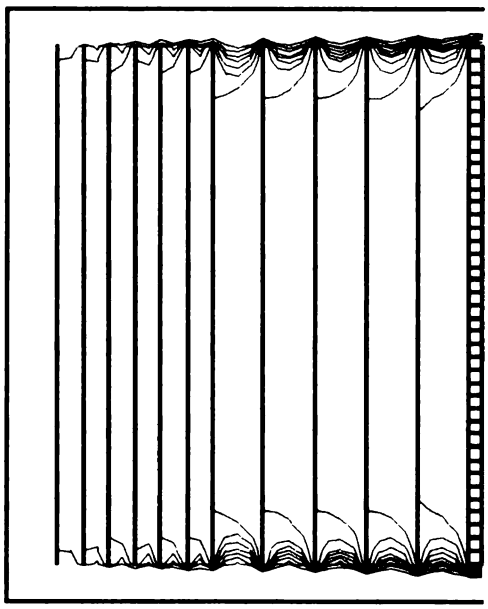

b)

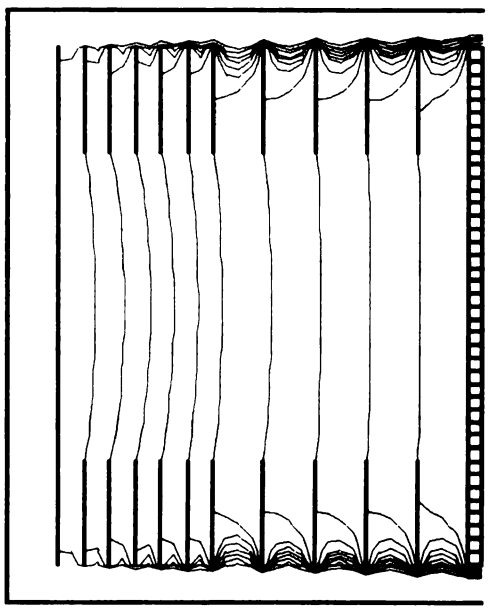

c)

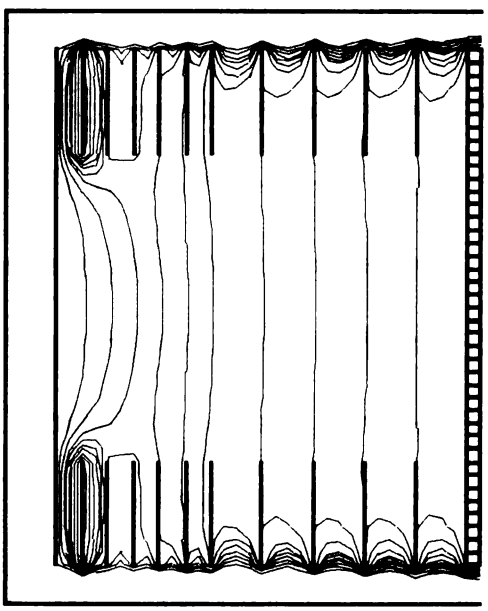

Figure 5.6 SIMION **a)** fully gridded reflectron, **b)** two-grid reflectron, and **c)** two-grid reflectron after adjustment of ring voltages.

Figure 5.7a shows the trajectories of 6 iso-mass ions having kinetic energies of 1950, 2100, 2250, 2400, 2550, and 2700 eV. These ions begin at the same point (a perfect space-focus plane at upper left) with a trajectory 2 degrees from the reflectron axis. Prior to entering the reflectron, the ions follow the same path, as would be expected for a collimated ion beam in a field-free region. The low energy ions spend less time in the reflectron, have a smaller velocity component perpendicular to the reflectron field, and do not penetrate the reflectron field as far as the high energy ions. Upon exiting the reflectron, the iso-mass ions follow parallel paths, eventually becoming focused temporally at a second space-focus plane. The tick marks in the ion trajectories are equal time markers. During the first leg of field-free flight, the ions having higher energy (and higher velocity) move ahead of the lower energy ions, but spend more time in the reflectron, exiting the reflectron later than the lower energy ions. At the second space-focus plane, the higher energy ions have caught up to the low energy ions, resulting in a narrow temporal distribution. Figure 5.7a′ is an expanded view of the portion of Figure 5.7a contained in the rectangle.

For purposes of comparison, the SIMION simulation results (indicated by the squares) are plotted along with the MathCad® calculated results (indicated by the line) in Figure 5.8. Simulations have been made for ions in the range of 1950 to 2700 eV at 25 eV intervals. It can be seen that these predictions are virtually identical.

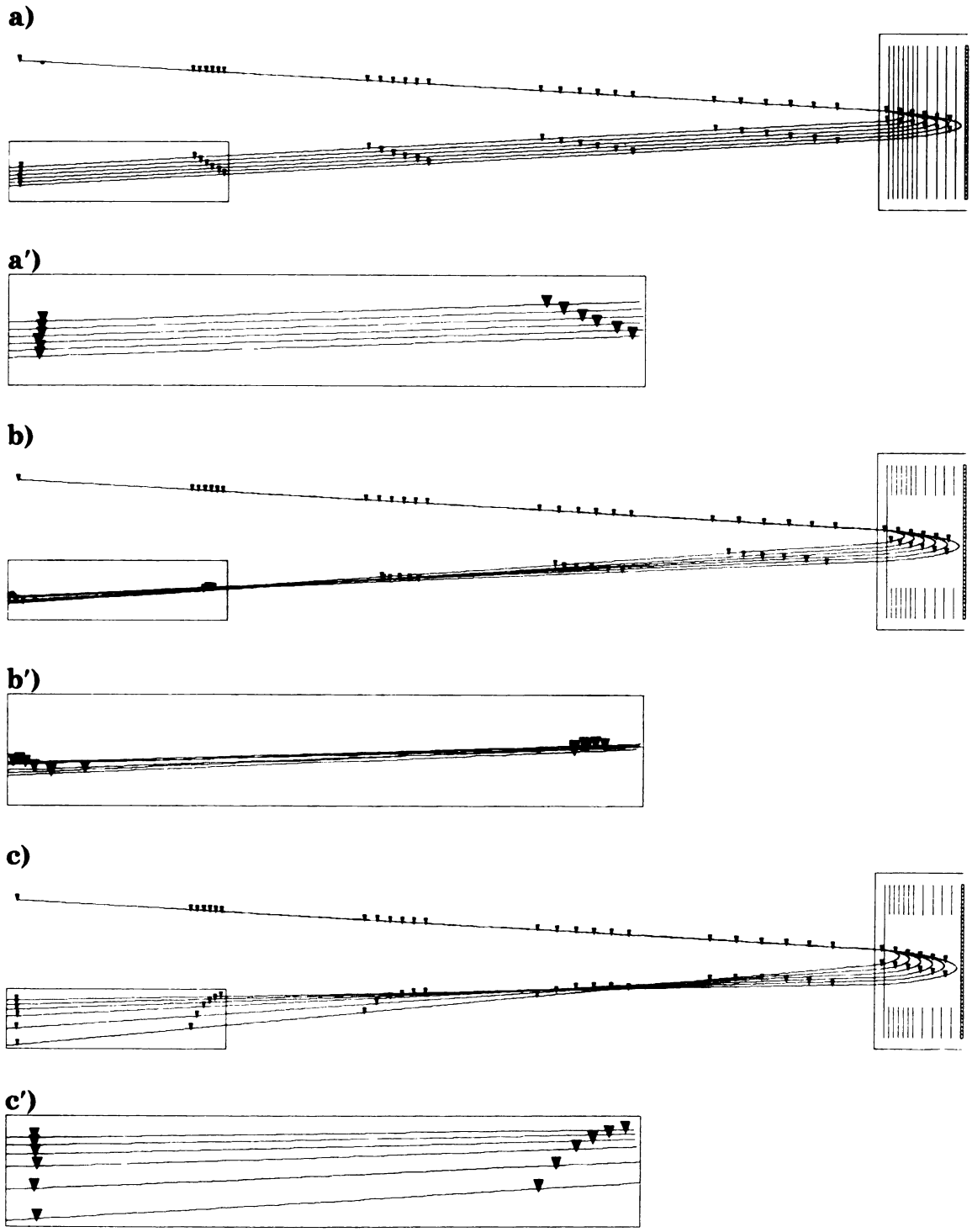

Figure 5.7 SIMION ion trajectories for **a, a')** the fully gridded reflectron, **b, b')** the two-grid reflectron, and **c, c')** the two-grid reflectron after adjustment of the ring electrode voltages.

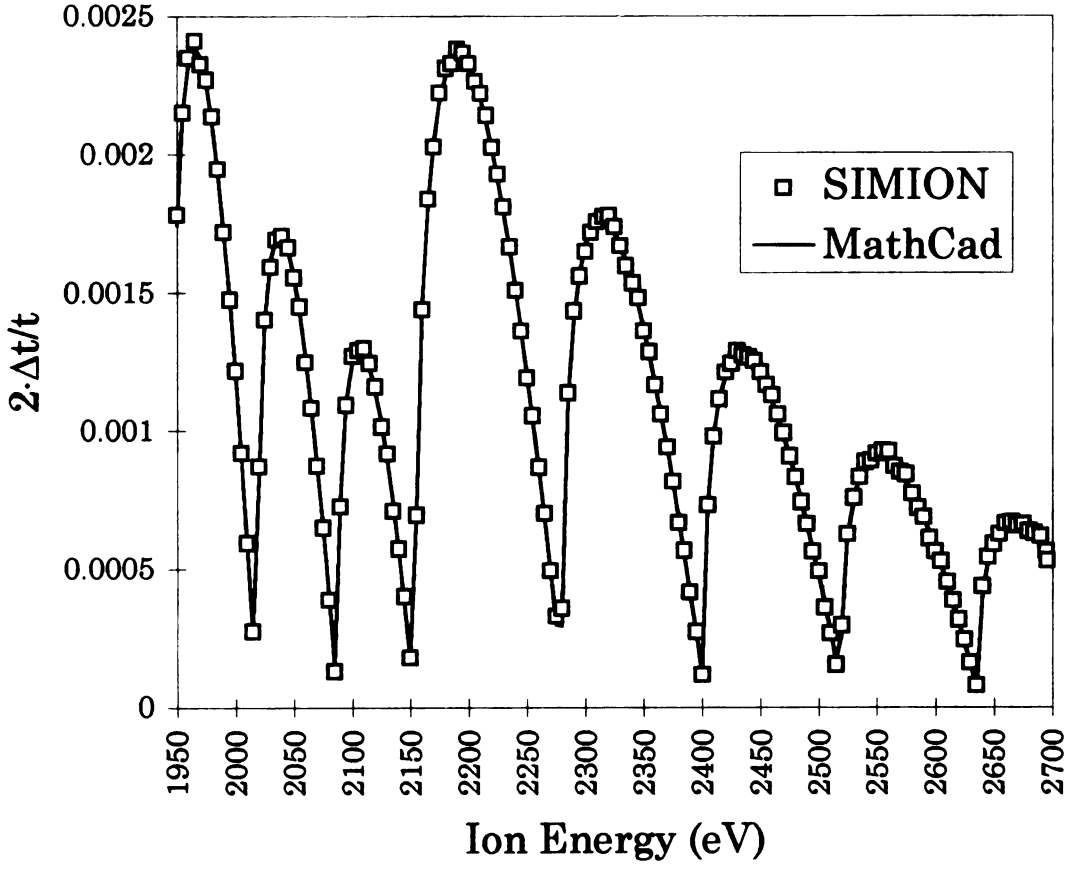

Figure 5.8 Comparison of MathCad® calculation and SIMION simulation.

In the SIMION simulation, the grids are assumed to have 100% ion transmission. However, because the grids actually have limited open area (88%), ion transmission through a real reflectron with many grids would be unacceptably low. Also, field distortions in the vicinity of grids can result in deflection of ions and loss of resolution [14]. To eliminate this limitation we replaced most of the virtual grids in the SIMION reflectron with open rings with the exception of the first two grids, which define the end of the field-free region and the steep initial rise, and the solid plate at the back of the reflectron. Removal of these grids results in distortion of the field in the reflectron. Figure 5.6b is a SIMION plot of the equi-potential contours that result from this new configuration using the calculated potentials given in Table 5.1. The equi-potential contours follow the ring electrodes but deviate from the original grid position as the distance from the ring electrodes increases. Also, the potential vs. distance profile along the reflectron axis is no longer that which was calculated.

These field distortions result in three major consequences. First, the focusing properties observed for the totally gridded reflectron simulation are degraded since the potential profile has changed. Second, the curved field affects radial ion motion, so that ions entering the reflectron at different positions or at slightly different angles are steered differently (spherical aberration). Third, ions entering the reflectron at the same position and angle, but having different energies are also steered differently (chromatic

aberration). The loss of temporal focus resulting from the field distortions can be observed in Figure 5.7b and Figure 5.7b′, which show trajectories for ions with kinetic energies in the range of 1950 to 2700 eV. Also apparent is the chromatic aberration, which in this case results in a narrower beam at the reflectron focal point. This reflectron yields a predicted resolution of less than 50.

In order to compensate for the field distortions seen in Figure 5.6b, the ring electrode voltages can be manually adjusted in SIMION by an iterative process. With each adjustment of electrode voltages, a contour plot is observed and trajectories simulated to determine effect. This procedure allows the calculated potential vs. distance profile to be achieved quite closely in the two-grid reflectron for the path that the ions are expected to travel in the reflectron. This results in improved temporal focusing, but increases the spherical and chromatic aberration by further increasing the curvature of the reflectron field. This effect can be seen in Figure 5.6c, which shows the equi-potential contours for the manually adjusted reflectron. The voltages applied to the rings in this simulation are the adjusted potentials given in Table 5.1. Figure 5.7c and Figure 5.7c′ show trajectories for ions in the range of 1950 to 2700 eV. The effects of chromatic aberration in this case result in a broad ion beam. The temporal distribution has decreased considerably as a result of the manual adjustment. Figure 5.9 is a plot of $2 \cdot \Delta t/t$ vs. ion energy Because the

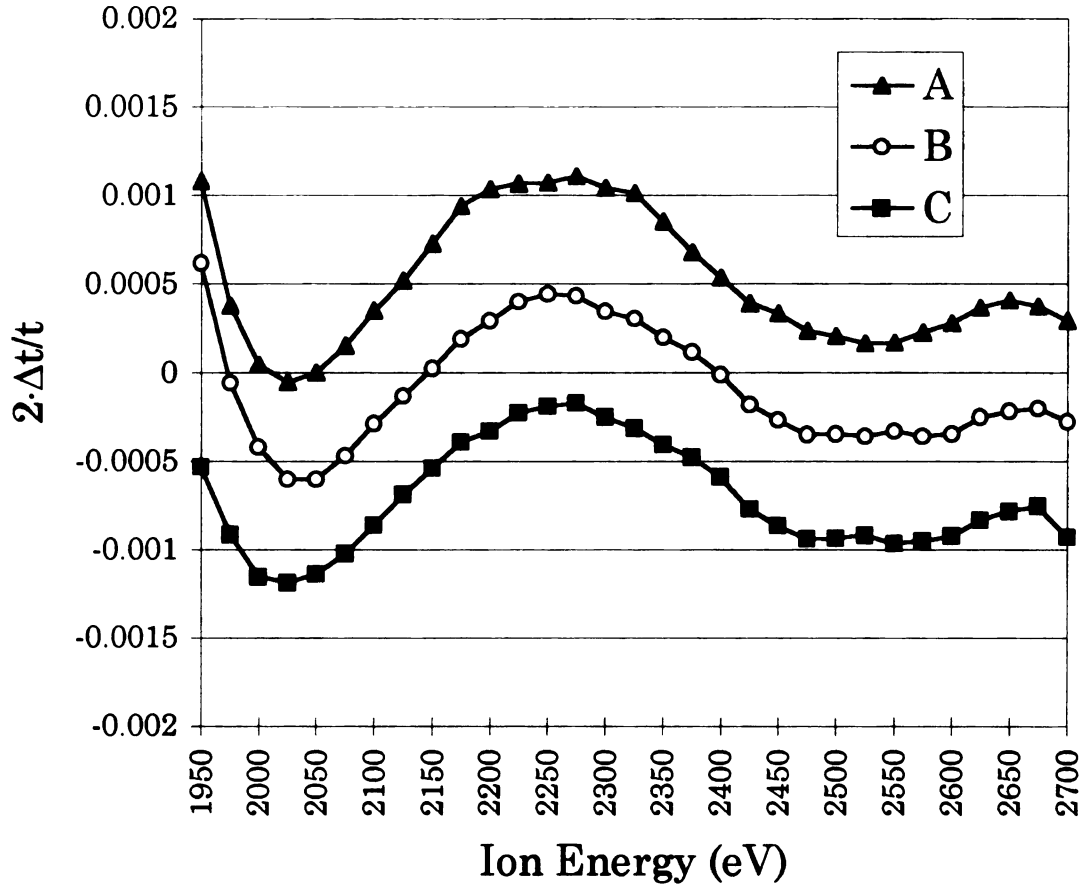

Figure 5.9 A plot of $2 \cdot \Delta t/t$ as a function of ion energy for the two-grid, empirically adjusted reflectron over the range of 1950 to 2700 eV at intervals of 25 eV.

ion beam is not infinitely narrow as modeled above, but rather has a finite diameter of about 1 cm, three traces are drawn in Figure 5.9. Curve B corresponds to the center of the beam (as modeled above), giving a theoretical resolution of approximately 800. Curve A corresponds to the same trajectories begun from a position 5 mm nearer the center of the reflectron while curve C indicates trajectories begun 5 mm further from the center of the reflectron, for an overall beam diameter of 1 cm. The differences between these traces are a result of spherical aberration. Including the effect of the beam width, an overall resolution of approximately 400 is predicted. This is the reflectron configuration we chose to emulate for the second reflectron in the tandem TOF instrument.

5.5.3 Construction

Reflectron 2 is constructed from stainless steel rings (outer diameter = 10.2 cm, inner diameter = 6.35 cm, thickness = 0.051 cm). Stainless steel mesh (90 LPI, 88% open area, Buckbee-Mears, St. Paul, MN) was spot-welded to the face of the first two rings to form the linear portion of the reflectron. The last electrode in the reflectron stack is a solid stainless steel plate. Ceramic spacers are used to hold the electrodes together in a stack and isolate them from one another electrically. The distances between the rings are given in Table 5.1 as are the adjusted voltages applied to the electrodes. The total length of the reflectron is 9.5 cm. The reflectron is mounted in the instrument by three posts attached to the back. Two of the

posts are connected to linear motion feedthroughs which allow optimization of mirror position while under vacuum.

5.5.4 Performance

Figure 5.10 is a product spectrum obtained using the two-grid, empirically-adjusted reflectron in the tandem TOF mass spectrometer. The precursor ion was m/z 91 from toluene which was isolated by the gate prior to dissociation. This spectrum represents a relative kinetic energy range of about 32%.

The mass resolution ($m/\Delta m$, FWHM) is about 300 for product spectra and about 1500 ($t/(2\cdot\Delta t)$, FWHM) for normal spectra. This resolution for normal spectra through reflectron 2 (collected without use of the gate or laser PID) is approximately the same resolution that is observed when a detector is placed near the position of the interaction region. One would normally expect resolution to improve with increased flight distance since the separation between adjacent iso-mass ion packets increases. Our result shows that the arrival time distribution for each iso-mass ion packet is being broadened at approximately the same rate as the distance between adjacent iso-mass ion packets increases. There are two factors which are believed to be primarily responsible for this effect. First, some flight time deviation is expected as a function of energy and beam width as depicted in Figure 5.9. Second, the introduction of seven grids in the second mass analyzer (the reflectron grids

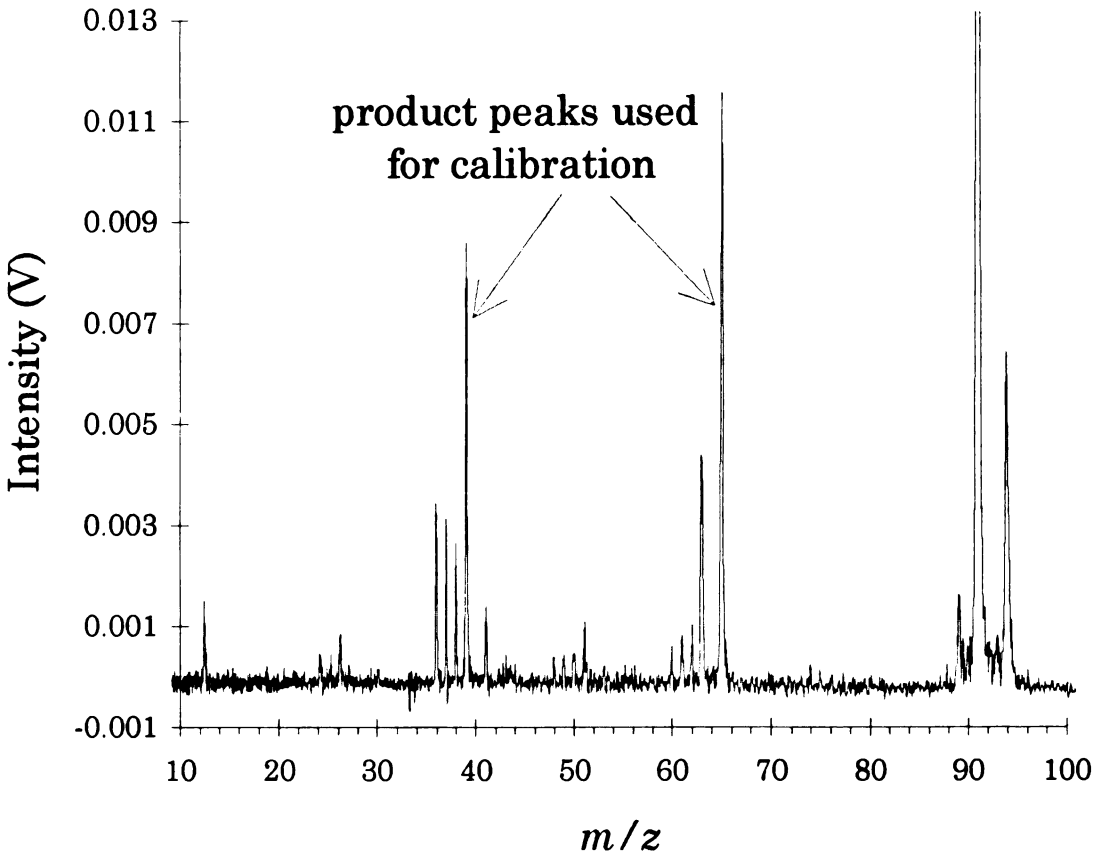

Figure 5.10 Product spectrum of m/z 91 from toluene.

counted twice) can also result in broadening of peaks since field distortions occur in the vicinity of these grids [14]. This effect is especially pronounced when the field strength changes drastically across the grid, as is the case for both the post-dissociation acceleration grids and the reflectron grids.

The fact that the product spectra are not as well resolved as normal spectra is not primarily a result of temporally broadened product ion peaks, but the compression of this spectrum in time as compared to the normal spectrum. Normal (undissociated) ion packets separate from one another continuously through the entire flight path beginning at the source, while product ion packets do not begin to separate from one another until they are accelerated after dissociation in the interaction region. The mass resolution of 300 observed for the product spectra is similar to the resolution of 400 predicted by the SIMION model. Because each iso-mass product ion packet has a small kinetic energy range rather than the entire energy range (which was used in making the resolution prediction), one would expect that the actual peak widths would be narrower than those predicted in this manner. However, the loss of resolution as a result of grid effects, spherical and chromatic aberration, uncertainties in the dimensions of instrument components, uncertainties in applied voltages, and uncertainties in the modeling itself apparently are offsetting. Uncertainties in the dimensions of the instrument are important since the reflectron voltages are calculated based on these dimensions, which include field-free drift length and distance

between reflectron electrodes. Distance between the two grid electrodes is of particular importance because of the large field applied between them. Unfortunately, this distance is particularly difficult to control since the wire mesh attached to the ring electrodes does not tend to stay flat. Attempts to apply tension to the wire mesh worsens the situation as the material then tends to ripple. The reflectron voltages are not tuned in any way to improve performance for two reasons. First, adjustment of individual voltages degrades resolution. Second, any change in the profile which does not make the profile more like that calculated is likely to affect applicability of the derived mass calibration equations described below. Indiscriminate tuning is effective for the first reflectron, however, since all m/z values have approximately the same energy distribution and therefore travel similar paths through the first reflectron.

It was previously mentioned that due to chromatic and spherical aberration, beam de-focusing effects may result in ion loss and m/z discrimination (see Figure 5.7). Evidence of this problem presents itself in the tandem TOF instrument since relative intensities of product m/z's are affected by the adjustment of the reflectron's angular position. When mirror position is optimized for maximum throughput of low m/z product ions rather than normal, undissociated ions, their intensity can be improved by approximately a factor of two, with a corresponding reduction in the normal ion peak intensities.

5.5.5 Possible improvements

As mentioned above, the specific reflectron used in the tandem TOF instrument was optimized within the constraints of pre-existing size limitations of the vacuum chamber. When a greater range was considered for the independent variables in the design calculation, it was found that extending the linear field region at the front of the reflectron resulted in a longer non-linear region with less curvature. Figure 5.11 is a comparison of two calculated profiles for the same choice of U_1, α, and L_{ff}, but curve A is calculated using L_1 of 1.054 cm as used previously in the tandem TOF reflectron 2 development, and curve B is calculated using L_1 of 10.54 cm.

There are several reasons why the longer profile is a more effective solution. Because the profile for the longer first stage is less curved, the flight time deviations for ions that turn around between grid positions is smaller. There is far less field distortion as a result of removal of the grids in the longer reflectron as compared to the shorter one, reducing the extent to which ring electrodes need to be adjusted to restore the calculated profile. The more homogeneous field of the longer reflectron causes less spherical and chromatic aberration. Because the change in field strength across the reflectron grids is smaller for the long linear stage than for the shorter linear stage, the detrimental field distortions in the vicinity of the reflectron grids will be smaller [14]. Besides the improvements in using a longer reflectron

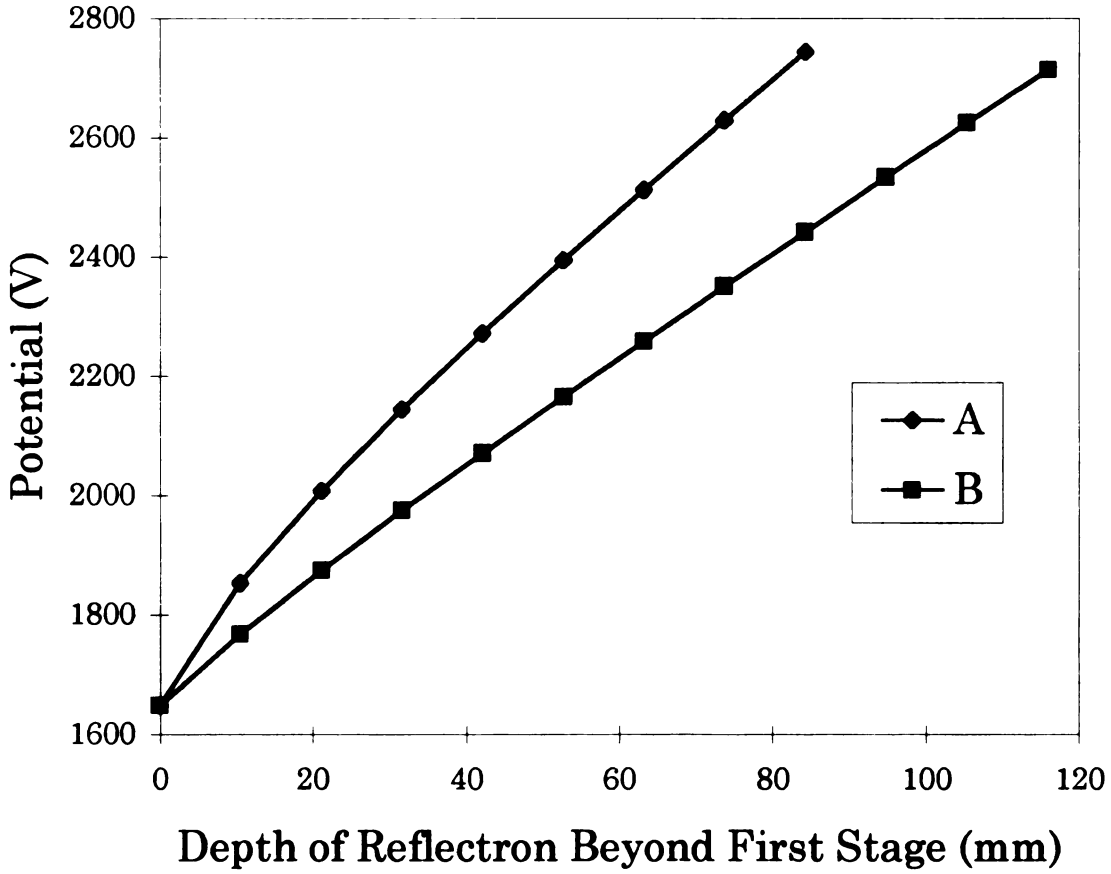

Figure 5.11 Comparison of resulting reflectron profiles for different lengths of the first stage.

design, it is expected that using a smaller angle, α, will result in improved performance. Since the field profile in the non-linear portion of these reflectrons varies from the outer edges to the center, with large curvature in the equi-potential lines near the edges (see Figure 5.6c), using only the center portion of the reflectron (by reducing α) should reduce aberration effects.

Unfortunately the physical size limitations of the tandem TOF vacuum chamber do not allow the testing of a significantly longer reflectron design. However, the IT/TOF instrument design incorporates the suggested improvements. The tandem TOF instrument and the IT/TOF instrument pose slightly different challenges, making a direct comparison of results difficult. The tandem TOF reflectron 2 must focus individual iso-mass ion packets having small energy ranges, but with a broad relative energy range over the mass range. In the IT/TOF, the relative kinetic energy range over each specific m/z ion packet is large (~30%). In the tandem TOF instrument, macroscopic inaccuracy in the field profile used will result primarily in calibration inaccuracy. In the IT/TOF instrument, inaccuracy in the field profile will result in reduced mass resolution. A direct comparison of the performance of a short and long reflectron can be performed in the IT/TOF instrument by constructing one reflectron of each type.

5.5.6 Significance of this design method

The reflectron design method presented here results in non-linear field reflectrons capable of focusing large energy ranges with the use of only two grids. The systematic progression of design results in a practical device in terms of performance and ease of construction despite geometric constraints. This design method provides an alternative to analytical solutions for energy-focusing and a new approach to ion optical design.

The method described above has been successfully used to design a reflectron which provides unit resolution for product ions having a relative kinetic energy range of about 32% in the tandem reflectron TOF mass spectrometer. While the performance of this specific reflectron is satisfactory in its application, we expect that the longer design under construction for the IT/TOF instrument will result in improved performance for broad energy range focusing for reasons mentioned above.

This design method is quite versatile. While one and two-stage reflectrons must be constructed in accordance with analytical solutions, reflectrons designed by this method have much more flexible geometry. As discussed above, however, longer reflectrons with smaller angles between ion flight path and reflectron axis are expected to perform better. In both the tandem TOF and the IT/TOF instrument, our needs require focusing of ions with relative energy spreads around 30%. This is certainly not the limit of this reflectron design method. We expect that any energy range can be

compensated for by adding stages to the back of the reflectron during the calculation step.

It is interesting to consider the case of reducing the distance between adjacent grids in the calculation to the point where the flight time deviations for ions stopping between grids becomes negligible. This is not useful as a practical device due to the large number of grids; however, the resulting profile would be an excellent solution to the broad energy range focusing problem for instruments with field-free regions, unlike the 'perfectron' solution described by Rockwood [15] which has no field-free region. Although our solution is more consistent with current reflectron instrument designs than the 'perfectron' design, the challenge again becomes the design and construction of a practical device which accurately produces this field profile without serious aberration.

5.6 Calibration of product ion spectra

Calibration of product ion spectra is easily accomplished using the derived relationship:

$$t_{prec} - t_{prod} = \sqrt{\frac{m_{prec}}{A + B}} - \sqrt{\frac{m_{prod}}{\left[\frac{m_{prod}}{m_{prec}} \cdot A\right] + B}} \qquad (16)$$

where t_{prec} is the precursor arrival time, t_{prod} is the product arrival time, with:

$$A = \frac{2 \cdot \overline{U}_{prec}}{(L_{ff})^2} \qquad (17)$$

$$B = \frac{2 \cdot U_{acc}}{(L_{ff})^2} \qquad (18)$$

where $\overline{U}_{prec}$ is the average kinetic energy of the precursor ions, and U_{acc} is the energy gained by post-dissociation acceleration.

Since A and B are difficult to determine by direct measurement, two product ion arrival times for known *m/z* values along with the arrival time and *m/z* value of the precursor ion are used in Equation 16 to solve for the two unknowns (A and B) using MathCad®. These constants can be used to calibrate product spectra collected from any *m/z* value precursor ion for the same instrument tune. For the spectrum in Figure 5.10, the peaks at m/z values 39 and 65 were used for calibration. Mass assignment is accurate to within 0.1 a.m.u. for most of the spectrum, with slightly larger error for masses in approximately the lowest 25% of the spectrum.

5.7 References

1 Wiley, W. C.; McLaren, I. H. *Rev. Sci. Instrum.* **1955**, *26(12)*, 1150.

2 Karataev, V. I.; Mamyrin, B. A.; Shmikk, D. V. *Sov. Phys. Tech. Phys.* **1972**, *16(7)*, 1177.

3 Mamyrin, B. A.; Karataev, V. I.; Shmikk, D. V.; Zagulin, V. A. *Sov. Phys.-JETP* **1973**, *37(1)*, 45.

4 Grix, R.; Gruner, U.; Li, G.; Stroh, H.; Wollnik, H. *Int. J. Mass Spectrom. Ion Processes* **1989**, *93*, 323.

5 Grix, R.; Kutscher, R.; Li, G.; Gruner, U.; Wollnik, H. *Rapid Commun. Mass Spectrom.* **1988**, *2(5)*, 83.

6 Gohl, W.; Kutscher, R.; Laue, H. J.; Wollnik, H. *Int. J. Mass Spectrom. Ion Processes* **1983**, *48*, 411.

7 *MathCad 5.0 ® for Windows*; Copyright © 1991-1994 by MathSoft, Inc., 101 Main Street, Cambridge, MA 02142.

8 Boesl, U.; Weinkauf, R.; Schlag, E. W. *Int. J. Mass Spectrom. Ion Processes* **1992**, *112*, 121.

9 Berger, C. *Int. J. Mass Spectrom. Ion Processes* **1983**, *46*, 63.

10 Frey, R.; Weiss, G.;Kaminski, H.; Schlag, E. W. *Z. Naturforsch. Teil A.* **1985**, *40*, 1349.

11 Walter, K.; Boesl, U.; Schlag, E. W. *Int. J. Mass Spectrom. Ion Processes* **1986**, *71*, 309.

12 Kutscher, G.; Grix, R.; Li, G.; Wollnik, H. *Int. J. Mass Spectrom. Ion Processes* **1991**, *103*, 117.

13 Bergmann, T.; Martin, T. P.; Schaber, H. *Rev. Sci. Instrum.* **1990**, *61(10)*, 2592.

14 Bergmann, T.; Martin, T. P.; Schaber, H. *Rev. Sci. Instrum.* **1989**, *60(3)*, 347.

15 Rockwood, A. L. *Proceedings of the 34th ASMS Conference on Mass Spectrometry and Allied Topics,* Cincinnati, Ohio, June 8-13, 1986, 173.

16 Della Negra, S.; Le Beyec, Y. *Int. J. Mass Spectrom. Ion Processes* **1984**, *61*, 21.

17 Della Negra, S.; Le Beyec, Y. *Anal. Chem.* **1985**, *57*, 2035.

18 Tang, X.; Beavis, R.; Ens, W.; LaFortune, F.; Scheuler, B.; Standing, K. G. *Int. J. Mass Spectrom. Ion Processes* **1988**, *85*, 43.

19 Weinkauf, R.; Walter, K.; Weickhardt, C.; Boesl, U.; Schlag, E. W. *Z. Naturforsch.* **1989**, *44a*, 1219.

20 Cornish, T. J.; Cotter, R. J. *Org. Mass Spectrom.* **1993**, *28*, 1129.

21 Cornish, T. J.; Cotter, R. J. *Rapid Commun. Mass Spectrom.* **1993**, *7*, 1037.

22 Cornish, T.J.; Cotter, R. J. *Proceedings of the 42nd ASMS Conference on Mass Spectrometry and Allied Topics,* Chicago, Illinois, May 29 - June 3, 1994, 1046.

23 Schey, K. L.; Cooks, R. G.; Kraft, A.; Grix, R.; Wollnik, H. *Int. J. Mass Spectrom. Ion Processes* **1989**, *94*, 1.

24 Seeterlin, M. A. *Ph. D. Thesis,* Michigan State University, **1993**.

25 Ji, Q.; Vlasak, P. R.; Holland, J. F.; Enke, C. G. *Proceedings of the 42nd ASMS Conference on Mass Spectrometry and Allied Topics,* Chicago, Illinois, May 29 - June 3, 1994, 1042.

26 Ji, Q.; Davenport, M. R.; Holland, J. F.; Enke, C. G. *presented at The 43rd ASMS Conference on Mass Spectrometry and Allied Topics,* Atlanta, Georgia, May 22, 1995.

27 Dahl, D. A.; Delmore, J. E. *SIMION PC/PS2 Version 5.0 (real mode),* 1988, Idaho Falls National Engineering Laboratory, EG&G Idaho Inc., P.O. Box 1625, Idaho Falls, ID 83415.

Chapter 6: TOF/TOF as an analytical tool

6.1 Unit resolution and efficient photo-fragmentation

The goal of this research project, as outlined in chapter 1, is the development of a tandem mass spectrometer capable of greatly increasing the amount of MS/MS data obtainable from sample components as they elute from a chromatographic column. Several steps along the road to this goal have been described in this thesis.

Time-of-flight mass spectrometry is especially suited to any application which requires a high spectral generation rate. The characteristically poor mass resolution of TOF has been an impediment to its development, however. This is especially true for applications which require a gas-phase ion source. In the TOF/TOF instrument, we have demonstrated a mass resolution of 1500 for separation of precursor ions (see chapter 2). We have demonstrated that focusing a laser pulse to the approximate dimensions of a single, iso-mass precursor ion packet allows unit resolution of selection at least to m/z 158. Calculations show that the limit of unit resolution for selection is around m/z 1200 (see chapter 3). Isolation of the precursor ion packet (prior to PID) is important in order to eliminate background. We have demonstrated that the use of an interleaved comb deflection gate allows unit

resolution for isolation to at least m/z 167 with calculations indicating that the actual limit is around m/z 300 (see chapter 4). Using a novel reflectron which can focus a broad energy range, we have demonstrated a mass resolution of 300 for the collection of product ion spectra. The development method used to create this reflectron represents a new approach in ion optical design (see chapter 5). Unit resolution over a mass range of at least 300 a.m.u. is consistent with the requirements of a detector for gas chromatography, showing that tandem TOF is an alternative to the more traditional tandem mass analyzers based on mass filters.

Given the known photodissociation cross-sections for organic ions and the photon density that can be generated by focusing a high-energy excimer laser pulse to a small volume, it follows that photo-fragmentation efficiencies should be high for ions which occupy this volume. This was demonstrated experimentally in the tandem TOF instrument (see chapter 3) when a fragmentation efficiency of 79% was observed for the molecular ion of bromobenzene. The efficiencies for a variety of ions were shown to be similar to the efficiencies observed for CID in a triple quadrupole mass spectrometer. A large number of precursor ions are focused to the interaction region volume, thereby making efficient use of sample as well as laser power.

6.2 Analytical utility of PID product spectra

The implementation of the novel reflectron in the second mass analyzer results in unit mass resolution for the product spectra. This development allows a more complete charactrization of photo-induced dissociation (at 193 nm) as a fragmentation technique in the tandem TOF mass spectrometer [1-4]. Photodissociation cross-sections for 45 ions originating from 27 different compounds have been determined. These cross-sections range from 2.9×10^{-19} to 1.4×10^{-18} cm^2 [2, 4]. Aliphatic ions originating from both saturated and unsaturated molecules are among those successfully photo-fragmented. This provides evidence that virtually all organic ions should photodissociate when 193 nm radiation is used and further indicates that PID will provide efficiencies that are useful in analytical applications when a system with high ion/photon overlap is employed.

The product spectra from photodissociation in the tandem TOF mass spectrometer were compared to product spectra collected using CID in a triple quadrupole mass spectrometer [1, 2, 4]. All ions observed in the CID spectra were also observed in the corresponding PID spectra. In general, the low m/z portions of the PID spectra were enhanced with respect to the corresponding CID spectra. In addition, peaks due to loss of hydrogen from various product ions were more frequently observed in the PID spectra than in the CID spectra. These factors both indicate that more energy is imparted

to the precursor ion through the use of 193 nm (6.4 eV) PID than is transferred collisionally in the triple quadrupole mass spectrometer. These data show that PID in the tandem TOF mass spectrometer provides at least as much analytical information as CID in the triple quadrupole mass spectrometer. Further studies of the PID process for organic compounds as a function of laser wavelength and power are being carried out in Professor Enke's laboratory.

6.3 Feasibility of GC/MS/MS

The collection of complete data sets for compounds as they elute from a gas chromatographic column is still not possible. Many of the barriers that stood in the way of this goal have been removed, however. Particularly, we have shown that useful product spectra can be generated at the repetition rate of an excimer laser. Monitoring GC effluents will require the implementation of an improved instrument control and data collection system. The current instrument control system is based on a LabWindows® program which communicates via GPIB with a delay generator and a transient recorder (see chapter 2). The GPIB cannot transfer data at an adequate rate to allow GC/MS/MS. Also, delay times, which specify precursor ion m/z, currently are entered manually.

The automated system which would allow GC/MS/MS will continuously collect normal spectra until a compound begins to elute. The

spectrum of this compound will then be assessed for m/z values having significant intensity. Next, the control system will sequentially implement the necessary delay times to collect a product ion spectrum for each significant m/z value in the normal spectrum. The control system will then continue to check for evidence of the next elution. An integrating transient recorder, like that developed at MSU [5-7], will be required for data collection. While custom electronics and sophisticated programming would be required to construct such a control system at this time, computer interfacing and data collection electronics are both high-growth technologies, and the building blocks of such a system may become commercially available in the relatively near future.

6.4 TOF/TOF in other analytical applications

There are numerous potential applications of tandem TOF beyond those which have previously been described in this thesis. Two of these, which involve the extension of this technique to non-volatile compounds, are described below. Besides the analytical diversity gained by extending this instrument's capabilities to higher mass compounds, this would allow characterization of PID as a potential fragmentation technique for high m/z ions.

The advantages of tandem TOF in the characterization of GC effluents are directly applicable to liquid separations. The successful coupling of LC

with TOF is challenging, however, since the ion sources (such as electrospray) which are generally used to interface LC with mass spectrometry operate in continuous rather than pulsed mode. A possible solution to this interface problem is being developed in Professor Enke's laboratory. Specifically, Qinchung Ji [8, 9] has coupled an ion trap storage device with a TOF mass spectrometer such that the storage device accumulates continuously generated ions between extractions. This will allow any type of ionization to be used with TOF, thereby taking advantage of the spectral generation rate and sensitivity of TOF without sacrificing duty cycle.

Matrix-assisted laser desorption ionization (MALDI) has proven itself as an extremely useful technique for ionizing large biomolecules or other polymers. MALDI is often used in conjunction with TOF since TOF analyzers have virtually unlimited mass range, are inexpensive, and are directly compatible with pulsed ionization. MALDI is a soft ionization technique which often yields exclusively the protonated molecule. While this is useful in determining molecular weight, it provides little structural information. The possibility of using tandem TOF to enhance the structural information obtainable is therefore attractive. Preliminary studies were performed in collaboration with Ben Gardner and Professor J. Throck Watson [10] in the tandem TOF instrument. The photodissociation of protonated bradykinin (m/z 1061) represents the first successful photo-fragmentation of a peptide

ion in a TOF mass spectrometer. Unfortunately, the low acceleration potential of this instrument (650 V) proved incompatible with MALDI, which generally employs accelerations on the order of 30 kV to overcome a large energy spread and to reduce ion loss due to radial divergence. Signal levels were simply too low to warrant further studies. The implementation of an ion trap storage source (as described above) would allow a more successful coupling.

6.5 References

1 Vlasak, P. R.; Beussman, D. J.; Enke, C. G. *Proceedings of the 42nd ASMS Conference on Mass Spectrometry and Allied Topics,* Chicago, IL, May 29 - June 3, 1994, 1036.

2 Beussman, D. J. *Ph. D. Thesis,* Michigan State University, **1995**.

3 Beussman, D. J.; Erickson, T. A.; Enke, C. G. (*submitted to J. Am. Soc. Mass Spectrom.*)

4. Beussman, D. J.; Erickson, T. A.; Vlasak, P. R.; Enke, C. G. (*in preparation for submission to Anal. Chem.*)

5 Erickson, E. D.; Enke, C. G.; Holland, J. F.; Watson, J. T. *Anal. Chem.* **1990**, *62(10)*, 1079.

6 Tecklenburg, R. E., Jr.; McLane, R. D.; Grix, R.; Sweeley, C. C.; Allison, J.; Watson, J. T.; Holland, J. F.; Enke, C. G.; Gruner, U.; Gotz, H.; Wollnik, H. *Proceedings of the 38th ASMS Conference on Mass Spectrometry and Allied Topics,* Tucson, AZ, June 3-8, 1990.

7 Holland, J. F.; Newcombe, B.; Tecklenburg, R. E., Jr.; Davenport, M.; Allison, J.; Watson, J. T.; Enke, C. G. *Rev. Sci. Instrum.* **1991**, *62(1)*, 69.

8 Ji, Q.; Vlasak, P. R.; Holland, J. F.; Enke, C. G. *Proceedings of the 42nd ASMS Conference on Mass Spectrometry and Allied Topics,* Chicago, IL, May 29 - June 3, 1994, 1042.

9 Ji, Q.; Davenport, M. R.; Holland, J. F.; Enke, C. G. *presented at The 43rd ASMS Conference on Mass Spectrometry and Allied Topics*, Atlanta, Georgia, May 22, 1995.

10 Gardner, B. D.; Vlasak, P. R.; Beussman, D. J.; Enke, C. G.; Watson, J. T. *Proceedings of the 42nd ASMS Conference on Mass Spectrometry and Allied Topics*, Chicago, IL, May 29 - June 3, 1994, 1037.